Application of electrochemical methods for the study and protection of heritage copper alloys

Thesis submitted in fulfilment of the requirements for the degree of

DOCTOR OF SCIENCE: CHEMISTRY

by

ALICE ELIA

Supervisor: Prof Dr A. Adriaens

Co-supervisor: Prof Dr M. Dowsett

Acknowledgements

This research has been possible thanks to the collaboration of many people: probably all of them will read this part, so I will try not to forget anyone.

Firstly, I would like to express my gratitude to prof. dr. Annemie Adriaens for her guidance: her kindness and support have been very precious to me along all these years and I would not be at this point without her determination.

I am also thankful to prof. dr. Mark Dowsett for his important help, especially in the final stages of this PhD, and all the fruitful discussions on scientific matters and particularly on copper carboxylates issues. Thanks to him, I was introduced to the unforgettable experience of performing experiments in a synchrotron facility. For this, I would also like to thank the staff of the UK CRG beam line (XMaS) and of the Dutch-Belgian beamline (Dubble) at ESRF in Grenoble. Thanks also to the staff of the beamline P06 at DESY in Hamburg.

My sincere acknowledgment also goes to prof. dr. Karel Strijckmans and prof. dr. Peter Vandenabeele for their assistance in the difficult moments.

I wish to acknowledge as well Sandra van Vlierberghe and Vincent Vermeersch (Ghent University) for the help with ATR-FTIR analyses, Tom Planckaert (Ghent University) and David Walker (University of Warwick) for collecting the XRD data.

A sincere acknowledgment should be reserved to prof. dr. Laszlo Vincze and the entire XMI group for the XRF measurements. Thanks to Bart and Giovanni for the help with the XRF mapping. Jan and Lien, I certainly owe you a big hug and you know why.

Furthermore, I have to thank the Bijzonder Onderzoeksfonds *(BOF) and the* Fonds Wetenschappelijk Onderzoek *(FWO), for the financial support, and the* Onroerend Erfgoed *(OE) and Leentje Linders for kindly providing the archaeological artefacts, without which my research would have been incomplete.*

And of course I have to thank all my colleagues of the ESA group: Elbeshary, Farzin, Roohangiz, Victoria and especially Pieter-Jan, for sharing his good mood when I needed it. Rosie, sorry if I often mistreat your mother tongue and thanks for smiling at me when I do it. Michel, thank you for your company and support: your being cool in every situation was for me a reference point: I am sure that the students will be in good hands!

I cannot forget the friends that accompanied me in all my Belgian years. Some of them made return to their home country, some other found a new home (warmer than Belgium), some

other just arrived in Ghent and many others (water- and windproof) are still here. Here I would like to thank Alessia, Andrei, Andrey, Deepti, Eleonora, Kris, Lara, Matthias, Sylvia, Tom and, of course, the entire Department of Analytical Chemistry, who gave me a warm hug on my 30th birthday.

I also would like to thank my family, mum, dad, Mario and Silvia, for their endless help and support despite the distance between us. Thank you for being with me in every moment.

A special thanks to Michela, Luca, Chiara, Chiara e Davide, who have reached me travelling all the way to Belgium (and beyond), and all the friends who supported me from Italy.

Simone, perhaps I've been a bit grumpier than usual in the past months, but you were always there for me with your love and infinite (?) patience. Thank you for taking care of me in all the difficult moments I went through.

Table of Contents

List of Appendixes in the enclosed CD-ROM:

Appendix A: XRF maps of corroded Cu-Sn alloys

Appendix B: XRD spectra of reference copper corrosion products and OE artefacts

Appendix C: photographs of OE artefacts

Appendix D: ATR-FTIR spectra of copper carboxylates

Appendix E: optical and electron microscopy images of copper carboxylates on copper

Appendix F: XRD spectra of copper carboxylates

List of abbreviations

EIS: Electrochemical impedance spectroscopy

FTIR: Fourier-transform infrared spectroscopy

LSV: Linear sweep voltammetry

OCP: Open circuit potential

SEM: Scanning electron microscope

SIMS: Secondary ions mass spectroscopy

SQWV: Square wave voltammetry

SR-XRD: Synchrotron X-ray diffraction

VMP: Voltammetry of microparticles

XAS: X-ray absorption spectroscopy

XEOL: X-ray excited optical luminescence

XRD: X-ray diffraction

XRF: X-ray fluorescence

XPS: X-ray photoelectron spectroscopy

1. Introduction

1.1 Objectives of the thesis

The aim of this work is to explore the use of electrochemical techniques for the study of corrosion and protection of the metallic cultural heritage. Among all the metals that have been used in history and can hence be studied, it was decided to focus the research on copper and its alloys, as copper was one of the first metals to be known and used by humans. Even today copper and its alloys are still used for electrical wires, roofing, plumbing and industrial machinery but also for the production of sculptures and jewellery.

This chapter will give a brief introduction to copper along with its history and will provide a description of the degradation phenomena arising in different corrosive environments. The chapter will be concluded by an overview of the applications of electrochemical techniques for the study of corrosion and protection of the metallic cultural heritage.

The research work of the thesis is divided into three parts. The first part (chapter 3), which follows a chapter on the methodology used in this work (chapter 2), investigates the corrosion rate of different copper-tin alloys in corrosive environments, including marine water and acid rain. The corrosion rate of the alloys has been measured by means of linear polarization experiments while analyses have been carried out using X-ray diffraction (XRD) and X-ray fluorescence (XRF) to identify the corrosion layers formed on the sample surfaces. The complementarity of electrochemistry and other analytical techniques is shown as necessary in order to describe the complexity of corrosion phenomena.

The second part (chapter 4) deals with the technique voltammetry of microparticles (VMP) and its application to the characterization of metals and the identification of copper corrosion products. Here reference metals, alloys and copper corrosion products were analysed to create a database containing the oxidation and reduction peaks to be used as reference. The VMP technique was then used for the characterization of historical bronze objects excavated in Flanders.

The last part of the research (chapters 5 and 6) is dedicated to the development of a protective coating for copper based on the use of carboxylic acids, successfully tested on lead and iron objects. The deposition of the coating was carried out by means of cyclic voltammetry (chapter 5) and by immersion in ethanolic solutions (chapter 6). The coatings have been studied by means of XRD and synchrotron radiation XRD, optical microscopy and electron microscopy. Linear polarization resistance was used to evaluate the inhibition efficiency of the coatings.

The major outcomes of the research are summarized in a conclusive chapter. Additional data, which are referred to in the text but have not been discussed in detail, are collected in the appendixes in the enclosed CD-ROM.

Copper and its alloys in history

This section presents copper and its alloys through a brief excursion into the use of the metal during history. The next section deals with corrosion phenomena, which are discussed in view of the preservation of heritage copper objects.

The Latin name for copper is *Cuprum* (hence the chemical symbol Cu) that derives from the words *aes cyprinum* or *cyprium*, meaning metal from Cyprus (*Cyprum*, in Latin) [1–3]. In the Roman period, in fact, the copper mines of Cyprus were well known for their richness and for the quality of the metal extracted so that the name of the island was used to be used to define the metal and its alloys [2-3].

The importance of this metal and its alloys in everyday life is clearly visible in the number of copper items that surround us: electrical wiring, pipes, but also cookware, musical instruments, roof plates and coins. Moreover, a large number of copper compounds are used as mineral pigments and colorants, but also as antibacterial agents [1,4].

Copper can be found in its native state in small quantities and this availability, together with its properties and appearance, made it one of the earliest metals to be used in ancient times [1–3]. The most ancient copper objects found in archaeological contexts are indeed made with native copper. Small items such as beads and pins have been found in Ali Kosh (western Iran) and Çayönü Tepesi (Anatolia, Turkey) in archaeological sites dating around the 9^{th}-7^{th} millennium BC [3]. In particular

some of the objects present signs of annealing, a process of heat-treatment that softens the metal hardened after cold working [2,3].

First traces of copper extraction from minerals date back to the 7th millennium BC in Anatolia and become more frequent in the Neolithic (6^{th}-5^{th} millennium BC) when mankind assists to the production of bigger and more sophisticated objects [2-3]. To the same period date also the first metallurgical evidences of copper smelting in Iran and Turkey. From this period on, the availability of copper objects increased exponentially, because of the possibility of smelting small fragments or broken objects [2].

Figure 1.1: Native copper nugget about 4 cm in size [5].

Copper is a metal characterized by a reddish-orange colour. It is an excellent thermal and electrical conductor and amongst its properties we can list the malleability (it can be hammered or pressed into a shape without breaking or cracking) and the ductility (the capability of being drawn out into a thin wire without cracking) [6]. When hammered, copper becomes harder, with the double effect of shaping the material and improving its mechanical properties [6,7].

Copper can be alloyed with other elements, zinc and tin among them, creating a large series of materials with different mechanical, physical and chemical properties usable for a wide range of applications [1–3,6]. The first example of copper alloying is arsenical copper (or arsenical bronze), an alloy with variable quantities of arsenic,

which appeared during the 3rd millennium BC [2,3]. It is likely that the earliest examples of arsenical copper were accidental, resulting from the extraction of copper from rocks containing copper and arsenic minerals, such as olivenite (Cu_2AsO_4OH), but there is no agreement on when the intentional production of the alloy actually started [2]. Moreover, there is a wide range of arsenic concentrations found in the objects, making the identification of intentional alloys difficult. Small amounts of arsenic in the alloy are sufficient to lower the melting temperature of the metal, to improve casting properties and workability and to increase hardness [7,8].

Copper-antimony alloys were also produced in the Early and Middle Bronze Age (3300-1800 BC), even though antimony rich ores were not as common as those rich in arsenic. They were mainly located in central Europe [3]. The presence of antimony in the alloy produces the same hardening effect of arsenic [3].

Bronze, strictly copper-tin alloys, appeared at the beginning of the 3rd millennium BC in Mesopotamia (current Iraq and Iran) and their abundant use during that time gave the name to the period, called the Bronze Age [2-3]. During the Bronze Age the production increased exponentially. The manufacture of bronze was characterized by finer details and more attention to the casting process [2]. After these alloys became wide-spread, the use of pure copper became limited to particular applications, such as small jewellery and coining [1,2].

Whether or not the addition of tin was done intentionally in the first phases of the bronze production is still debated even today. While arsenic (and antimony) deposits were sometimes associated with copper ores, only few copper ores containing tin contamination have been documented [3]. Considering the rarity of the tin deposits, the distribution of copper-tin alloys began only when various civilizations began trading over considerable distances, around the beginning of the 3rd millennium BC [2-3].

Similar to the addition of arsenic, copper-tin alloys have a lower melting point than pure copper. The casting is therefore more fluid and the mechanical strength is increased [3,7]. The simplest process for the fabrication of bronze is to melt in the same crucible metallic copper and metallic tin. An alternative is to use metallic copper and mineral cassiterite (SnO) and melt them in a reducing atmosphere (under coal for example). Tin melts at 232°C and starts to diffuse into the copper

matrix, lowering its melting point to around 950°C while the melting point of pure copper is 1084°C and hence more difficult to achieve with primitive furnaces [3,6,7].

Figure 2 [3] illustrates the increase in hardness of copper, copper-arsenic and copper-tin alloys when cold worked, as in the case of plastic deformation to shape an object (i.e. hammering to obtain metal sheets) [7].

The graph shows the increase in hardness (expressed in terms of the Vickers hardness) as a function of the plastic deformation (in this case the thickness reduction to obtain metal sheets) for copper, As-bronze and Sn-bronze. The addition of 8 % of arsenic or tin to the copper produces the same increase in hardness.

The uses of bronze have ranged from weapons, to vessels, religious items, ornaments, statuary and also tools for daily activities. The applications depend in particular on the percentage of tin contained in the alloy. A small amount of tin in the alloy does not affect the alloy properties. Changes are visible from few percentage points [2-3,6,7].

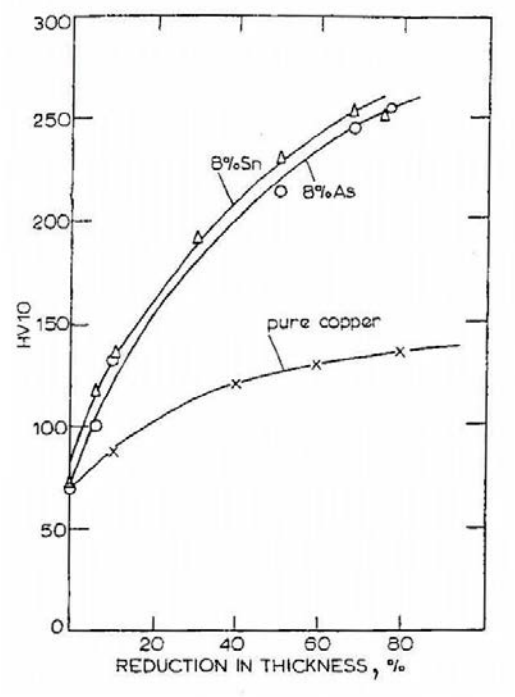

Figure 1.2: Increase of the hardness of copper during cold working as a function of the thickness reduction of the metal piece. The addition of tin or arsenic increases the hardness of the alloy ([3], © Maney Publishing).

A notable increase in hardness is already visible with 8 % of tin. Tin percentages between 6 and 12 produce an alloy with good mechanical properties such as hardness and fluid casting, good cold-workability. More than 13 % of tin accentuates the hardness and the alloy becomes brittle and not easily cold-workable [2-3,7].

Percentages between 20 and 30 % of tin make a bronze that is characterized by a particular sonority and a silvery colour. This is the preferred material for the realization of bells. High percentages of tin are also found in mirrors. The alloy cannot be worked anymore cold, but it can be polished until a mirror-like surface. Higher percentages of tin are not found in historical artefacts, due to the difficulty in casting [6-7]. A more detailed description of copper-tin alloys properties, together with the phase diagram, will be given in chapter 3.

In general bronze objects also contain other elements, contained as impurities in the original materials (such as nickel and iron), or added intentionally, such as in the case of lead. Small percentages of lead (less than 4 %) improve the workability and increase the fluidity of the casting [7].

The presence of zinc, which gives a gold-like colour to the alloy, is also found in bronze artefacts. The production of quaternary bronze, containing copper, tin, lead and zinc started towards the end of the Iron Age (2nd century BC) and it became common during the Roman period [2].

The alloy containing just copper and zinc is called brass and its first applications were quite limited due to the large popularity of bronze [2-3]. Brass became popular only when the technique called cementation was introduced (from the 2nd century BC) [3].

Cementation is a process that allows the production of brass from zinc minerals. It is not possible to obtain brass from metallic zinc because it melts at 419 °C and evaporates at 917 °C [1,7]. Zinc minerals, such as zincite (ZnO), smithsonite ($ZnCO_3$) and hemimorphite ($Zn_4Si_2O_7(OH)_2 \cdot H_2O$), finely grounded were put in a closed crucible with copper and coal. The temperature of the crucible was then kept around 950 °C so that the reduced zinc evaporated, thereby generating vapours that diffuse in the metallic copper. The alloying of zinc lowers the melting point of copper to a minimum around 1000 °C, a point at which the maximum content of Zn

is 30 %, as can be deduced from the Cu-Zn phase diagram presented in Figure 1.3 [6,7].

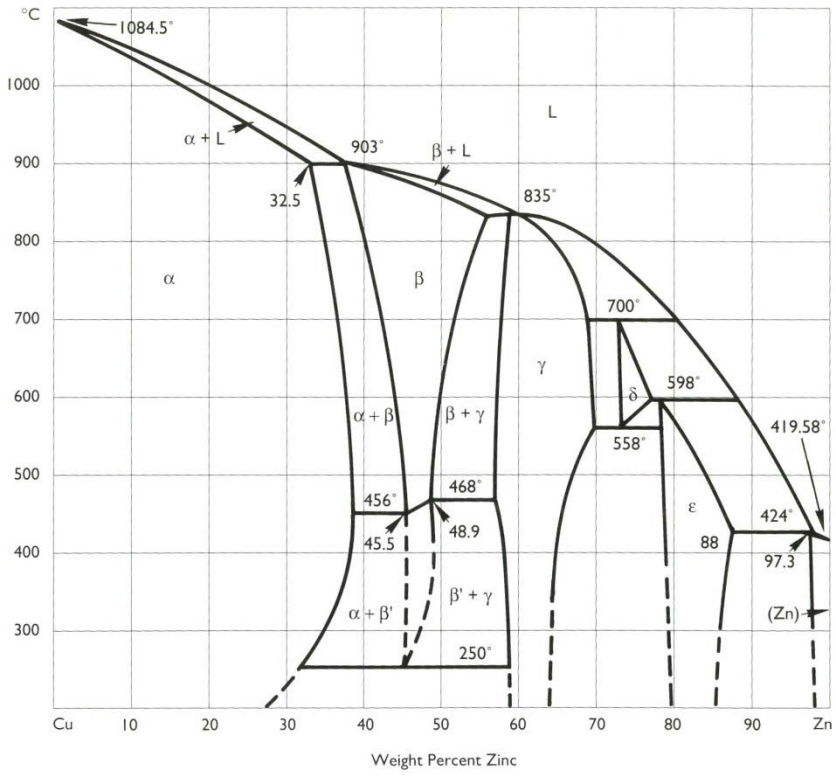

Figure 1.3: Phase diagram of Cu-Zn ([7], © The Getty Conservation Insitute).

Ancient brasses contain usually 10-25 % of zinc and the alloy is characterized by a yellow colour. It is cold or hot workable. In antiquity it was described as a material particularly precious (called orichalcum) for its colour resembling gold and for the difficulty of production. Alloys with 4 % of zinc were also produced and were particularly used for coinage [1–3,8].

With the collapse of Roman empire, and the lack of tin supply from other regions of the empire, brass became more common [2-3], until the Middle Ages when brass and quaternary alloys were also used for liturgical objects, doors of cathedrals and many other objects used in daily life [2-3].

The repetitive annealing and remelting of brass in order to recycle pieces of alloy can cause a loss of zinc because of its low boiling temperature (as visible in Figure 1.3). This reflects in changes of the casting properties. It is quite common to find

lead and zinc and no tin in late brasses. The addition of small quantities of lead increases the fluidity of the casting compensating the loss of zinc [2,3].
Apart from the composition of the alloy and the types of phases present in the system, it must be emphasized that the workability of metals and alloys is also influenced by the shape and the dimension of the grains. The presence of small and elongated grains, in fact, increases the hardness of the metal [7,9].

1.2 Corrosion

Corrosion can be defined as the natural degradation of the metal. Metals occur in nature for the larger part in the form of minerals and the reduction to their metallic state requires energy. The metallic state is therefore thermodynamically unstable and they naturally tend to a lower energy state, the one of minerals [10,11]. Corrosion is an electrochemical process that involves the exchange of ions. Two types of corrosion can be distinguished: wet and dry corrosion. In the case of wet corrosion, , the surface is in contact with water in different forms (water, steam or condensation from humid air on the surface). Wet corrosion is the most important because is creating more damage, since the kinetic of the reactions is faster in presence of water. Damp soils may also be considered as electrolytes because of the high humidity. On the surface there are two electrochemical reactions: an anodic reaction in which the metal is oxidized and loses electrons, and a cathodic reaction, in which a chemical species present in the environment is reduced accepting the electrons of the metal [10,12].
In the case of dry corrosion, the kinetics of the formation of corrosion products (such as oxidation layers) on the surface are more complex, but since they involve the exchange of ions also the dry corrosion is related to an electrochemical mechanism [1,6].
A typical corrosion cell is presented in Figure 1.4. The electrochemical reaction that leads to the formation of corrosion products can be divided into two half-reactions: anodic and cathodic. The anodic half-reaction describes the oxidation of the metal:

$$M\ (s) \rightarrow M^{+} + e^{-} \tag{1.1}$$

Here the electrons produced are released in the metallic phase, while the ions generated by the oxidation are released in the solution or they react with other species to form insoluble compounds, thereby forming a deposit of corrosion products.

In the cathodic process the electrons released at the anodic site reduce chemical species present in the environment. The principal cathodic half-reaction describes the reduction of oxygen in alkaline or neutral environment:

$$½\ O_2 + H_2O\ +\ 2e^- \rightarrow\ 2\ OH^- \tag{1.2}$$

However, it may also involve the reduction of other species than oxygen. As an example, in acidic solutions the cathodic reaction involves the reduction of hydrogen [6,12-13]:

$$2\ H^+ + 2\ e^- \rightarrow\ H_2(g) \tag{1.3}$$

The electrons produced and the electrons used are in equal number, so that the two half-reactions are balanced in equilibrium conditions. Because of the movements of the electrons in the material, a current flows in the metal, by convention from the cathodic to the anodic region. Ions also migrate, generating a current flow from anodic to cathodic region and closing the circuit. The magnitude of this current is an indication of the corrosion rate of a metal in a given environment [8,10,14].

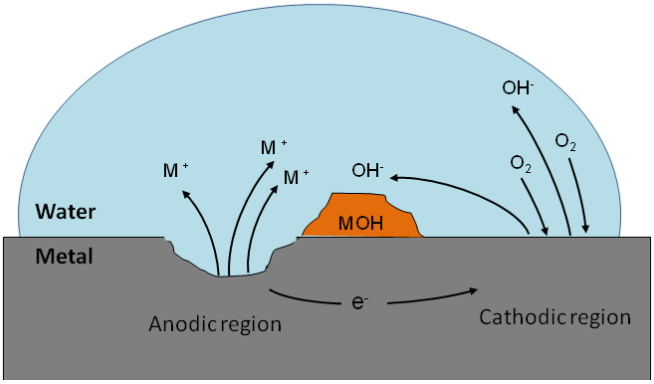

Figure 1.4: Schematic representation of a corrosion cell.

Metals are classified according to their susceptibility to oxidation. Their redox potential is the parameter used for the classification. In the electrochemical series, elements are listed in descending order according to their redox potential. At the highest point stand metals which are difficult to oxidize and are therefore defined as noble metals [8,10,14]. The durability of copper is related to its high redox potential [6].

1.2.1 Forms of corrosion

Corrosion can develop on a surface in a uniform or localized way. One can then distinguish between general corrosion and localized corrosion [1,8,10,15].

In the case of general corrosion, the most common form of corrosion,. the process is is distributed over the entire surface exposed without any appreciable localization of the attack.

Localized corrosion, on the other hand, occurs only on specific parts of the surface and may be due to surface heterogeneity. Forms of localized corrosion [11,16] (schematically presented in Figure 1.5 [16]) can be:

Galvanic corrosion, which occurs when two different metals are in contact. The metal with the lower redox potential becomes the anode and the metal with the higher potential becomes the cathode.

Crevice corrosion, which is an intense and localized form of corrosion and is usually associated with small amounts of water stagnant in the crevices, holes and joints.

Pitting corrosion, which occurs in small areas on the surface and develops in a vertical direction. This corrosion can be due to a failure in the protective film or to a local inhomogeneity. It is one of the most dangerous forms of corrosion since it can damage the metal in depth without obvious metal loss or visual changes as the pits are often covered with corrosion products.

Intergranular corrosion, which is a localized attack at the grain boundaries with a relatively slow corrosion of the grains. As a result, the alloy disintegrates. It can be caused by impurities at the grain boundaries, enrichment of one of the alloying elements, or depletion of one of these elements in the grain-boundary areas.

Selective leaching, which is the removal of one element from a solid alloy by corrosion processes. The most common example is the selective removal of zinc in brass alloys (dezincification).

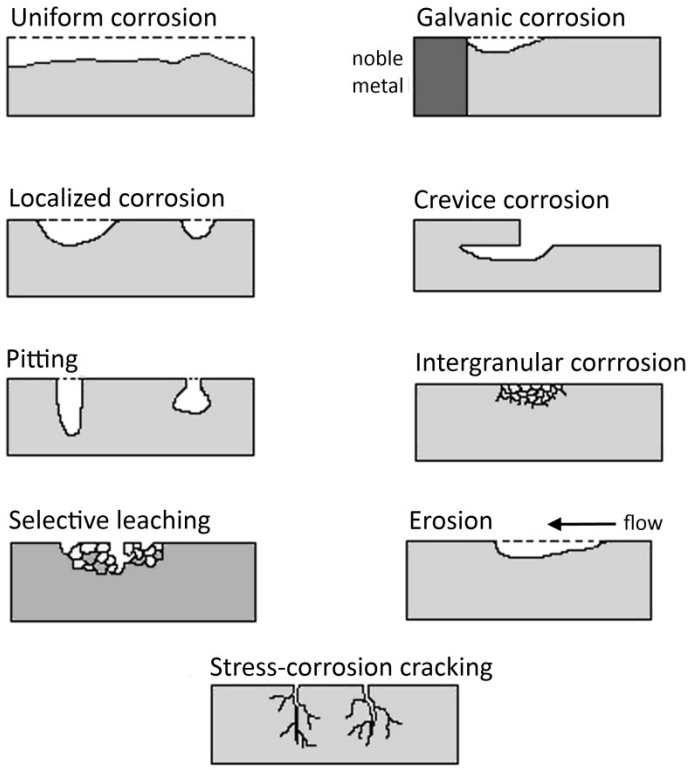

Figure 1.5: Different forms of corrosion (drawing based on information in [16]).

Erosion corrosion, which is the acceleration in the corrosion rate of a metal due to mechanical wear and abrasion by the movement of a corrosive fluid on the metal surface. The metal is removed as dissolved ions, or it forms solid corrosion products that are mechanically swept from the metal surface.

Stress-corrosion cracking, which is caused by the simultaneous presence of tensile stress and a corrosive medium.

The surface of a metal exposed to the environment will alter according to the type of environment (see also section 1.3.3). The latter can be considered as a combination of factors such as humidity, chemical composition, temperature and many other parameters.

There are three types of behaviour of a metal in contact with an aggressive environment: immune, active and passive. In the first case, the metal does not react with the environment and there is no corrosion. This is the case for noble metals, such as gold or platinum that remain stable in most of the natural environments.
A metal in a passive state reacts with the surrounding environment and the corrosion products form on the surface a protective film (called passivation layer) that slows down the corrosion process. The characteristics of the passivation layer (adhesion, thickness, solubility) influence its protective properties. This is the case of the film of copper (I) oxide formed on copper surfaces exposed to air.
A metal in an active state, on the other hand, reacts with the surrounding environment. The corrosion products formed are soluble. There is no formation of a passivation layer, but a deposit through which the exchange of ions is not slowed down. Because of the properties of the corrosion layer, the metallic surface is continuously exposed to the environment and the corrosion proceeds actively. Active corrosion is characterized by a significant weight loss from the metal, until the metallic core is completely destroyed. An example of active corrosion occurs when iron is exposed to marine water.
The corrosion behaviour of a metal in an aqueous solution can be predicted using the appropriate Pourbaix diagrams [17]. These diagrams plot the electrode potential versus the pH, under the conditions of a fixed pressure and temperature, and allow the determination of pH and potential interval that characterize conditions of immunity, passivity or active corrosion.

1.2.2 Corrosion mechanisms in copper and copper alloys

When it comes to the terminology of corrosion products, this text uses in accordance with literature two different terms: patina and corrosion layer. A patina generally indicates a smooth, continuous and homogeneous layer of corrosion products on the metal surface. The patina usually preserves most of the details and the shape of the object. The term corrosion layer is used to describe deposits of copper minerals which do not present continuity and make the reading of the surface detail difficult. Accretions may also be present on the external layer and they can be defined as a

mixture of other minerals and fragments of other materials (such as small pieces of wood, stones or even shells) adherent to the patina or the corrosion layer [1].

1.2.2.1 The influence of alloying elements

In the previous sections the effect of the properties of the environment upon the degradation of a metal was described, but the corrosion behaviour of a metal is also correlated with the composition of the alloy [7]. The result of the corrosion process on an alloy is often a de-alloying effect, leading to the dissolution or removal of one of the components of the alloy, such as de-stannification, in the case of the selective removal of tin.

In bronze (copper-tin) alloys the mechanism suggested by Robbiola [18] presents the existence of two types of structures.
Type-I structures, commonly found in low corrosion environments, are characterized by a de-cuprification of the surface (the selective removal of copper), leaving the outer layer tin-enriched, and thereby preserving the details of the original surface underneath. The exterior appearance shows a uniform corrosion layer consisting of a tin oxide layer which passivates the surface inhibiting further copper oxidation and dissolution. The mechanism of de-cuprification can be explained by the selective oxidation of tin, which is less noble in respect to copper. An outer layer made of copper corrosion products may be present beyond the tin-enriched surface. In some cases, inter- and trans-granular granular corrosion have been observed in objects showing a type-I structure.
Type-II structures occur in aggressive environments, often in the presence of chloride ions. A layered structure is observable, with the formation of cuprous oxide and a high chloride content on the metallic interface. Large amounts of chloride ions in contact with the alloy give rise to a selective and progressive dissolution of copper with respect to tin or the other elements of the alloy. The structure consists of several layers characterized by an inner layer rich in tin, a middle layer, mainly composed of cuprite and an external layer of copper (II) compounds. Chlorides ions are typically present at the interface between the inner and the middle layer. Pits

and cracks are frequently observed. A type-II structure is found in case of bronze disease (see 1.3.3.1).
In the case of brasses the selective dissolution of one of the two components of the alloy can be observed (e.g. decuprification and dezincification, when the zinc is removed).
Lead is a common constituent of copper alloys but it is segregated in globules as a separated phase because the two metals are not mutually soluble at room temperature. Galvanic corrosion is a typical phenomenon in copper-lead alloys: the less noble metal (lead) will act as an anodic region and will be oxidized first. These areas rich in corrosion products are weak points in the alloy, leading to the formation of internal cracks and fractures [19].

1.2.3 Corrosive environments

This section describes the corrosive environments together with the corrosion products encountered, which are typical for copper and bronze corrosion. They include burial environments, including corrosion in water and soils, indoor environments and outdoor environments, which comprise corrosion phenomena in urban and rural area, and the effects of acid rain and salt spray. It must also be kept in mind that a single object may be exposed to different environments during its lifetime, giving rise to the formation of a complex group of minerals on the surface [1].

1.2.3.1 Burial environment

Burial is the most frequent corrosion condition for copper alloys. Here, the soil characteristics are responsible for the development of the corrosion layers on the artefact. The definition of parameters for the classification of soils on the basis of their corrosion behaviour is still far from being complete [1]. The main parameters used, however, include the level of drainage, the resistivity, pH and the water composition.
A model of corrosion of copper is presented in Figure 1.6 [1]. The left image presents a typical cross section of a corroded copper object. An inner layer (b), in contact with

the metal core (a), is composed mainly of copper(I) oxide, a mineral called cuprite (b). Usually the cuprite layer is covered by a second layer (c), which is mainly constituted of copper (II) salts. In the case of copper-tin alloys, this scheme can be related to the type-I structure described by Robbiola [18] (see paragraph 1.3.2.1), where the metallic surface is preserved by an inner layer which is enriched in tin. The composition of the outer layer is influenced by the composition of the soil, but in general the most encountered minerals on buried copper objects include copper carbonates such as malachite ($Cu_2CO_3(OH)_2$) and azurite ($Cu_3(CO_3)_2(OH)_2$). The formation of copper basic carbonates is caused by the presence of high levels of carbonate ions in the soil and groundwater. Azurite is rarely found alone, but occurs frequently as crystal aggregates in malachite. It is less stable and in the presence of a high humidity it can be converted to malachite according to the reaction 1.4 [1,6]:

$$2\ Cu_3\left(CO_3\right)_2\left(OH\right)_2 + H_2O \rightarrow 3\ Cu_2CO_3\left(OH\right)_2 + CO_2 \qquad (1.4)$$

On the outer part an encrustation may adhere to the surface forming a further layer on the object (d). It can include materials such as clay, wood and charcoal, which are present in the environment,.

A patina composed of carbonates is usually stable and protective and the metal core is usually preserved. In particular conditions, such as extremely damps soils or sites which are characterized by a high organic content [1,20], pitting phenomena may occur giving rise to a more intense corrosion activity, while soils with a low content in oxygen and low humidity are considered as less aggressive towards metal objects [20,21]. In the last decades attention has been focused on archaeological sites situated in the proximity of agricultural areas. Here increased acid levels have been encountered in soils where organic fertilizers have been used, leading to a higher aggressiveness of the soil towards metal objects [21–23].

The image on the right side of Figure 1.6 presents the cross section of a copper object corroded in the presence of chloride ions (a scheme comparable with the type-II structure mentioned earlier in paragraph 1.3.2.1). The formation of nantokite (copper(I) chloride), promoted by high chloride ion concentrations, acidity and low

oxygen conditions, occurs at the interface between the cuprite layer and the external layer or within the layer of copper (II) compounds (e). Nantokite is very unstable in presence of humidity and causes corrosion phenomena that are classified under the name of bronze disease.

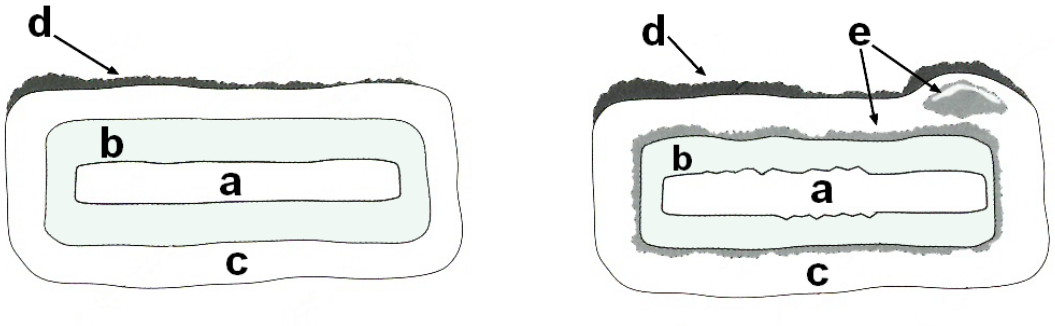

Figure 1.6: The figure on the left shows a schematic structure of a corroded copper object. The right image shows the same object corroded in an environment particularly rich in chlorides (modified from [1], © The Getty Conservation Insitute).

The term bronze disease describes a progressive deterioration of copper and bronze caused by the presence of nantokite (CuCl) in contact with the metal surface. It appears as light green powdery eruptions upon the surface of copper based materials. In the presence of moisture and oxygen, nantokite reacts to form a copper hydroxychloride as is shown in the reaction below (1.3).

$$4\ CuCl\ +\ 4\ H_2O\ +\ O_2 \rightarrow\ 2\ Cu_2\left(OH\right)_3 Cl\ +\ 2\ HCl \qquad (1.5)$$

The copper hydroxychlorides are larger in volume and introduce physical stress within the object, leading to cracking and fragmentation phenomena on the surface [1,6,24,25]. Bronze disease is a particularly dangerous form of corrosion because is often localized in pits that deepen the corrosion locally. The hydrochloric acid produced in the reaction promotes the progressive corrosion of the metal to form CuCl, followed by copper hydroxychlorides. This process can lead to the complete destruction of the metal.

Inclusions of nantokite may also be found underneath a cuprite layer, implying serious conservation problems for the objects. The humidity of the environment plays a fundamental role in the conversion to copper hydroxychlorides.

In a burial environment we can also consider marine water including archaeological sites situated underwater, as is the case of shipwrecks. The exact composition of the seawater varies depending on the location, but generally contains chlorides, sulphates, carbonates, magnesium, sodium and potassium ions. The low levels of oxygen and carbon dioxide dissolved determine the type of corrosion: aerobic or anaerobic, which, in its turn, influences the type of corrosion products present on the object [1].

In an aerobic marine environment, corrosion is promoted by the presence of oxygen. Oxygen rich water is considered as aggressive since the oxygen reduction reaction is not limited by the amount of the reactant. The corrosion rate may also be influenced by the wave motion of the water, causing erosion corrosion phenomena, which are enhanced by the presence of abrasive materials such as sand or particulates. Also copper and bronze objects recovered from marine environments present a layered structure, showing an inner layer of cuprite covered by a thicker layer of copper(II) compounds, typically copper hydroxychlorides. The presence of nantokite is also frequent at the interface between copper oxide and copper hydroxychlorides [1,26,27].

In anaerobic conditions, on the other hand, corrosion is promoted by the presence of microorganisms and, in particular, by sulphate-reducing bacteria that grow under these conditions. These organisms produce elevated amount of sulphide ions, which lower the pH of the water and attack the metal surface. The main mineral formed in the corrosion layer is chalcocite (Cu_2S). Marine life, rotting timbers, coral and other factors also contribute to the formation of a thick encrustation on the surface of the objects, despite the biocide activity of copper [1,26–28].

1.2.3.2 Outdoor environment

The development of corrosion layers on copper objects exposed to the outdoors depends on many factors, including the presence of gaseous pollutants, particulate matter, rain, wind, and their proximity to industrial or marine areas. Until the 19th century, atmospheric corrosion of copper alloys was limited to the formation of an inner layer of cuprite and an eventual external layer of carbonates, mainly

malachite, promoted by the presence of humidity in the air. With the industrial revolution, mankind caused dramatic changes in the chemical composition of the atmosphere with an increase in gaseous and particulate pollutants produced by industrial and combustion processes resulting in a more aggressive environment for exposed metals [1,6,29-30].

Among the most dangerous gaseous pollutants one can list sulfur dioxide (SO_2). This gas minimally attacks the metal surface, but it is easily oxidised to SO_3, which reacts with the humidity present in the atmosphere thereby forming sulfuric acid, one major components of the so-called acid rain [1].

$$2\,SO_2 + O_2 \rightarrow 2\,SO_3 \tag{1.6}$$

$$SO_3 + H_2O \rightarrow H_2SO_4 \tag{1.7}$$

In the presence of humidity, sulfuric acid reacts with the copper oxide layer to form copper sulphates, such as brochantite (reaction 1.6) and antlerite (reaction 1.7).

$$2\,Cu_2O + H_2SO_4 + O_2 + 2\,H_2O \rightarrow Cu_4(OH)_6\,SO_4 \tag{1.8}$$

$$6\,Cu_2O + 4\,H_2SO_4 + 3\,O_2 + 4\,H_2O \rightarrow 4\,Cu_3(OH)_4\,SO_4 \tag{1.9}$$

Brochantite ($Cu_4(OH)_6SO_4$) and antlerite ($Cu_3(OH)_4SO_4$) are insoluble in water and form a uniform green patina on the copper and the bronze surfaces. Brochantite is a very stable compound and is the most common copper sulphate present on copper exposed to urban atmosphere. Antlerite is soft and brittle and thus less frequently encountered in corrosion layers on outdoor copper alloys. Posnjakite ($Cu_4(OH)_6SO_4 \cdot H_2O$), less common, is characterized by a blue colour and is considered as a precursor to the formation of brochantite. The occurrence of hydrated copper sulphates on outdoor bronzes is related to the presence of active corrosion [1,6,31–34].

Among other gases present in the atmosphere we can list nitrogen oxides (NO_x). Through oxidation and reaction with water they can form nitrous (reaction 1.8) and nitric acid (reaction 1.9).

$$2\ NO\ + H_2O\ +\ ½\ O_2 \rightarrow\ 2\ HNO_2 \quad (1.10)$$

$$2\ NO_2 + H_2O\ +\ ½\ O_2 \rightarrow\ 2\ HNO_3 \quad (1.11)$$

Nitrous and nitric acids promote the formation of copper nitrates on copper surfaces, but they are rarely found in corrosion layers because they are highly soluble in water and are washed off by the rain.

Chloride ions are also present in atmospheres contaminated by industrial processes and marine aerosols in coastal areas [1]. On outdoor bronzes, chloride ions react with copper and cuprite to form CuCl. Nantokite is very unstable and easily oxidizes to $CuCl_2$, a very hydrophilic molecule. The most common copper hydroxychlorides are atacamite and paratacamite, which give the typical blue-green colour to copper, together with the copper sulphates. Botallackite is also formed on the surface, but it is a metastable product and recrystallizes to atacamite, clinoatacamite or paratacamite [1,35]. There is still discussion on the actual name and formula of paratacamite [1]. It is now accepted that the mineral with monoclinic crystalline structure and formula $Cu_2(OH)Cl_3$ has to be called clinoatacamite, and not paratacamite, which has rhombohedral symmetry and contains zinc atoms [36]. In this work, nevertheless we will still use the term paratacamite to define the monoclinic structure since the International Center for Diffraction Data (ICDD) database (ICDD PDF2) has not been updated yet in this regard and uses the name paratacamite (card number 01-086-1391) for classifying the monoclinic compound [37].

Copper sulphates and copper hydroxychlorides are thus the most common copper corrosion products present on outdoor bronzes. Copper basic carbonates such as malachite and azurite are also present in outdoor corrosion layers as minor components since they tend to recrystallize in sulphates or chlorides under the action of strong acids (H_2SO_4 and HCl).

Outdoor corrosion layers may also contain a variety of copper organometallic compounds, such as copper oxalates. These products, usually present in very small quantities (less than 1% in weight), act as a binder forming a cohesive corrosion layer. The characterization of these compounds is rather difficult because of their small amount and the complexity of the corrosion layer stratigraphy [1,31–34].

1.2.3.3 Indoor environment

The lower humidity range that occurs in indoor spaces, such as museums and storage rooms, ensures that the corrosion rate of bronze and copper objects is smaller in comparison to outdoor environments. Nevertheless the gaseous pollutants present in this environment are the same as those in the outdoor atmosphere, among them NO_x, SO_2, H_2S, which can react with the metallic surface to form sulphates, chlorides and nitrates. Volatile organic compounds (VOCs), such as formaldehyde and benzene, can also be present [1]. The origin of gaseous pollutants is in part from the outdoor environment, but a consistent amount of pollutants, such as organic acids and H_2S are produced by the display or storage cases, furnishings, paints and other materials present in the room [1,20,38]. Wooden display cases, in particular, easily emit organic acids and aldehydes that can seriously damage the metal surface.

Table 1-I : Most common corrosion products found on historical copper objects [1,39].

Mineral	Formula	Colour	Crystal system
Cuprite	Cu_2O	From cochineal-red to dark red or almost black	Cubic
Tenorite	CuO	Dark grey or black	Monoclinic
Malachite	$Cu_2(OH)_2CO_3$	Bright green, dark green	Monoclinic
Azurite	$Cu_3(OH)_2(CO_3)_2$	Very dark to pale blue	Monoclinic
Brochantite	$Cu_4SO_4(OH)_6$	Emerald-green, blackish green, pale green	Monoclinic
Posnjakite	$Cu_4SO_4(OH)_6 \cdot H_2O$	Light to dark blue	Monoclinic
Antlerite	$Cu_3SO_4(OH)_4$	Emerald-green, blackish green, pale green	Orthorhombic
Atacamite	$Cu_2Cl(OH)_3$	Bright green, dark emerald-green to blackish green	Orthorhombic
Paratacamite	$Cu_2Cl(OH)_3$	Green to dark green, greenish black	Monoclinic
Botallackite	$Cu_2Cl(OH)_3$	Dark-green, bluish green to green	Monoclinic
Nantokite	CuCl	Colourless, white; greyish to greenish	Cubic
Chalcocite	Cu_2S	Blackish lead-grey	Monoclinic

The presence of hydrogen sulphide, even if in small concentration, produces a darkening of the copper and bronze surfaces resulting from the formation of a thin layer of copper sulphide (chalcocite, CuS) known as tarnish [1,31]. Eventual visitors can also introduce skin particles, fibres and dust. The main problem of the presence of this particulate matter is connected to their deposition on the surfaces. The particles are able to retain humidity, increasing locally the amount of water and accelerating the localized corrosion rate.

Bronze disease is also one of the major problems encountered in indoor environment. Cases of post excavation corrosion are also possible. The humidity levels in museums and storage depot, in fact, are too high (above 45 % RH) and they cannot prevent the conversion of nantokite to copper hydroxychlorides [1].

Table 1.I provides an overview of the most common copper corrosion products on copper and its alloys.

1.3 Electrochemistry and cultural heritage

Electrochemical techniques have been developed and applied to the cultural heritage field since the end of the 19th century with the first works on the corrosion of metals and copper in particular [40–42]. The main objective was the characterization of the corrosion layers on bronze objects, with a particular attention to the presence of copper chlorides and the development of bronze disease [42]. Among the first techniques applied is electrolysis, which has been widely used for stabilizing and cleaning archaeological artefacts and even today it is still applied in restoration laboratories [20,43–45].

Nevertheless, in the last decades the application of electrochemical techniques to conservation science has undergone a large development. A multidisciplinary approach involving conservators and scientists has led to a broadening of the field and an improvement of the treatments and materials used in conservation procedures [45]. The value of electrochemistry for the study of heritage objects has been highlighted during the workshop *Electrochemistry in historical and archaeological*

conservation, held in Leiden (the Netherlands, 11-15 January 2010) [46]. In this event the wide range of possible applications has been summarized in four themes:

Analysis: identification and characterization of the material

Testing and monitoring

Electrolytic cleaning and stabilization of artefacts

Protection

1.3.1 Analysis: identification and characterization of the material

The identification of metals and the characterization of alloys can be done with many analytical techniques, including scanning electron microscopy coupled with energy-dispersive X-ray spectroscopy (SEM-EDS), X-ray fluorescence spectroscopy, secondary ion mass spectrometry (SIMS), X-ray photoelectron spectroscopy (XPS) as the most common ones [47–51]. The use of electrochemistry for this purpose was in the past limited by the need to immerse the object in the electrolyte in order to use it as an electrode. The development of the technique called voltammetry of microparticles (VMP) overcame to this problem. VMP, introduced by Fritz Scholz in 1976, is a powerful tool for the analyses of solid particles by using a supporting electrode [52–54]. This method can be successfully applied in the conservation field since it gathers characteristics required when working with heritage materials, such as non-invasiveness and sensitivity and versatility. In fact VMP can be used for the identification of metals and alloy components, but also for the identification of corrosion products even in complex systems such as archaeological corrosion layers. The technique can provide qualitative and quantitative information on the composition of solid solutions [45,55,56].

1.3.2 Testing and monitoring

This theme includes all studies related to the development and the application of electrochemical techniques for the understanding and the monitoring of the electrochemical processes which occur on heritage metallic artefacts.

Like the identification of metals, the study of corroded layers on artefacts usually involves the use of a wide range of analytical techniques (see 1.4.2) [47,57–71]. From

the perspective of a multidisciplinary approach, electrochemistry appears to be complementary to these techniques, while it can be considered the preferred method for the investigation of corrosion processes and their inhibition. The study of corrosion mechanisms is obviously not limited to the field of cultural heritage, but touches a variety of research fields because of the widespread use of metals in daily life. Understanding the degradation processes is fundamental to the development of efficient strategies against corrosion.

Considering the limited use of pure copper for the production of historical artefacts [1–3,6], most of the literature investigates the corrosion processes of copper alloys. Brasses and bronzes are tested in different aggressive environments, e.g. rich in chlorides [18,72–84]. Atmospheric corrosion of copper and its alloys has also been studied in order to predict the durability of copper objects exposed to urban environment [26,29–31,85–87]. For the characterization of the formation of corroded layers and their properties artificially corroded samples are often used in order to simulate the behaviour of real artefacts and determine the correct parameters for eventual electrochemical treatments [68,88–91].

1.3.3 Electrolytic cleaning and stabilization of artefacts

Electrolytic cleaning has been used for more than a century. Together with mechanical and chemical cleaning, it is still commonly used in restoration laboratories for the removal of concretion on archaeological pieces. In maritime archaeology, in fact, it is one the most versatile techniques for conserving metal artefacts recovered from the sea [27,92–94].

The treatment of metallic artefacts ideally tends to reverse the corrosion process that modified the original aspect of the objects. In the case of electrolytic cleaning the object is immersed in an electrolyte and connected to a power supply [20,27,92,95]. The reduction at the cathode (the artefact) produces hydrogen bubbles that can mechanically remove the crust or promote its removal. The crust can also react to form other compounds, more easily removable [92,95].

The stabilization and storage of metallic artefacts may also be supported by electrochemistry: a weak polarization of the object can be used to selectively reduce

corrosion products and remove aggressive species (such as chlorides) or to prevent further corrosion of the metal [44,93,96,97].

Despite the efficacy of these methods, there are some inconveniences connected with the difficulty of immersing objects of large dimensions or composite artefacts, in which the presence of wood, textile and leather makes the treatment by immersion impossible.

To overcome these difficulties, one can use a gel, prepared with the chosen electrolyte and a supporting agent (such as agar, a polysaccharide gum) to be applied in selected areas of the object. Localized treatments can also be done by using small electrolytic cells adapted to the area or by using electrolytic pencils, characterized by a small probe (similar to a pencil) able to treat very small areas [98].

1.3.4 Protection

The inhibition of corrosion processes is also a common trend in the metal conservation field and electrochemical tests have been presented as new techniques and very valuable tools for research on the protectiveness of coatings and films applied to metal objects and artefacts. There are different approaches to protect metals: among them, the storage of metals under a controlled potential or current [44], or the isolation of the metallic surface from the surroundings through the application of a protective layer often containing a corrosion inhibitor [74,99–104]. The evaluation of the effectiveness of an inhibitor or a protective coating is easily performed by means of electrochemical techniques such as linear polarization [103–106] or electrochemical impedance spectroscopy (EIS) [29,106,107]. The need for intervention on immovable objects, such as bronze monuments and big sculptures, urged the development of small electrochemical cells and set-ups able to perform in-situ measurements.

References

[1] D.A. Scott, Copper and Bronze in Art – Corrosion, Colorants, Conservation, Getty Publications, Los Angeles, 2002.

[2] C. Giardino, I Metalli nel Mondo Antico. Introduzione all'Archeometallurgia, Editori Laterza, Roma, 2002.

[3] R.F. Tylecote, A History of Metallurgy, Institute of Materials, London, 2002.

[4] D.A. Scott, A review of copper chlorides and related salts in bronze corrosion and as painting pigments, Studies in Conservation, 45 (2000) 39–53.

[5] http://commons.wikimedia.org/wiki/File:Native_Copper_Macro_Digon3.jpeg, copyright Jonathan Zander (accessed 2/07/2013).

[6] L. Selwyn, Metals and Corrosion. A Handbook for the Conservation Professional, Canadian conservation institute, Ottawa, 2004.

[7] D.A. Scott, Metallography and Microstructure of Ancient and Historic Metals, Getty Conservation Institute, Marina del Rey, 1991.

[8] W. O'Brien, Arsenical copper in early Irish metallurgy, in: S.M.M. Young, A.M. Pollard, P. Budd, R.A. Ixer (Eds.), Metals in Antiquity, Archeopress, Oxford, 1999: pp. 33–42.

[9] L. Delannay, M.R. Barnett, Modelling the combined effect of grain size and grain shape on plastic anisotropy of metals, International Journal of Plasticity, 32-33 (2012) 70–84.

[10] E. D. Verink, Corrosion Testing Made Easy, vol. 3. The Basics, NACE, Houston, TX, 1994.

[11] J.R. Davis, Corrosion: Understanding the Basics, ASM International, Materials Park, OH, 2000.

[12] G.S. Haynes, R. Baboian, eds., Laboratory Corrosion Tests and Standards, ASTM, Philadelphia, 1985.

[13] J.W. Evans, S. Kim, Elements of corrosion, in: J.W. Evans, J.Y. Evans (Eds.), Product Integrity and Reliability in Design, Springer-Verlag, London, 2001: pp. 178–203.

[14] W.F. Hosford, Materials for Engineers, Cambridge University Press, Cambridge, 2008.

[15] H. H. Uhlig, Corrosion and Corrosion Control. An Introduction to Corrosion Science and Engineering, 2nd ed., J. Wiley & Sons Inc., 1971.

[16] D.A. Jones, Principles and Prevention of Corrosion, Ed Macmillan, New York, 1991.

[17] M. Pourbaix, Atlas d'Equilibres Electrochemiques, Gauthier-Villars, Paris, 1963.

[18] L. Robbiola, J.-M. Blengino, C. Fiaud, Morphology and mechanisms of formation of natural patinas on archaeological Cu-Sn alloys, Corrosion Science, 40 (1998) 2083–2111.

[19] A. Dorigo, C. Fiaud, J.-P. Labbé, L. Robbiola, P. Brunella, H. Böcking, Characterization of the corrosion structures of Roman copper alloys by SEM and EDSX. IMMACO: Improvement of Means of Measurements on Archaeological Copper Alloys for Characterization and Conservation, in: W. Mourey, L. Robbiola (Eds.), Metal 98: Proceedings of the International Conference on Metals Conservation, Draguignan-Figanières, France, 27-29 May 1998, James & James Ltd, 1998: pp. 145–151.

[20] H. Plenderleith, The Conservation of Antiquities and Works of Art: Treatment, Repair and Restoration, Oxford University Press, London, 1956.

[21] A.G. Nord, E. Mattsson, K. Tronner, Factors influencing the long-term corrosion of bronze artefacts in soil, Protection of Metals, 41 (2005) 309–316.

[22] A.G. Nord, K. Tronner, E. Mattsson, G.C. Borg, I. Ullén, Environmental threats to buried archaeological remains., Ambio, 34 (2005) 256–62.

[23] M. Fjaestad, I. Ullén, A.G. Nord, K. Tronner, G.C. Borg, M. Sandberg, Are recently excavated bronze artifacts more deteriorated than earlier finds? Second report, in: W. Mourey, L. Robbiola (Eds.), Metal 98: Proceedings of the International Conference on Metals Conservation, Draguignan-Figanières, France, 27-29 May 1998, James & James Ltd, London, 1998: pp. 71–79.

[24] I.D. MacLeod, Bronze disease: an electrochemical explanation, in: Bulletin AICCM 7, AICCM, 1981: pp. 16–26.

[25] W.R. Fischer, B.D. Wagner, H. Siedlarek, B. Fussinger, I. Hanssel, N. von der Bank, The influence of chloride ions and light on the corrosion behavior of copper alloys in aqueous environments with special regard to bronze disease, in: I. MacLeod, S.L. Pennec, L. Robboiola (Eds.), Metal 95, Proceedings of the International Conference on Metals Conservation, Semur En Auxois 25-28 September 1995, James & James Ltd, London, 1997: pp. 89–94.

[26] L. Veleva, P. Quintana, R. Ramanauskas, R. Pomes, L. Maldonado, Mechanism of copper patina formation in marine environments, Electrochimica Acta, 41 (1996) 1641–1646.

[27] N.A. North, Conservation of Metals, in: C. Pearson (Ed.), Conservation of Marine Archaeological Objects, Butterworths, London, 1987.

[28] A.G. Nord, K. Lindahl, K. Tronner, A note on spionkopite as a corrosion product on a marine copper find, Studies in Conservation, 38 (2012) 133–135.

[29] P. Letardi, Laboratory and field tests on patinas and protective coating systems for outdoor bronze monuments, in: J. Ashton, D. Hallam (Eds.),

Metal 04: Proceedings of the International Conference on Metals Conservation, Canberra, Australia, 4 - 8 October 2004, National Museum of Australia, Canberra, 2004: pp. 379–387.

[30] L.S. Selwyn, N.E. Binnie, J. Poitras, M.E. Laver, D.A. Downham, Outdoor bronze statues: analysis of metal and surface samples, Studies in Conservation, 41 (1996) 205–228.

[31] E. Franceschi, L. Macció, D. Palazzi, L. Rosa, The corrosion of metallic artifacts within different environments. Archaeological objects and laboratory simulations, in: W. Mourey, L. Robbiola (Eds.), Metal 98: Proceedings of the International Conference on Metals Conservation, Draguignan-Figanières, France, 27-29 May 1998, James & James Ltd, London, 1998: pp. 92–93.

[32] C. Leygraf, Atmospheric corrosion, in: P. Marcus, J. Oudar (Eds.), Corrosion Mechanisms in Theory and Practice, Marcel Dekker Inc., New York, 1995: pp. 421–455.

[33] G. Wranglén, An Introduction to Corrosion and Protection of Metals, Chapmann and Hall, London-New York, 1985.

[34] T. Stambolov, The Corrosion and Conservation of Metallic Antiquities and Works of Art, Central Laboratory for Objects of Art and Science, Amsterdam, 1985.

[35] J.B. Sharkey, S.Z. Lewin, Conditions governing the formation of atacamite and paratacamite, The American Mineralogist, 56 (1971) 179–192.

[36] N. Eastaugh, V. Walsh, T. Chaplin, R. Siddal, Pigment Compendium: a Dictionary of Historical Pigments, Elsevier Science, Amsterdam, 2004.

[37] International Centre for Diffraction Data database, release 2008, http://www.icdd.com/ (accessed 2/07/2013).

[38] L. Robinet, D. Thickett, A New Corrosion Testing, Studies in Conservation, 48 (2011) 263–268.

[39] J.W. Anthony, R.A. Bideaux, K.W. Bladh, M.C. Nichols, Handbook of Mineralogy, Mineralogical Society of America, Chantilly, VA 20151-1110, USA, Http://www.handbookofmineralogy.org/%20 (accessed 21/01/2013).

[40] A. Doménech-Carbó, Electrochemistry for conservation science, Journal of Solid State Electrochemistry, 14 (2009) 349–351.

[41] L. Mond, G. Cuboni, On the nature of antique bronze patina, Atti Reale Accademia Dei Lincei, 52 (1893) 498–499.

[42] M. Berthelot, Sur l'altération lente des objets de cuivre, au sein de la terre et dans les musées, Comptes Rendus Hebdomadaires Des Seances De l'Academie Des Sciences, 118 (1894) 768–770.

[43] V. Costa, Electrochemistry as a conservation tool: an overview, in: J. Townsend, K. Eremin, A. Adriaens (Eds.), Conservation Science 2002: Papers from the Conference Held in Edinburgh, Scotland 22-24 May 2002, Archetype, London, 2003: pp. 88–95.

[44] R. Bertholon, R. Bell, J.-M. Blengino, N. Lacoudre, Stabilisation de la corrosion d'un objet archéologique en alliage cuivreux par electrolyse á faible polarization dans le sesquicarbonate de sodium, in: I. MacLeod, S.L. Pennec, L. Robbiola (Eds.), Metal 95, Proceedings of the International Conference on Metals Conservation, Semur En Auxois 25-28 September 1995, James & James Ltd, London, 1997: pp. 209–219.

[45] A. Doménech-Carbó, M.T. Doménech-Carbó, V. Costa, Electrochemical Methods in Archaeometry, Conservation and Restoration, Springer, Berlin, 2009.

[46] http://www.lorentzcenter.nl/lc/web/2010/364/info.php3?wsid=364 (last accessed 31/05/2013).

[47] L. Bertrand, L. Robinet, M. Thoury, K. Janssens, S.X. Cohen, S. Schöder, Cultural heritage and archaeology materials studied by synchrotron spectroscopy and imaging, Applied Physics A, 106 (2011) 377–396.

[48] A. Adriaens, C. Degrigny, J. Cassar, eds., Benefits of Non-Destructive Analytical Techniques for Conservation. Papers from a COST Action G8 Workshop held in Kalkara, Malta 8 January 2004, Office for official publications of the European communities, Luxembourg, 2005.

[49] G. Demortier, A. Adriaens, eds., Ion Beam Study of Art and Archaeological Objects. A Contribution by Members of the COST G1 Action, Office for official publications of the European communities, Luxembourg, 2000.

[50] A. Denker, A. Adriaens, M. Dowsett, A. Giumlia-Mair, eds., Cost Action G8. Non-Destructive Testing and Analyses of Museum Objects, Fraunhofer IRB Verlag, München, 2006.

[51] K. Janssens, R. Van Grieken, Eds., Comprehensive Analytical Chemistry, vol. 42: Non-destructive Micro Analysis of Cultural Heritage Materials, Elsevier, Amsterdam, 2004.

[52] F. Scholz, L. Nitschke, G. Henrion, A New Procedure for Fast Electrochemical Analysis of Solid Materials, Naturwissenschaften, 76 (1989) 71–72.

[53] F. Scholz, L. Nitschke, G. Henrion, A Technique to Study the Electrochemistry of Minerals, Naturwissenschaften, 76 (1989) 167–168.

[54] F. Scholz, L. Nitschke, G. Henrion, Abrasive stripping voltammetric analysis of tin—bismuth, Electroanalysis, 2 (1990) 85–87.

[55] V. Costa, K. Leyssens, A. Adriaens, N. Richard, F. Scholz, Electrochemistry reveals archaeological materials, Journal of Solid State Electrochemistry, 14 (2009) 449–451.

[56] V. Costa, Characterisation of cultural artefacts using electrochemical techniques, in: J.H. Townsend, L. Toniolo, F. Cappitelli (Eds.), Conservation Science 2007: Paper from the Conference Held in Milano, Italy 10-11 May 2007, Archetype, London, 2007: pp. 209–211.

[57] M. Wadsak, I. Constantinides, G. Vittiglio, A. Adriaens, K. Janssens, M. Schreiner, F.C. Adams, P. Brunella, M. Wuttmann, Multianalytical study of patina formed on archaeological metal objects from Bliesbruck-Reinheim, Mikrochimica Acta, 133 (2002) 159–164.

[58] G.P. Cicileo, M.A. Crespo, B.M. Rosales, Comparative study of patinas formed on statuary alloys by means of electrochemical and surface analysis techniques, Corrosion Science, 46 (2004) 929–953.

[59] I. Constantinides, M. Gritsch, A. Adriaens, H. Hutter, F. Adams, Microstructural characterization of five simulated archaeological copper alloys using light microscopy, scanning electron microscopy, energy dispersive X-ray microanalysis and secondary ion mass spectrometry, Analytica Chimica Acta, 440 (2001) 189–198.

[60] F. Munnik, K.A. Sjöland, G. Vittiglio, G. Ingelbrecht, U. Wätjen, Nuclear microprobe study of metal segregation in quaternary bronze, Nuclear Instruments and Methods in Physics Research B, 158 (1999) 281–286.

[61] M.L. Young, F. Casadio, S. Schnepp, J. Almer, D.R. Haeffner, D.C. Dunand, Synchrotron X-ray diffraction and imaging of ancient Chinese bronzes, Applied Physics A, 83 (2006) 163–168.

[62] M. Serghini-Idrissi, M.C. Bernard, F.Z. Harrif, S. Joiret, K. Rahmouni, A. Srhiri, H. Takenouti, V. Vivier, M. Ziani, Electrochemical and spectroscopic

characterizations of patinas formed on an archaeological bronze coin, Electrochimica Acta, 50 (2005) 4699–4709.

[63] I. De Ryck, A. Adriaens, E. Pantos, F. Adams, A comparison of microbeam techniques for the analysis of corroded ancient bronze objects, The Analyst, 128 (2003) 1104–1109.

[64] H. Ling, Z. Qingrong, G. Min, Characterization of corroded bronze Ding from the Yin Ruins of China, Corrosion Science, 49 (2007) 2534–2546.

[65] A. Paulin, S. Spaić, A. Zalarb, N. Trampuž-Orelc, Metallographic analysis of 3000-year-old Kanalski Vrh hoard pendant, Materials Characterization, 51 (2003) 205–218.

[66] E.S. Friedman, A.J. Brody, M.L. Young, J.D. Almer, C.U. Segre, S.M. Mini, Synchrotron radiation-based x-ray analysis of bronze artifacts from an Iron Age site in the Judean Hills, Journal of Archaeological Science, 35 (2008) 1951–1960.

[67] A. Adriaens, Non-destructive analysis and testing of museum objects: An overview of 5 years of research, Spectrochimica Acta Part B: Atomic Spectroscopy, 60 (2005) 1503–1516.

[68] V. Hayez, V. Costa, J. Guillaume, H. Terryn, A. Hubin, Micro Raman spectroscopy used for the study of corrosion products on copper alloys: study of the chemical composition of artificial patinas used for restoration purposes, The Analyst, 130 (2005) 550–6.

[69] E. Pantos, W. Kockelmann, L.C. Chapon, L. Lutterotti, S.L. Bennet, M.J. Tobin, J.F.W. Mosselmans, T. Pradell, N. Salvado, S. Butí, R. Garner, a. J.N.W. Prag, Neutron and X-ray characterisation of the metallurgical properties of a 7th century BC Corinthian-type bronze helmet, Nuclear Instruments and Methods in Physics Research Section B: Beam Interactions with Materials and Atoms, 239 (2005) 16–26.

[70] M.C. Squarcialupi, G.P. Bernardini, V. Faso, A. Atrei, G. Rovida, Characterisation by XPS of the corrosion patina formed on bronze surfaces, Journal of Cultural Heritage, 3 (2002) 199–204.

[71] M.P. Casaletto, G.M. Ingo, M. Albini, A. Lapenna, I. Pierigé, C. Riccucci, E. Faraldi, An integrated analytical characterization of corrosion products on ornamental objects from the necropolis of Colle Badetta-Tortoreto (Teramo, Italy), Applied Physics A, 100 (2010) 801–808.

[72] M.M. Antonijević, S.C. Alagić, M.B. Petrović, M.B. Radovanović, A.T. Stamenković, The influence of pH on electrochemical behavior of copper in presence of chloride ions, International Journal of Electrochemical Science, 4 (2009) 516–524.

[73] N. Souissi, E. Sidot, L. Bousselmi, E. Triki, L. Robbiola, Corrosion behaviour of Cu–10Sn bronze in aerated NaCl aqueous media – Electrochemical investigation, Corrosion Science, 49 (2007) 3333–3347.

[74] F. Ammeloot, C. Fiaud, L. Robbiola, E. Sutter, Some new photoelectrochemical insights into the oxidation mechanisms of a Cu-13Sn alloy in a NaCl aqueous solution with and without 0.1 M BTA, in: W. Mourey, L. Robbiola (Eds.), Metal 98: Proceedings of the International Conference on Metals Conservation, Draguignan-Figanières, France, 27-29 May 1998, James & James Ltd, London, 1998: pp. 229–233.

[75] G. Kear, B.D. Barker, F.C. Walsh, Electrochemical corrosion of unalloyed copper in chloride media––a critical review, Corrosion Science, 46 (2004) 109–135.

[76] Y. Feng, K.-S. Siow, W.-K. Teo, K.-L. Tan, A.-K. Hsieh, Corrosion mechanisms and products of copper in aqueous solutions at various pH values, Corrosion, 53 (1997) 389–398.

[77] Y. Feng, K.-S. Siow, W.-K. Teo, K.-L. Tan, A.-K. Hsieh, The corrosion behaviour of copper in neutral tap water. Part I: corrosion mechanisms, Corrosion Science, 38 (1996) 369–385.

[78] Y. Feng, K.-S. Siow, W.-K. Teo, K.-L. Tan, A.-K. Hsieh, The corrosion behaviour of copper in neutral tap water. Part II: determination of corrosion rates, Corrosion Science, 38 (1996) 387–395.

[79] D. Starosvetsky, O. Khaselev, A. M, Y. Ein-El, I, Initiation of copper dissolution in sodium chloride electrolytes, Electrochimica Acta, 51 (2006) 5660–5668.

[80] M.P. Sánchez, M. Barrera, S. González, R.M. Souto, R.C. Salvarezza, Electrochemical behaviour of copper in aqueous moderate alkaline media, containing sodium carbonate and bicarbonate and sodium perchlorate, Electrochimica Acta, 35 (1990) 1337–1343.

[81] N. Souissi, L. Bousselmi, S. Khosrof, E. Triki, Electrochemical behaviour of an archaeological bronze alloy in various aqueous media: new method for understanding artifacts preservation, Materials and Corrosion, 54 (2003) 318–325.

[82] G. Bech-Nielsen, M. Jaskula, I. Chorkendorff, J. Larsen, The initial behaviour of freshly etched copper in moderately acid aerated chloride solutions, Electrochimica Acta, 47 (2002) 4279–4290.

[83] I. Mabille, A. Bertrand, E.M.. Sutter, C. Fiaud, Mechanism of dissolution of a Cu–13Sn alloy in low aggressive conditions, Corrosion Science, 45 (2003) 855–866.

[84] I. MacLeod, S. Pennec, The effects of composition and microstructure on the corrosivity of copper alloys in chloride media, in: K. Grimstad (Ed.), ICOM Committee for Conservation, Preprints 9th Triennial Meeting, Dresden, Getty Conservation Institute, Los Angeles, 1990: pp. 732–739.

[85] M. Wadsak, T. Aastrup, I.O. Wallinder, C. Leygraf, M. Schreiner, Multianalytical in situ investigation of the initial atmospheric corrosion of bronze, Corrosion Science, 44 (2002) 791–802.

[86] J. Nairn, K. Fitzgerald, A. Atrens, Atmospheric corrosion of copper, in: I. MacLeod, S.L. Pennec, L. Robboiola (Eds.), Metal 95, Proceedings of the International Conference on Metals Conservation Semur En Auxois 25-28 September 1995, James & James Ltd, London, 1997: pp. 86–88.

[87] M.A. Crespo, G.P. Cicileo, B.M. Rosales, Electrochemical characterization of patina protectiveness evolution on outdoor bronze sculptures, in: J. Ashton, D. Hallam (Eds.), Metal 04: Proceedings of the International Conference on Metals Conservation, Canberra, Australia, 4 - 8 October 2004, National Museum of Australia, Canberra, 2004: pp. 185–194.

[88] K. Marušić, H. Otmačić-Ćurković, Š. Horvat-Kurbegović, H. Takenouti, E. Stupnišek-Lisac, Comparative studies of chemical and electrochemical preparation of artificial bronze patinas and their protection by corrosion inhibitor, Electrochimica Acta, 54 (2009) 7106–7113.

[89] J. Virtanen, J. Aromaa, O. Forsén, T. Korpinen, Durability of artificial patina on copper, in: Proceedings of the 15th International Corrosion Congress, Granada 23-27 September 2002, Curran associates Inc., 2007: pp. 697–702.

[90] F. Noli, P. Misaelides, a. Hatzidimitriou, E. Pavlidou, M. Kokkoris, Investigation of artificially produced and natural copper patina layers, Journal of Materials Chemistry, 13 (2003) 114–120.

[91] B. Rosales, R. Vera, G. Moriena, Evaluation of the protective properties of natural and artificial patinas on copper, Corrosion Science, 41 (1999) 625–651.

[92] D.L. Hamilton, Methods of Conserving Underwater Archaeological Material Culture. Conservation Files: ANTH 605, Conservation of Cultural Resources

I. Nautical Archaeology, Texas A&M University Program 1998, http://nautarch.tamu.edu/class/ANTH605 (accessed 15/01/2013).

[93] I. MacLeod, Stabilization of corroded copper alloys: a study of corrosion and desalination mechanisms, in: K. Grimstad (Ed.), ICOM Committee for Conservation, Preprints of the 8th Triennial Meeting, Sydney, Australia, 6-11 September 1987, Getty Conservation Institute, Los Angeles, 1987: pp. 1079–1085.

[94] I.D. MacLeod, Conservation of corroded copper alloys: a comparison of new and traditional methods for removing chloride ions, Studies in Conservation, 32 (1987) 25–40.

[95] C. Degrigny, Introduction to the use of electrolytic techniques in conservation, internal report, Instituut Collectie Nederland, Amsterdam, 2003.

[96] O. Berger, Mise au point de prétraitements d'un composite fer forgé-bois issu du milieu sous-marin. Compatibilité entre la déchloriration de la partie métallique et la preservation de la surface originelle, in: I. MacLeod, J.M. Theile, C. Degrigny (Eds.), Metal 2001: Proceedings of the International Conference on Metals Conservation, Santiago, Chile 2-6 April 2001, Western Australian Museum, Perth, 2004: pp. 97–103.

[97] C. Lamy, Stabilisation d'objets archéologiques chlorurés en alliage cuivreux, internal report ARC'Antique, Nantes, France (1997).

[98] A. Aldaz, T. Espania, V. Montiel, A simple tool for the electrolytic restoration of archaeological metallic objects with localized corrosion, Studies in Conservation, 31 (2011) 175–176.

[99] G. Brunoro, A. Frignani, A. Colledan, C. Chiavari, Organic films for protection of copper and bronze against acid rain corrosion, Corrosion Science, 45 (2003) 2219–2231.

[100] M. Finšgar, I. Milošev, Inhibition of copper corrosion by 1,2,3-benzotriazole: A review, Corrosion Science, 52 (2010) 2737–2749.

[101] G. Bierwagen, T.J. Shedlosky, K. Stanek, Developing and testing a new generation of protective coatings for outdoor bronze sculpture, Progress in Organic Coatings, 48 (2003) 289–296.

[102] Ž. Petrović, M. Metikoš-Huković, R. Babić, Modification of copper with self-assembled organic coatings, Progress in Organic Coatings, 61 (2008) 1–6.

[103] A. Elia, K. De Wael, M. Dowsett, A. Adriaens, Electrochemical deposition of a copper carboxylate layer on copper as potential corrosion inhibitor, Journal of Solid State Electrochemistry, 16 (2012) 143–148.

[104] A. Adriaens, F. De Bisschop, M. Dowsett, B. Schotte, Growth and real time corrosion resistance monitoring of lead decanoate coatings, Applied Surface Science, 254 (2008) 7351–7355.

[105] A. Elia, M. Dowsett, A. Adriaens, On the use of alcoholic carboxylic acid solutions for the deposition of protective coatings on copper, in: P. Mardikian, C. Chemello, C. Watters, P. Hull (Eds.), Metal 2010: Proceedings of the International Conference on Metals Conservation, Charleston, South Carolina, USA, 11-15 October 2010, Clemson University, Clemson, 2010: pp. 144–150.

[106] S. Varvara, L.M. Muresan, K. Rahmouni, H. Takenouti, Evaluation of some non-toxic thiadiazole derivatives as bronze corrosion inhibitors in aqueous solution, Corrosion Science, 50 (2008) 2596–2604.

[107] M. Metikosï, M. Lonc, R. Babic, Impedance and photoelectrochemical study of surface layers on Cu and Cu-10Ni in acetate solution containing benzotriazole, Electrochimica Acta, 44 (1999).

2. Methods

This chapter briefly discusses the analytical techniques that were used in this work, which comprise various electrochemical methods, but also spectroscopy including optical and scanning electron microscopy (SEM), Fourier transform infrared spectroscopy (FTIR) and X-ray-based techniques: X-ray fluorescence (XRF), X-ray diffraction (XRD) and synchrotron X-ray diffraction (SR-XRD). For detailed information regarding these methods, the reader is referred to literature [1–22].

2.1 Electrochemical methods

As corrosion is an electrochemical process, electrochemical methods are the preferred analysis methods to study the corrosion behaviour of metals

Electrochemical reactions occur spontaneously at the electrode surface. The oxidation (anodic) and reduction reactions occur simultaneously and the corrosion potential (E_{corr}) is the potential of the metal surface at equilibrium [12–14]. The current that is flowing in equilibrium conditions, equal for the anodic and the cathodic reaction, is called exchange current density (i_0).

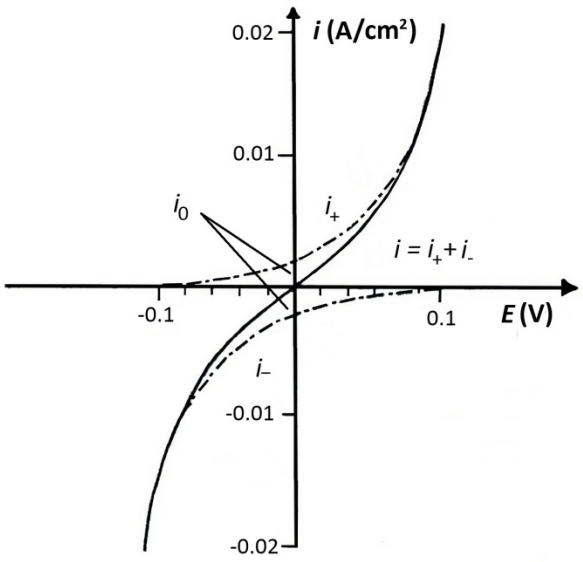

Figure 2.1: The net current density (*i*,represented by the full line) (given by the sum of anodic (i_+) and cathodic (i_-) current density, represented by dotted lines) as a function of the potential (E) (from [23]). i_0 is the exchange current density.

Figure 2.1 shows a representation of the anodic and cathodic current densities. In absence of an applied potential (E), the electrode adjusts its potential to the value for which the two reactions (anodic and cathodic) are equivalent. Since E_{corr} is connected to the electrochemical reactions that occur at the metal surface, its value will be strongly influenced by the surface characteristics of the substrate (e.g. composition, roughness, presence of coatings) and the electrolyte properties (pH, conductivity, concentrations, temperature, stirring, presence of O_2).

In order evaluate the corrosion rate of a metal, one can proceed by determining the polarization resistance (R_p) or the corrosion current density (i_{corr}) [7,8].

The calculation of the polarization resistance is based on Ohm's law that describes the linear (for small overpotentials) relationship existing between the polarization potential and the current density according to equation 2.1 [9,11,13,24]:

$$R_p = \left(\frac{\partial E}{\partial i} \right)_{E \to Ecorr} \tag{2.1}$$

Here E is the polarization potential, i the current density (in $A \cdot cm^{-2}$) and R_p the polarization resistance (in $\Omega \cdot cm^2$). When an electrode corrodes at a higher rate, with more electrons passing easily into the solution, then a higher current density will flow in the cell. If the application of a small voltage produces a large current density, then the R_p is small and the surface is easily corroded. Conversely, if R_p is higher, the surface corrodes more slowly [8–10].

The polarization resistance can be thus calculated as the inverse of the slope of the polarization curve. Figure 2.2 presents a schematic view of the measurements of the polarization resistance using linear sweep voltammetry (LSV).

According to Faraday's law (Equation 2.2), a linear correlation exists between the dissolution rate of the metal considered and the corrosion current. The corrosion rate increases proportionally with the corrosion current density, which depends on the kinetics of anodic and cathodic reactions [11,24].

$$R_M = \frac{M}{nF\rho} i_{corr} \tag{2.2}$$

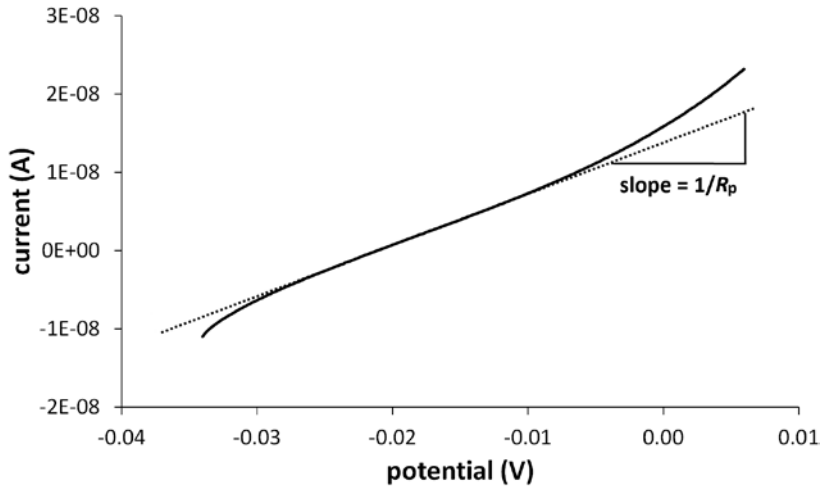

Figure 2.2: Example of a linear polarization curve. The polarization resistance (R_p) is calculated from the slope of the line tangent to the polarization curve.

Here R_M is the dissolution rate of the metal, M the atomic weight, ρ the density, n the number of electrons exchanged in the dissolution reaction, F the Faraday constant (96.485 C/mol) and i_{corr} the current density.

The relationship between the current density and the potential is given by the Butler-Volmer equation (Equation 2.3), which describes how the current density is related to the electrode potential, considering that both a cathodic and an anodic reaction occur on the same electrode:

$$i = i_{corr}\left(e^{\left(\frac{E-E_{corr}}{\beta_a}\right)} - e^{\left(\frac{E-E_{corr}}{\beta_c}\right)} \right) \tag{2.3}$$

Here i is the current density measured experimentally, β_a and β_c the anodic and cathodic slopes and E the applied potential. E_{corr} is the corrosion potential [8–10].

At large positive or negative values of the overpotential (the potential difference between the applied potential and E_{corr}), the second or the first term of equation becomes negligible. For this reason, simple exponential relationships between

current density and overpotential are obtained so that the overpotential can be considered as logarithmically dependent on the current density. Plots of the logarithm to base 10 of the current versus the potential are known as Tafel plots, named after the Swiss chemist Julius Tafel (1862-1918) who first explained how the logarithm of the current density varies linearly with the potential. The graph in Figure 2.3 illustrates a typical Tafel plot. The slopes of the anodic and cathodic semilogarithmic curves are shown. From the two slopes it is possible to extrapolate the β_a and β_c values. These parameters, determined experimentally, are used for the calculation of the corrosion current, according to the Stern-Geary equation (Equation 2.4) [8–10].

$$i_{corr} = \frac{B}{R_p} \tag{2.4}$$

Here B is the Tafel constant and is defined according to Equation 2.5:

$$B = \frac{\beta_a \beta_c}{2.303\left(\beta_a + \beta_c\right)} \tag{2.5}$$

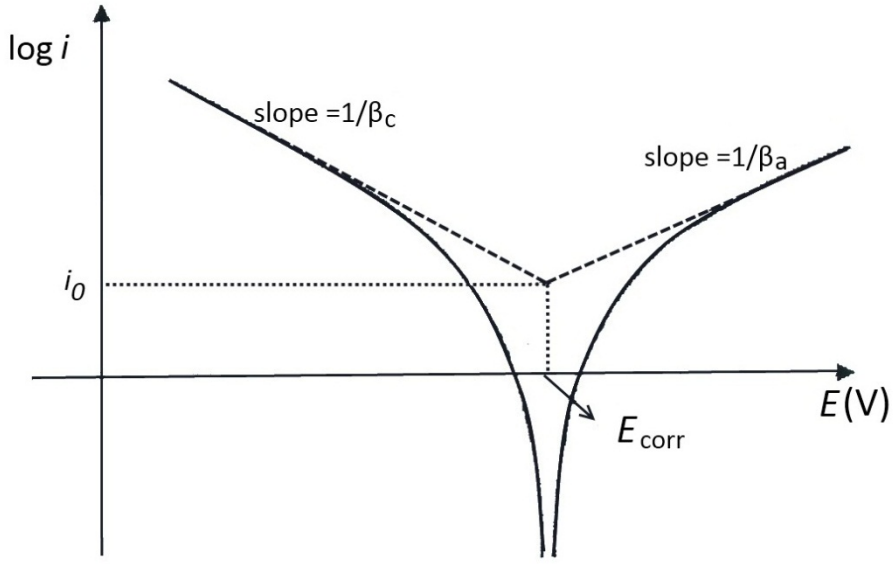

Figure 2.3: Schematic representation of the Tafel extrapolation: i_0 is the exchange current density and represents in this case the corrosion current density [23].

2.1.1 Chronopotentiometry

The technique called chronopotentiometry (at zero current) measures the open circuit potential (OCP), which is the potential difference between the metal surface (so-called working electrode) and a reference electrode as a function of time without applying a current. When the potential has reached a stable value, an equilibrium is reached and the OCP represents E_{corr}.

The measurement of E_{corr} vs time provides information on the corrosion behaviour of the metal in a given electrolyte. Figure 2.4 shows the four typical situations of the corrosion potential behaviour when a metal is immersed in a solution [25]. Curve 1 shows a passivation behaviour, presenting a process in which the anodic current is reduced by the formation of a passivating layer. Curve 2, on the contrary shows active corrosion, in which the E_{corr} decreases constantly. Curve 3 can be explained by a first stage of active corrosion (3a) followed by the formation of a passivation layer on the surface (3b). Curve 4 shows the presence of passivation (4a), followed by a breakdown of the protective layer that causes the start of a corrosion process (4b) [25].

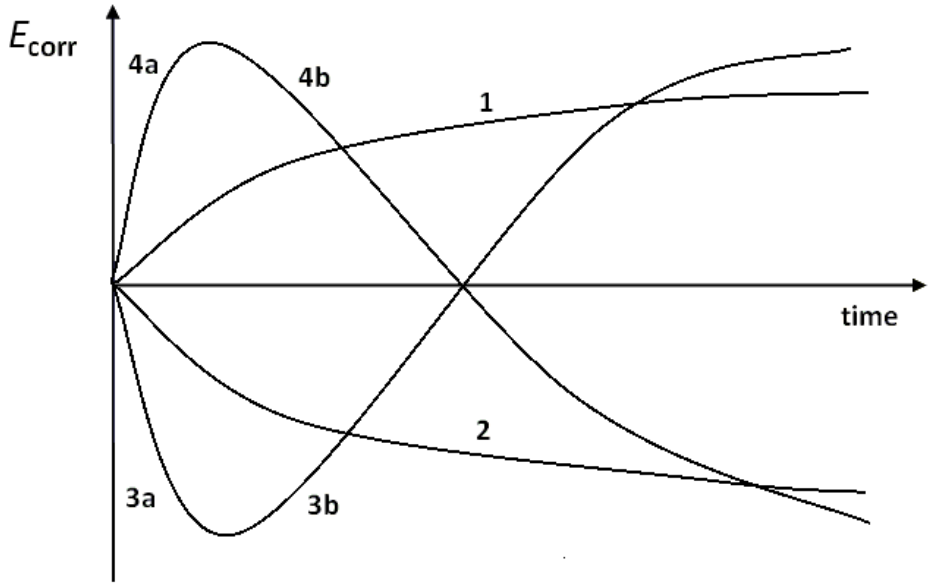

Figure 2.4: E_{corr} as a function of time in case of passivation (1), corrosion (2) and the co-occurrence of the two behaviours (3 and 4).

2.1.2 Polarization methods

The main characteristic of polarization techniques is the application of a potential to the working electrode and the measurement of the Faraday current through the electrochemical cell. The current is monitored at the counter electrode [12–15].
Different from chronopotentiometry, these techniques may be considered "active" since the application of a potential forces a change (reduction or oxidation) upon the metal surface. In this work we used linear sweep voltammetry, cyclic voltammetry and square wave voltammetry.

2.1.2.1 Linear sweep voltammetry

In linear sweep voltammetry (LSV) the potential of the working electrode is swept linearly as a function of time. The polarization of the working electrode produces a current flow. In the current vs potential plot electrochemical reactions, such as oxidation or reaction are identifiable by the presence of positive or negative (respectively) waves and peaks at determined potentials [6].
In this study LSV has been used to measure the polarization resistance and to calculate the corrosion current through Tafel extrapolation.

2.1.2.2 Cyclic voltammetry

Cyclic voltammetry follows the same principle as linear sweep voltammetry, but the potential scan is cyclic. Figure 2.5 shows a graphical representation of the sweeping of the potential vs time (a) and the resulting current vs potential curve (b). Depending on the type of analysis one or more cycles can be performed.
Amongst various applications, cyclic voltammetry analyses provide information on the electrode kinetics and the reversibility of a reaction [6,15]. In this study, this technique has been used to monitor the deposition of carboxylate coatings on copper surfaces (chapter 5).

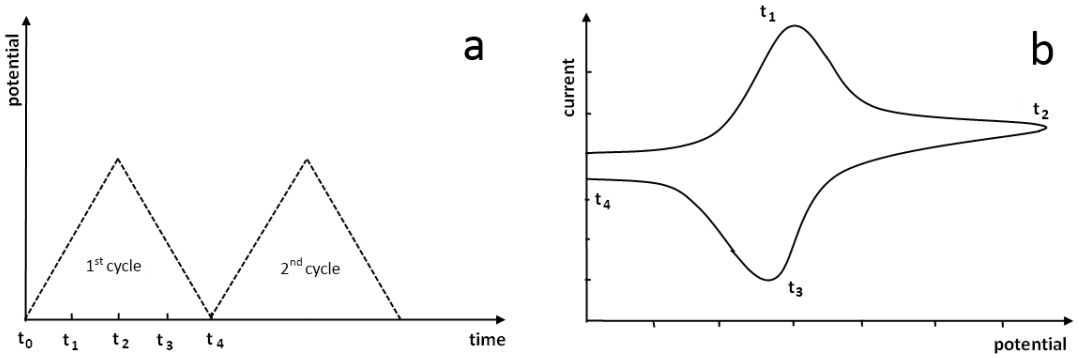

Figure 2.5: Variation of the potential as a function of time (a) in a cyclic voltammetry analysis and an example of its resulting current vs potential plot (b).

2.1.2.3 Square wave voltammetry

Square wave voltammetry (SQWV) is one of the pulse techniques, together with normal pulse voltammetry and differential pulse voltammetry. These techniques are widely adopted in electroanalytical chemistry for the determination of electroactive species because of their high sensitivity [6,15].

The main difference between SQWV and the linear polarization techniques is the type of the potential ramp. In the case of square wave voltammetry the increase of the potential ramp is not linear but follows a square wave, as is shown in Figure 2.6.

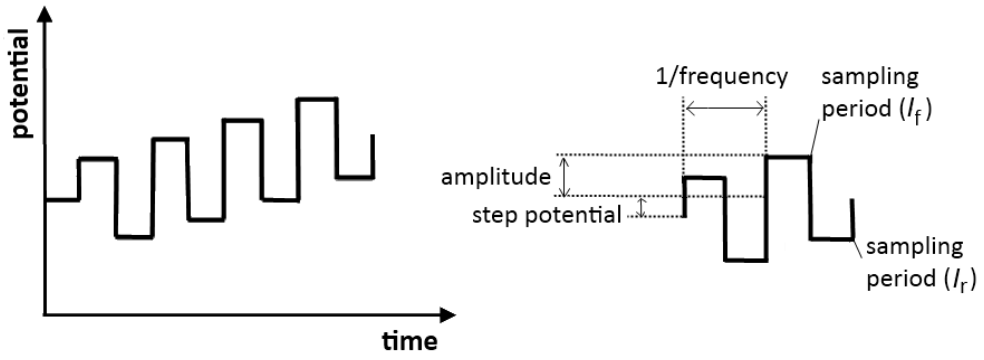

Figure 2.6: Variation of the potential as a function of time in square wave voltammetry and the parameters of the square wave. The current is measured at the end of each half cycle [16].

The current is measured at the end of each half-cycle, whereby the current measured on the reverse half-cycle (reverse or backward current, I_r) is subtracted from the one measured on the forward half-cycle (forward current, I_f). The current difference is displayed as a function of the applied potential [16,26], as is shown in Figure 2.7.

The main advantage of using square wave voltammetry is that plotting this difference minimizes the influence of the capacitive current. The capacitive current is not connected to electrochemical reactions, but it is the current flowing at the electrode interface due to charging/discharging of the double layer capacitance caused by the application of a potential. The presence of the capacitive current therefore interferes with the voltammetric response given by the redox reaction, leading to difficulties in the detection of oxidation/reduction peaks because of the presence of higher background current [14,16].

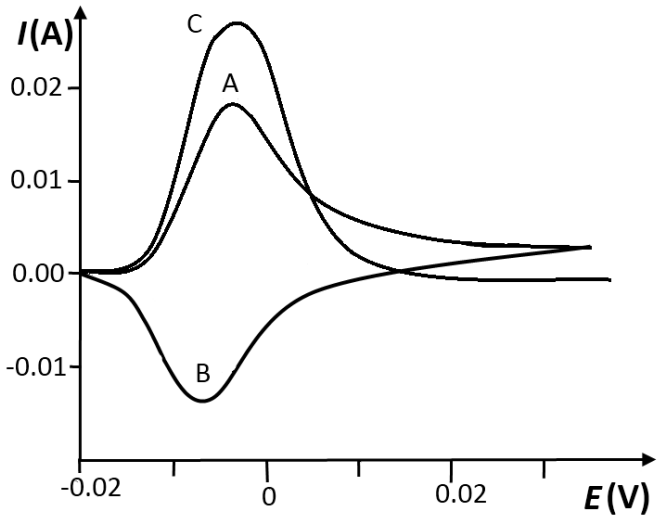

Figure 2.7: Square wave voltammogram: forward current (A), backward current (B) and the difference curve (C).

The use of square wave voltammetry enhances the resolution of the voltammetric peaks. In fact, considering an oxidation reaction at a potential more negative than the redox potential, forward and backward currents will be equal to zero and their difference will be zero as well [6,16]. At a potential more positive than the redox potential, instead, the reaction will be diffusion-controlled and the current difference will be again zero, since backward and forward current are equal. The

largest different between backwards and forward currents will be at the redox potential and the voltammogram will be characterized by peak-shaped curves (Figure 2.7).
Because of the capability of SQWV of discriminating between capacitive and Faradaic currents, the sensitivity of the technique is much higher than with the conventional linear sweep voltammetry [16,26].

Electrochemical experiments were carried out in a three electrode electrochemical cell, using a saturated calomel electrode (SCE, chapter 3, 4 and 5) or a mercury/*mercurous sulphate (MSE, chapter 6)* as a reference electrode (Radiometer Analytical, France). The counter electrode used is a platinum grid. The working electrode is a copper or bronze disc (2 mm thick, 12.6 mm diameter). The electrode is connected to the potentiostat via a specially designed holder. The structure of the holder is shown in Figure 2.8. It contains a phosphor bronze spring which assures the electrical connection between the back side of the copper coupons and the metallic screw connected to the potentiostat cable. For the electrochemical deposition of copper carboxylates layer the working electrode used was a pure copper rod (diameter 2 mm, purity 99.99% purchased from Goodfellow) embedded in epoxy resin.
A computer controlled potentiostat with the software package GPES 4.9005 (Autolab PGSTAT20, ECO Chemie) was used for all measurements.

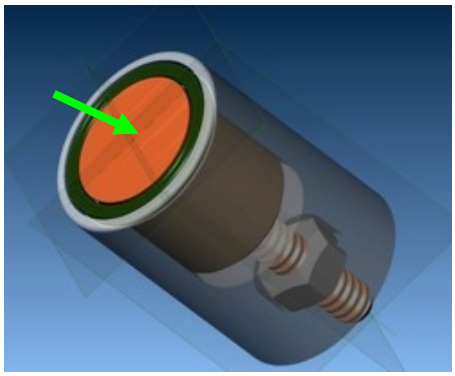

Figure 2.8: Electrode holder. The green arrow indicates the position of the coupons (© Mark Dowsett).

2.2 Optical microscopy

In this research, the visual examination of the samples has been carried out with a stereomicroscope. It uses two separate optical paths with two objectives and two eyepieces that to provide slightly different viewing angles to the left and right eyes. This produces a three-dimensional visualization of the object. The light source is a fiber-optic source, equipped with halogen bulbs, of which the intensity and position can be adjusted in order to provide adequate illuminating conditions[17,18].

Optical microscopy examinations in this study were carried out with a Nikon SMZ800 stereoscopic microscope equipped with a colour camera head DS-Fi1.

2.3 Scanning electron microscopy (SEM)

Scanning electron microscopy is based on the interaction between an electron beam and the sample to be measured. One of the ways to create an electron beam is by thermionic emission from a metallic filament and the emitted electrons are accelerated through a potential difference. The beam is then focused through magnetic lenses and scanned over the surface. The instrument is under vacuum (0.3 x 10^{-3} mbar) to avoid enlargement of the beam size [27]. When the surface is hit by a beam of electrons, the emission of secondary electrons and backscattered electrons occurs as one of the secondary processes. Secondary electrons have low energy (< 50 eV) and provide information on the morphology of the sample, giving a topographical image of the surface [1].
Backscattered electrons (BSE) are electrons that belong to the primary beam and that undergo an elastic collision with the nuclei of the atoms present in the target and are scattered with energy close to the initial one. Backscattered electrons give information about the nature of the atoms, i.e. when a surface is rich in elements with high atomic number, more electrons will be backscattered and this will correspond to a lighter area on the image. Figure 2.9 clarifies the difference between the types of images taken on the surface of a leaded bronze. The secondary electron image (a) shows the morphology of the surface, while the backscattered electron

image (b) gives an elemental map of the same area: the element with higher atomic number (lead, in this case) is characterized by the lighter colour.
The resolving power is theoretically given by the beam size, but due to scattering effects on the surface is slightly worse and depends also on the sample surface properties [1].

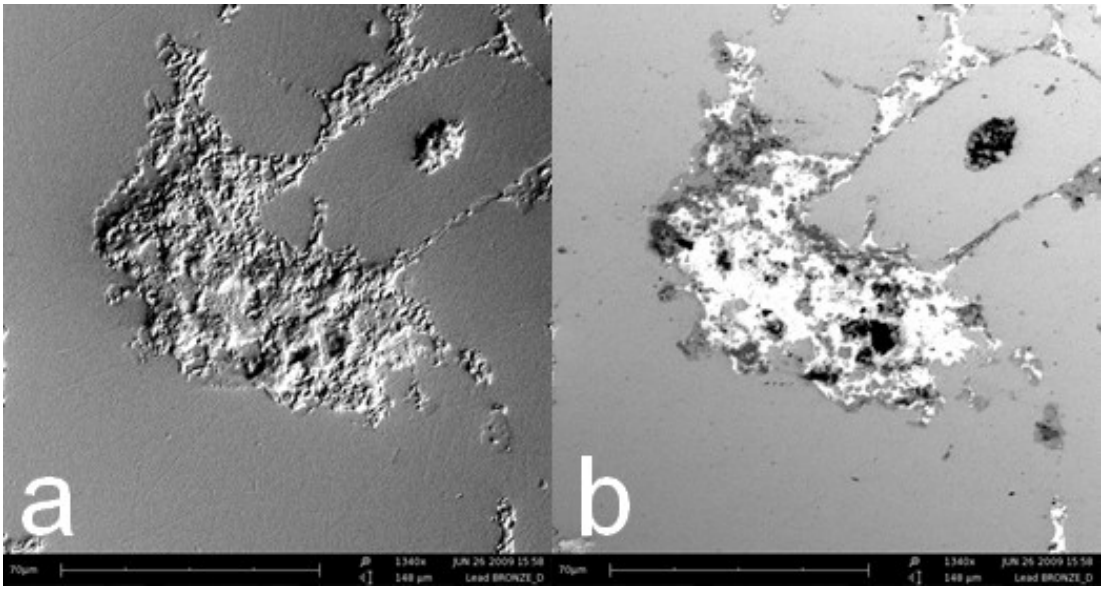

Figure 2.9: Secondary electron image (a) and backscattered electron (b) image of the surface of leaded bronze. Scale bar is 90 µm.

Scanning electron microscopy analyses have been performed with a Phenom table top instrument (FEI, USA). Electrons are created through thermionic emission using a CeB_6 filament and the electrons are accelerated through a potential difference of 5 kV.

2.4 Thickness measurements: eddy current principle

The measurement of the thickness of the corroded layers and the protective coatings has been performed with a thickness probe. The probe non-destructively measures the thickness of the coatings on metal substrates using the eddy currents principle. The probe contains an air-cored coil. A high frequency alternating current flows through the coil and generates an electromagnetic alternating field around the coil. When the probe is placed near a conductive surface, the alternating magnetic field

will induce an alternating current is induced in the material. This in turn generates another alternating electromagnetic field which perturbs the original field. Variations in the phase and the magnitude of these eddy currents can be thus monitored by measuring changes to the current flowing in the coil. Variations in the electrical conductivity of the test surface are determined by the presence of a coating or defects [19]. The probe must be calibrated with references of certified thickness so that the the result can be displayed in millimiters or micrometers.

Thickness measurements have been performed with the instrument Surfix® Pro S equipped with a FN1.5 probe (Phynix Gmbh & Co KG, Germany). For this study, the eddy current probe has been preferred to the use of cross section because it is totally non-destructive and it does not require any sample preparation.

2.5 Fourier transform infrared spectroscopy

Fourier transform infrared spectroscopy (FTIR) is a vibrational spectroscopy and is able to provide information on the molecular structure of compounds on the basis of a selective absorption of infrared radiation made by functional groups present in the sample.

Atoms in molecules are in continuous vibration with respect to each other. When the frequency of the infrared radiation (IR) is equal to the frequency of the vibrational mode, the molecules absorb the radiation and the energy is converted into vibrations such as stretching and bending (the major type of molecular vibration). The infrared spectrum presents the changes in absorbance (or transmittance) as a function of the frequency [3].

Different functional groups absorb characteristic frequencies of IR radiation. Moreover, additional bands are generated by the appearance of overtones (integral multiples of the fundamental absorption frequencies) and interference phenomena. The combination of these factors creates a unique IR spectrum or fingerprint for each compound [2]. The identification of an unknown sample can thus be done by comparison with reference infrared spectra.

There are different acquisition modes of the spectrum, which allows one to analyse the sample in every physical state. In transmission mode the detector collects the radiation that passes through the sample, producing a transmittance spectrum. In order to perform the analysis, a thin layer of sample is deposited on a pellet transparent to infrared radiation (usually made with KBr and NaCl). Insoluble samples are usually powdered and mixed with a medium in order to create a pellet.
In the case of attenuated total reflection (ATR) the infrared beam is directed onto an optically dense crystal with a high refractive and undergo multiple reflections that extend beyond the crystal surface and into the sample, for a thickness of around 4 μm. This acquisition mode is particularly important because, in the case of sample of reduced dimensions, it allows the performance of totally non-destructive analyses [2].

In this study infrared spectroscopic analyses were performed to obtain qualitative proof of the deposition of a copper carboxylate layer (chapter 5). The spectra were recorded in reflectance mode in the range 4000-600 cm^{-1} using a Biorad FT-IR spectrometer FTS 575C equipped with a "Golden Gate" ATR accessory fitted with a diamond crystal.

2.6 X-Ray fluorescence (XRF)

X-ray fluorescence (XRF) provides qualitative and quantitative information on the elemental composition of a material. Here, an X-ray beam is focused on a material and interacts with atoms present in the material. If the primary X-ray beam has sufficient energy, it can transfer its energy to an electron of an inner shell, which will then be ejected creating core level hole (Figure 2.10a). A core level hole is an unstable condition. An electron from an outer shell will transfer to a lower energy level to fill the vacancy. The transition to a lower energy shell can cause the emission of characteristic X-rays, a phenomenon called X-ray fluorescence (Figure 2.10b) [1]. This radiation will have a lower energy respect to the incident beam and the energy is equal to the difference in binding energies of the corresponding levels. Since each element has a unique set of energy levels, each element produces X-rays

at a unique set of energies, allowing the identification of the atomic species present in the sample [1,20]

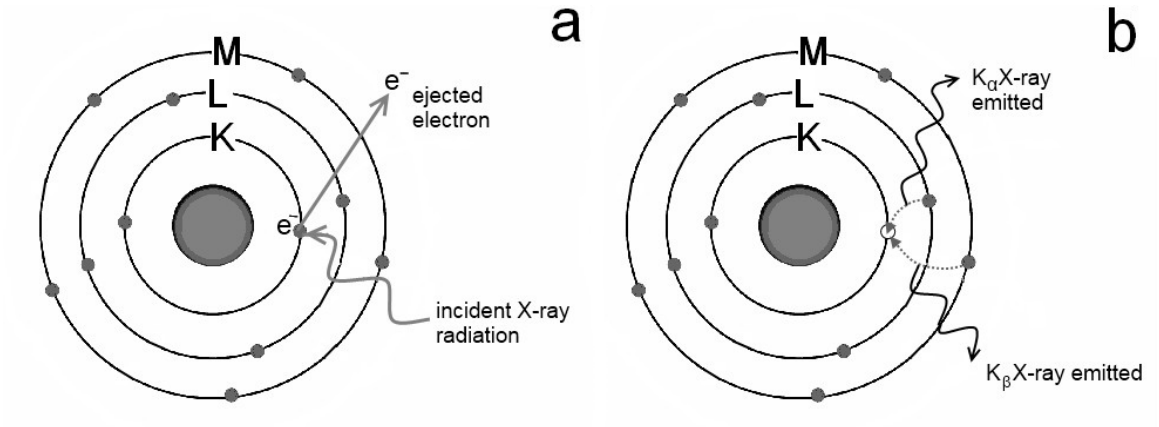

Figure 2.10: Principle of XRF - characteristic X-rays are emitted when an electron from an outer shell fill the vacancy created after the ejection of an electron by the incident radiation.

For an estimation of depth of the analysis, the depth of penetration of the primary X-ray beam into the sample and the escape depth from which fluorescent X-rays can be detected need to be considered. In general, X-rays will penetrate through and escape from a few micrometres down to several millimetres, depending on the material properties and on their energy. In particular, elements with low atomic number (in example Na, Mg, Al) have very low energy characteristic X-rays and they will be difficult to detect, even at small depths. Heavier elements (e.g. Cu, Sn, Pb) have much more energetic X-rays which will be able to pass through large thickness within the sample. The sample composition is thus an important factor: in the case of a high concentration of heavy elements, these atoms will strongly absorb the radiation, reducing the number of X-rays that can escape from deep in the sample (matrix effect) [1,20].

X-ray fluorescence mapping (chapter 3 and 4) was carried out with a laboratory micro-XRF system (Eagle-III microprobe, EDAX, Inc., Mahwah, NJ, USA). This spectrometer is equipped with a microfocus X-ray tube with a rhodium anode, a polycapillary lens for X-ray focusing and a 80 mm^2 energy dispersive Si-(Li) detector. The sample chamber, which incorporates a XYZ motorized stage for sample positioning, was brought under vacuum to improve the sensitivity on low Z

elements. The XRF spectra obtained were evaluated using the software Analysis of X-ray Spectra by Iterative Least Squares fitting (AXIL) [28].
In order to map the cross section of the artefact labelled tonn07-204 (chapter 4), a sample was cut using a drill equipped with a diamond cutting disc (Micromot 50, Proxxon) and embedded in resin (Epofix, Struers).

The micro X-ray fluorescence (XRF) measurements on the Danish coffin decoration (chapter 4) were performed using a laboratory micro-XRF instrument developed by the XMI group in the Department of Analytical Chemistry at Ghent University and based on the X-ray beam source manufactured by X-ray Optical Systems Inc. (XOS), Albany, USA. The X-ray beam source is focused and monochromatised at the energy of Mo-Kα (17.4 keV) by a double curved silicon crystal. The use of a monochromatic beam improves the quality of the XRF spectra by reducing the contribution of the bremsstrahlung radiation. In this way lower detection limits can be achieved [29].

2.7 X-ray diffraction (XRD)

X-ray diffraction provides information on the mineralogical composition and the crystalline structure of a material. The atoms interact with X-rays scattering the radiation. The diffraction pattern is characteristic for each crystalline structure (called lattice) and allows the identification of crystalline materials. The relationship between the interplanar distance and the wavelength is explained by Bragg equation:

$$n\lambda = 2d\sin\theta \tag{2.6}$$

where λ is the wavelength of the incoming beam, n an integer number, d the d-spacing (the distance between the planes) and θ the angle between the crystallographic plane and the incident radiation when constructive interference occurs for scattering of successive planes [21], as shown in Figure 2.11.

The wavelength of the incident beam is known (depending on the X-ray tube used and the presence of a monochromator) and the X-rays diffracted for every 2θ angle (the scattering angle) are measured by a diffractometer.

The diffraction pattern obtained can be used for identification of unknown sample by comparison with diffraction patterns of reference compounds [21]. Other applications of XRD analyses include: definition of the crystal structure and percentage of crystallinity, determination of size and shape of crystals and their orientation.

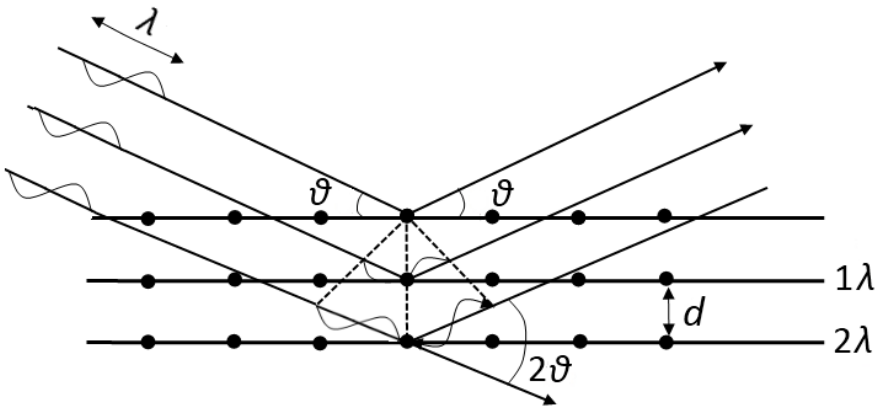

Figure 2.11: Scheme of the Bragg diffraction. Constructive interference occurs when the length $2d\sin\theta$ is equal to an integer multiple of the wavelength of the radiation.

X-ray diffraction (XRD) measurements on copper corrosion products and archaeological artefacts (chapter 4) were performed on an ARL X'TRA Diffractometer (Thermo Scientific) using $CuK_{\alpha 1}$ radiation. The diffractograms were processed using the software esaProject, written by M. Dowsett, © EVA Surface Analysis 2006-2013) [30].

The XRD analysis on copper carboxylates samples (chapter 6) were performed on a PANalytical X'Pert PRO multipurpose diffractometer using filtered copper Kα X-rays (1.5406 Å).

2.8 Synchrotron XRD

A synchrotron is a source of electromagnetic radiation in which charged particles (electrons or positrons, previously accelerated in the booster synchrotron) are

injected into a large storage ring where they circulate in a vacuum environment at a constant energy. Synchrotron radiation is emitted when the particle beam is forced to bend by a bending magnet. The radiation is produced to compensate the change of direction along the tangent under the form of a fan emanating from each bending magnet. Every bending magnet is then a "source" of synchrotron radiation which is characterized by a broad range of energies, from microwave to hard X-rays. Undulators may also be present along the ring: these are structures containing arrays of small magnets that force the particles to follow an undulating trajectory. They generate a more focused and narrower bandwidth beam of radiation compared to the bending magnets. Like bending magnets, wigglers produce a polychromatic radiation, but more intense [22,31]. The beam lines are positioned tangentially to the ring so as to intercept part of the emitted X-ray fan. There, the beam energy can be tuned to obtain a monochromatic radiation [22].

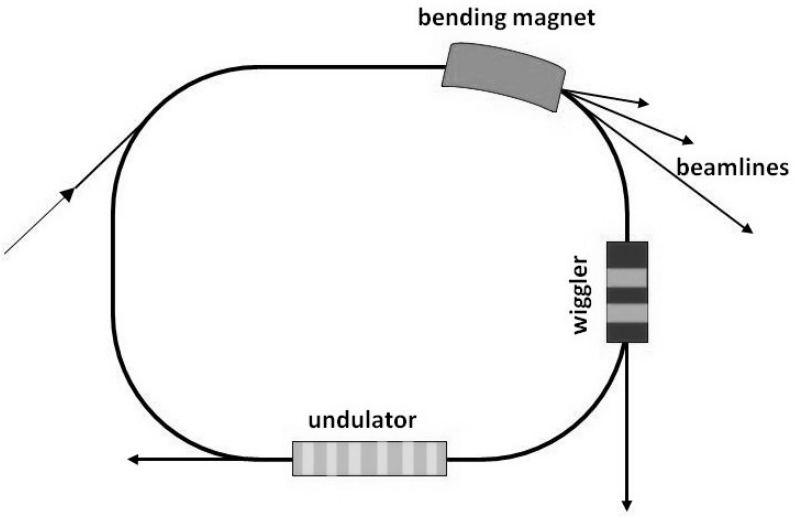

Figure 2.12: Schematic representation of a synchrotron (drawing based on information in [32]).

These properties allow the application of synchrotron radiation to a wide range of disciplines, from medicine, to physics, to art and archaeology. In this study synchrotron radiation has been used to perform time-resolved XRD studies on the growth of carboxylate layers on copper surfaces. The high intensity of the beam allows in fact to reduce considerably the measuring time, in comparison to a

laboratory X-ray diffractometer, so that time-lapse studies can be undertaken on surface changes occurring on the surface in a time-frame from 10 ms to hours .

SR-XRD has been performed at the UK CRG beam line (XMaS) at the European Synchrotron Radiation Facility (ESRF) in Grenoble (France). The XMaS beamline is located on a bending magnet and it has been designed to provide a focussed monochromatic beam with an energy range tuneable from 2.4 to 15 keV [33]. The beam size is also adjustable from a minimum of 20 x 20 μm^2 to a maximum of 0.3 x 0.8 mm^2 [33]. XRD images were taken using a Mar CCD camera and they were processed using the software esaProject© . The software first converts the raw XRD images to a map of intensity vs scattering angle where the elliptical arcs produced by the intersection of the Scherrer cones with the detector are straight. This produces egg-shaped images, like the one in figure 2.13, showing the diffraction lines of a copper surface. The image can be then integrated to obtain a spectrum [34,35]. The use of a two-dimensional detector, like a Mar camera, for the collection of XRD patterns provides more information respect to a conventional laboratory diffractometer, in particular for samples characterized by texture or large grain size. Moreover, a two-dimensional detector reduces the acquisition time of the XRD pattern [36-38]. The SR-XRD study on the formation of a carboxylate layer on copper surfaces (chapter 6) has been performed using a special environmental or electrochemical cell (eCell) [39]. The eCell is made of poly(chlorotrifluroethylene) (PCTFE), a material characterized by high-resistance to a wide range of chemicals [40]. A schematic representation of the eCell is shown in Figure 2.14. The eCell has been developed for time-resolved X-ray analyses coupled with electrochemical measurements, such as E_{corr} monitoring or cyclic voltammetry, for example. For this reason a reference electrode and a counter electrode are present in the eCell. The working electrode, in this study a copper coupon, is mounted in a special holder, positioned onto a piston in the centre of the cell. The eCell has a volume of around 30 mL. It is liquid-tight and it is sealed on the top by a window made of *Kapton® HN* polyimide film, so that it can positioned in any orientation without risk of liquid leaks on the instrumentation. The Kapton window used is 8 µm thick, it is transparent to X-rays and does not give a diffraction pattern which may interfere with the XRD pattern studied.

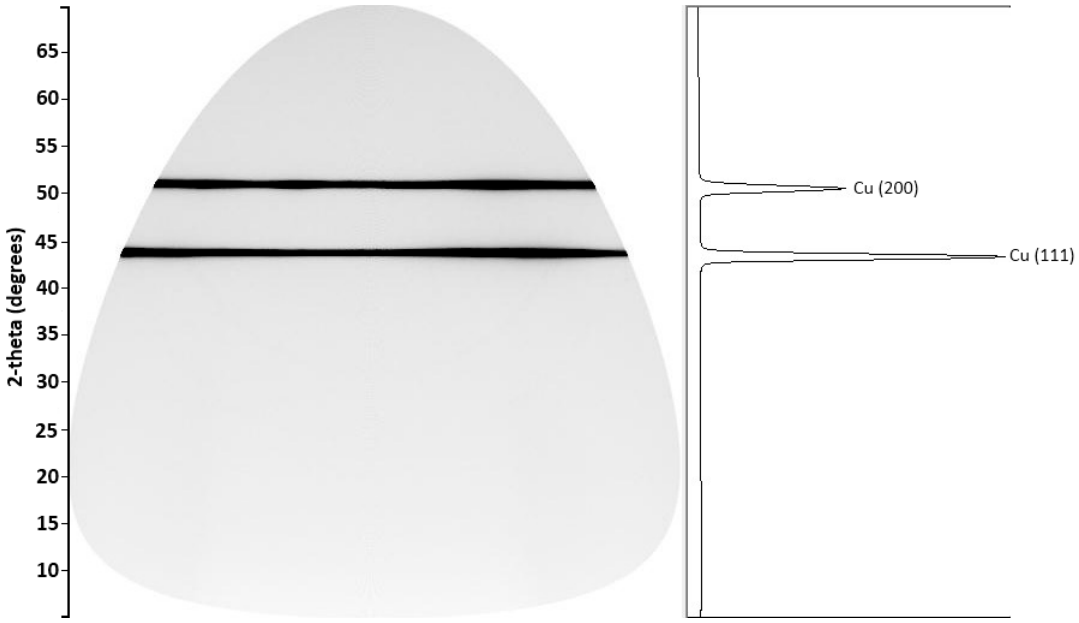

Figure 2.13: XRD image of copper and the correspondent XRD diffractogram.

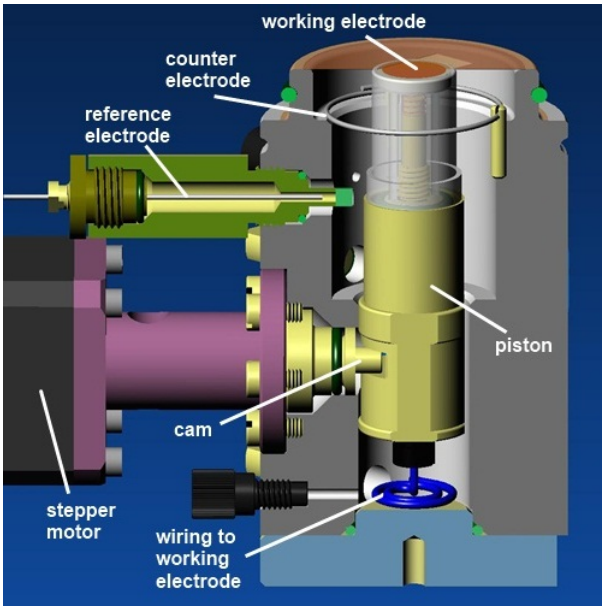

Figure 2.14: Graphical representation of the eCell [38], © Maney Publishing. .

The piston with the working electrode can be moved upwards and downwards by a stepper motor, whereby the upper position allows the acquisition of the X-ray data. The maximum thickness of the fluid in this position does not exceed 200 µm, which minimizes scattering and the absorption of the X-rays in the liquid [39]. The lower

position favours the reactions occurring on the electrode surface, which may be instead limited by a reduced amount of solution when the electrode is in the upper position. In this work, the eCell has been used to study the deposition of a carboxylate layer on a copper surface, by the recording of a sequence of XRD spectra without any electrochemical measurements.
Recent applications of the eCell include the monitoring of the corrosion processes of copper by XRD, X-ray absorption spectroscopy (XAS) and X-ray excited optical luminescence (XEOL) and the study of the growth of lead carboxylate layers on a lead surface by means of time resolved XRD [30,35,39,41-43].

References:

[1] G. Lawes, A.M. James, Scanning Electron Microscopy and X-ray Microanalysis. Analytical Chemistry by Open Learning, J. Wiley & Sons Inc., Chichester, UK, 1987.

[2] B. George, P. McIntyre, Infrared Spectroscopy. Analytical Chemistry by Open Learning, J. Wiley & Sons Inc., Chichester, UK, 1987.

[3] C.-P. Sherman Hsu, Infrared spectroscopy, in: F. Settle (Ed.), Handbook of Instrumental Techniques for Analytical Chemistry, Prentice Hall PTR, Upper Sadle River, 1997: pp. 247–284.

[4] M. Birkholz, Thin Film Analysis by X-ray Scattering, Weinheim, 2006.

[5] R. Lee, Scanning Electron Microscopy and X-ray Microanalysis, Prentice Hall PTR, Englewood Cliffs, 1993.

[6] A.J. Bard, L.R. Faulkner, eds., Electrochemical Methods. Fundamentals and Applications., 2nd ed., J. Wiley & Sons Inc., 2001.

[7] E. D. Verink, Corrosion Testing Made Easy, vol. 3. The Basics, NACE, Houston, TX, 1994.

[8] G.S. Haynes, R. Baboian, eds., Laboratory Corrosion Tests and Standards, ASTM, Philadelphia, 1985.

[9] D.A. Jones, Principles and Prevention of Corrosion, Ed Macmillan, New York, 1991.

[10] R. Baboian, ed., Electrochemical Techniques for Corrosion Engineering, NACE, Houston, 1986.

[11] J.R. Davis, Corrosion: Understanding the Basics, ASM International, Materials Park, OH, 2000.

[12] D. Pletcher, R. Greff, R. Peat, L.M. Peter, Instrumental Methods in Electrochemistry, Hellis Horwood Ltd, Chichester, UK, 1985.

[13] C.M.A. Brett, A.M. Oliveira Brett, Electrochemistry. Principles, Methods and Applications, Oxford University Press, Oxford, 1993.

[14] T. Riley, C. Tomlinson, Principles of Electroanalytical Methods. Analytical Chemistry by Open Learning, J. Wiley & Sons Inc., Chichester, UK, 1987.

[15] T. Riley, A. Watson, Polarography and Other Voltammetric Methods. Analytical Chemistry by Open Learning, J. Wiley & Sons Inc., Chichester, UK, 1987.

[16] S.P. Kounaves, Voltammetric Techniques, in: F.A. Settle (Ed.), Handbook of Instrumental Techniques for Analytical Chemistry, Prentice Hall, 1997.

[17] P.E. Nothnagle, W. Chambers, M.W. Davidson, Introduction to stereomicroscopy, http://www.microscopyu.com/articles/stereomicroscopy/stereointro.html (Accessed 29/05/2013).

[18] J.N. Turner, Introduction to stereo imaging, in: J.N. Turner (Ed.), Three-Dimensional Ultrastructure in Biology, Academic Press, 1981: pp. 1–11.

[19] Coating thickness measurement. Non-destructive measurements according to the magnetic-induction and eddy-current principle, Phynix GmbH & Co, Köln, 2001.

[20] M.S. Shackley, ed., X-ray fluorescence spectrometry (XRF) in geoarchaeology, in: Geoarchaeology, Springer, 2011.

[21] B.D. Cullity, Elements of X-ray Diffraction, 2nd ed., Addison Wesley, Reading, MA, 1978.

[22] H. Wiedemann, Synchrotron Radiation, Springer, Berlin, 2002.

[23] A. Adriaens, Elektrochemische Analysemethoden, Acco Leuven, 2009.

[24] S.D. Cramer, B.S. Covino Jr, eds., ASM Handbook, Volume 13A. Corrosion: Fundamentals , Testing and Protection, ASM International, 2003.

[25] C. Degrigny, Introduction to the use of electrolytic techniques in conservation, internal report Instituut Collectie Nederland, Amsterdam, 2003.

[26] A.B. Miles, R.G. Compton, The theory of square wave voltammetry at uniformly accessible hydrodynamic electrodes, Journal of Electroanalytical Chemistry, 487 (2000) 75–89.

[27] J. Lawrance, J. Carruthers, J. Jiao, S. Berger, Comparison of materials characterization performed by low voltage desktop SEM and standard high resolution SEM, Microscopy and Microanalysis, 13 (2007) 1728–1729.

[28] B. Vekemans, K. Janssens, L. Vincze, F. Adams, P. Vanespen, Analysis of x-ray-spectra by iterative least-squares (AXIL) - new developments, X-Ray Spectrometry, 23 (1994) 278–285.

[29] Personal communication with J. Garrevoet (XMI group, Department Analytical Chemistry, Ghent University).

[30] A. Adriaens, M. Dowsett, K. Leyssens, B. Van Gasse, Insights into electrolytic stabilization with weak polarization as treatment for archaeological copper objects, Analytical Bioanalytical Chemistry, 387 (2007) 861–868.

[31] What is SR, how is it generated and what are its properties. http://photon-science.desy.de/research/studentsteaching/primers/synchrotron_radiation/index_eng.html (last accessed 23/05/2013) (2013).

[32] http://hasylab.desy.de/science/studentsteaching/primers/storage_rings_beamlines/ index_eng.html#e29324 (last accessed 31/05/2013).

[33] S.D. Brown, L. Bouchenoire, D. Bowyer, J. Kervin, D. Laundy, M.J. Longfield, et al., The XMaS beamline at ESRF : instrumental developments and high resolution diffraction studies, Journal of Synchrotron Radiation, 8 (2001) 1172–1181.

[34] A. Adriaens, F. De Bisschop, M. Dowsett, B. Schotte, Growth and real time corrosion resistance monitoring of lead decanoate coatings, Applied Surface Science, 254 (2008) 7351–7355.

[35] M. Dowsett, A. Adriaens, B. Schotte, G. Jones, L. Bouchenoire, In-situ spectroelectrochemical study of the growth process of a lead decanoate coating as corrosion inhibitor for lead surfaces, Surface and Interface Analysis, 41 (2009) 565–572.

[36] M.B. Dickerson, K. Pathak, K.H. Sandhage, R.L. Snyder, U. Balachandran, B. Ma, et al., Applications of 2D Detectors in X-ray Analysis, Advances in X-ray Analysis, 45 (2002) 338–344.

[37] B.B. He, U. Preckwinkel, K.L. Smith, Comparison between conventional and two-dimensional XRD, Advances in X-ray Analysis, 46 (2003) 37–42.

[38] B.B. He, U. Preckwinkel, K.L. Smith, Fundamentals of two-dimensional X-ray diffraction, Advances in X-ray Analysis, 43 (2000) 273–280.

[39] M.G. Dowsett, A. Adriaens, Cell for simultaneous synchrotron radiation X-ray and electrochemical corrosion measurements on cultural heritage metals and other materials., Analytical Chemistry, 78 (2006) 3360–5.

[40] J.A. Brydson, Plastics Materials, 7th ed., Butterworth-Heinemann, Oxford, 1999.

[41] A. Adriaens, M. Dowsett, Time resolved spectroelectrochemistry studies for protection of heritage metals, Surface Engineering, 24 (2008) 84–89.

[42] M. Dowsett, A. Adriaens, C. Martin, L. Bouchenoire, The use of synchrotron X-rays to observe copper corrosion in real time., Analytical Chemistry, 84 (2012) 4866–72.

[43] M. Dowsett, A. Adriaens, B. Schotte, G. Jones, L. Bouchenoire, Real time spectroelectrochemical growth and corrosion resistance monitoring of lead carboxylate coatings in an environmental cell (eCell), in: C. Degrigny, R. van Langh, I. Joosten, B. Ankersmit (Eds.), Metall 07: Proceedings of the International Conference on Metals Conservation, Amsterdam 17-21 September 2007, Rijksmuseum Amsterdam, Amsterdam, 2007: pp. 26–31.

3. Corrosion study of Cu-Sn alloys

3.1 The Cu-Sn system

The wide distribution of bronze (copper–tin or Cu-Sn) objects in history is connected to the variety of properties of this alloy. The characteristics of copper-tin alloys depend on the tin content and have resulted in the manufacturing of different categories of objects, from precious items to daily life tools and weapons [1,2].

Bronze properties can be understood by looking at the phase diagram in Figure 3.1 [2]. This diagram will be discussed here only for the part concerning those tin percentages lower than 30-35 %, which are commonly found in historical bronzes.

The structure of the Cu-Sn system is not a monophasic structure because of the partial solubility of tin in the copper matrix. The solubility of tin in copper decreases with decreasing of temperature, leading to the formation of different metallic phases [2–4]. The phases that can be found in a Cu-Sn alloy depend on the composition, the temperature and the cooling rate. Every phase is characterized by its own mechanical properties [4] and their combination will define the final characteristics of the bronze objects.

Depending on the composition and the cooling rate, the phases formed during the cooling may also recrystallize as more thermodynamically stable phases [2,4]. The α phase is a homogeneous solid solution of tin and copper. Crystals of α phase are the first to precipitate in the form of dendrites (since copper has the highest melting temperature). The left diagram in Figure 3.1 represents the Cu-Sn system in equilibrium conditions, characterized by an extremely slow cooling rate. On the right the Cu-Sn phase diagram under usual casting conditions in the past and in modern times is shown. In an equilibrium situation, for example for an alloy containing 10 % of tin, all of the tin is dissolved in the α phase at high temperature. Below 300 °C the alloy recrystallizes in two phases, α and ε. Under the usual casting conditions, the ε phase never appears in bronzes with less than 38 % of tin. The recrystallization in the ε phase occurs extremely slowly and requires a long

annealing treatment. In practice, monophasic bronzes are characterized by a tin percentage lower than 10 %. With a higher content of tin, the alloy is characterized by the presence of dendrites of α phase (copper rich) and an interdendritic phase, δ (tin rich). Increasing the tin content in the alloy will increase the amount of the interdendritic phases. Depending on the casting condition and the cooling rate, there may be segregation phenomena occurring in the dendrites. The core of the dendrites is more copper rich and, if the cooling rate is slow enough, the successive growth of the arms is characterized by a higher tin content [2,4].

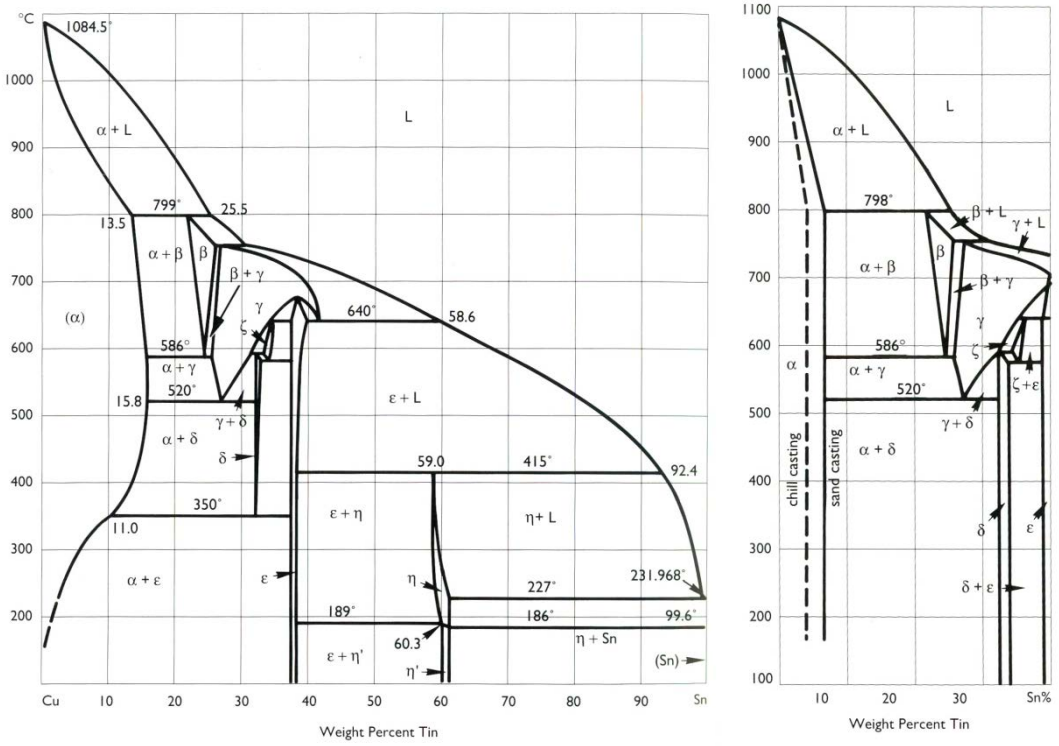

Figure 3.1: Theoretical phase diagram of copper and tin under equilibrium conditions (left) and phase diagram of copper and tin under standard casting conditions [2], © The Getty conservation Institute.

The complexity of the Cu-Sn system reflects then the multiplicity of properties of bronze and the variety of applications in art, industry and daily life. The differences in the alloy structure moreover influence their corrosion resistance.

3.1.1 Studies of the corrosion behaviour of Cu-Sn alloys

Different trends can be observed in the field of corrosion studies of bronze samples. Amongst them, the morphology and characteristics of patinas and corroded layers have been studied on archaeological objects [5–19] and on artificially corroded samples [15,20–29]. The characterization of corroded layers can be done using various analytical techniques. These include XRD [12,15,19,21,30–37], XRF [6,14,30–32,35,36,38], X-ray photoelectron spectroscopy (XPS) [22,39–42], SEM [11,19,21,27,43] and Raman spectroscopy [17,44–46]. Electrochemical techniques are the main analytical tool for the investigation of corrosion mechanisms and corrosion inhibition [5,9,18,20,21,28,37,42,47–51].

Research on copper-tin alloys has focussed on different aspects and includes the study of the corrosion formation in various corrosive media for both copper and alloyed copper [5,9,18,28,42,48,49,52–54]. In this regard, for instance, atmospheric corrosion has been studied, considering the influence of several parameters, such as type and concentration of pollutants, relative humidity, temperature and alloy composition [17,18,21,28,40,52,53,55–58]. In addition the positive role of tin (together with other alloying elements) in reducing the corrosion rate has been considered [27,48,59–61]; the latter also in different electrolytes [9,23,48–50,57,61–69]. An example of this includes the electrochemical study of monophasic copper-tin alloys with three different percentages of tin (7, 11 and 14 %) [70,71], while other research work has focussed on the combination of EIS and colorimetric analyses [72,73].

The present study focuses on bi-phasic copper-tin alloys and extends the range of compositions considered. Six different percentages of tin (varying between 3 and 18 %) have been studied with the aim of evaluating the effect of the concentration of tin on the bronze corrosion behaviour in different corrosive environments. The corrosion rate of the alloys has been studied by electrochemical means in a sodium sulphate electrolyte. The characterization of the corroded surfaces was carried out by means of thickness measurements, optical microscopy, XRF and XRD.

3.2 Experimental

3.2.1 The Cu-Sn alloys

In this work a set of six Cu-Sn samples with a tin content varying from 3 to 18 % were used. This range of tin content reflects the most common bronze composition found in cultural heritage objects.

Table 3-I: Composition of the six copper-tin alloys used. Data were obtained by XRF measurements ([74]).

Name	Cu % w/w	Sn % w/w
CuSn 97-3	97.0 ± 0.2	3.0 ± 0.1
CuSn 94-6	93.4 ± 0.2	6.6 ± 0.1
CuSn 91-9	90.8 ± 0.2	9.2 ± 0.1
CuSn 88-12	87.2 ± 0.2	12.8 ± 0.1
CuSn 85-15	84.0 ± 0.2	15.9 ± 0.1
CuSn 82-18	80.9 ± 0.2	19.1 ± 0.1

The alloys were cast in the metal workshop at the Academy of Fine Arts of Antwerp (Academie voor Schone Kunsten Antwerpen). The composition of the alloys was verified by means of XRF [74]. Table 3-I lists the composition of the alloys and their denomination used in this chapter. XRF measurements were performed also on the pure metals used for the bronze manufacturing and impurities of lead, iron and copper were detected in the tin [74].

3.2.2 Electrochemical tests

Prior to each experiment the electrode was mechanically cleaned with silicon carbide (SiC) paper of P1200 grit to obtain a fresh surface. The surface was subsequently polished using a polishing cloth and an alumina (Al_2O_3) water suspension (1 µm particle size). To remove any adhering Al_2O_3 particles, the electrode was rinsed with deionized water and ultrasonically cleaned in ethanol for 15 minutes.

The polarization resistance (R_p) was measured by means of linear sweep voltammetry (LSV) in a 0.1 M Na_2SO_4 solution in a range of ± 20 mV vs the open circuit potential (OCP) at a scan rate of 1 mV/s. The corrosion current was calculated via the Tafel extrapolation from the LSV curve recorded in a range of ± 250 mV vs OCP with a scan rate of 0.2 mV/s. The reference electrode used for this work is a saturated calomel electrode (SCE) and the counter electrode is a platinum grid.

3.2.3 Corrosive environments

The alloys were corroded by immersing them in different corrosive solutions with the aim of simulating different aggressive environments. The samples, bronze discs of 2 mm thickness and 12.6 mm diameter, were immersed for one year in a solution of synthetic acid rain and a solution of synthetic seawater.

Table 3-II: Composition of the synthetic acid rain solution [59].

Component	Concentration
H_2SO_4	31.85 mg/L
$(NH_4)_2SO_4$	46.20 mg /L
Na_2SO_4	31.95 mg /L
$NaNO_3$	15.75 mg /L
HNO_3	21.25 mg /L
NaCl	84.85 mg /L

Table 3-III: Composition of the synthetic seawater solution [75].

Component	Concentration
NaCl	34.24 g/L
$MgCl_2$ $6H_2O$	11.09 g/L
Na_2SO_4	4.09 g/L
$CaCl_2$	1.16 g/L
KCl	0.69 g/L
$NaHCO_3$	0.20 g/L
KBr	0.10 g/L

Their composition is based on the ASTM recommendations [54, 76]. Another set of samples was exposed for one year to the atmospheric environment in the city of Ghent. Because of the reduced number of samples available, for each alloy and each environment, only one bronze disc was used.

3.2.4 Thickness measurements

The thickness of the corroded layers was measured on 10 different spots of each sample using a coating thickness probe, described in the paragraph 2.4.

3.2.5 XRF measurements

XRF mapping of the surface was carried out using a laboratory micro-XRF system (Eagle-III microprobe. For the description of the technique and the instrument, the reader is referred to paragraph 2.6. The measurements were performed using an X-ray tube voltage of 40 kV, a tube current 50 µA, with a step size 20 µm and beamsize 25 µm. Each map covers a square region of the surface with a side of 500 µm and the measuring time was 50 seconds per point.

3.2.6 XRD analysis

XRD analyses were performed at the UK CRG beam line XMaS at the ESRF. The Mar CCD camera was positioned in plane with its axis at an angle of 40° to the incoming beam which was incident at 10° to the sample surface. The acquisition time was 10 seconds and the X-ray wavelength was 1.55 Å.

In this work all the alloys were analysed by means of linear sweep voltammetry and electron microscopy. Because of the limited number of bronze coupons available, the immersion test in the corrosive solutions was carried out only for three of the alloys (containing 3, 9 and 15% of tin). As a consequence, the characterization of the corroded layers by means of optical microscopy, XRD and XRF were done on these three alloys only.

3.3 Results

3.3.1 SEM examination of the bare alloys

The microstructure of the alloy CuSn 94-6 was previously examined using metallographic techniques [74], which showed the presence of two metallic phases. The backscattered electron microscopy images of a selection of the bronze alloys are presented in Figure 3.2. The analyses verify the presence of two distinct phases in all the alloys. According to the phase diagram, shown in Figure 3.1, alloys containing less than 10 % of tin should present a monophasic structure.

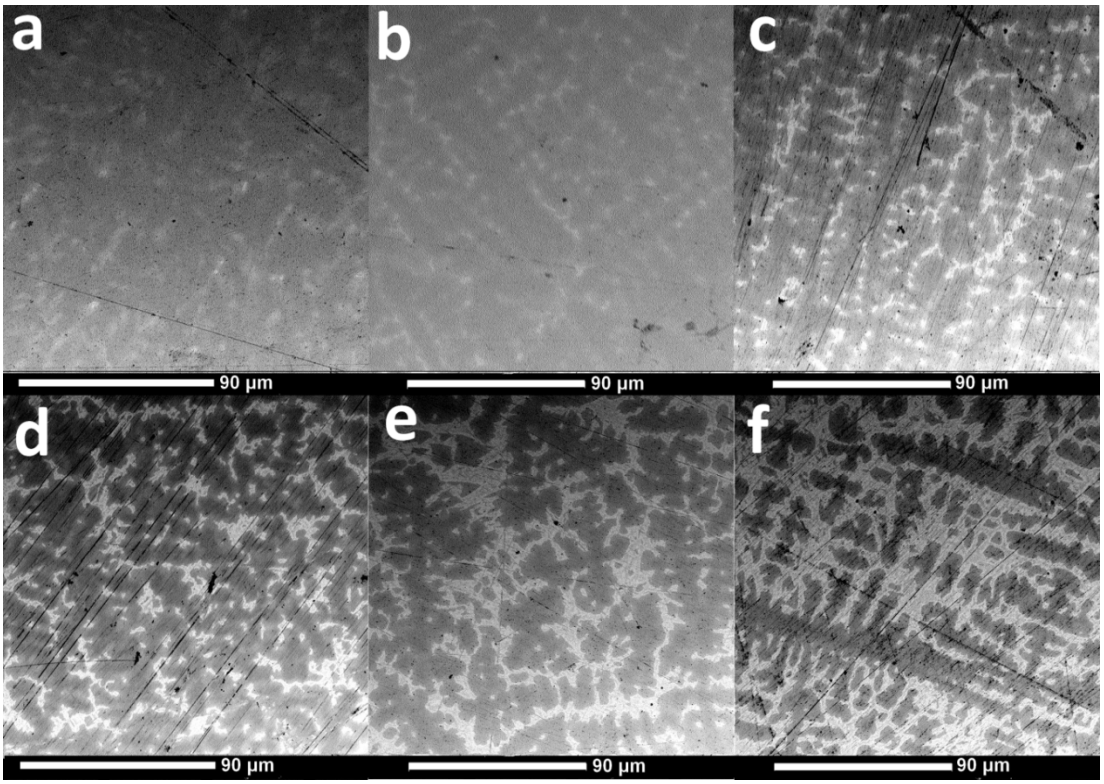

Figure 3.2: Backscattered electron micrographs of CuSn 97-3 (a), CuSn 94-6 (b), CuSn 91-9 (c), CuSn 88-12 (d), CuSn 85-15 (e), CuSn 82-18 (f). Scale bar is 90 µm.

The simultaneous presence of copper rich dendrites (α phase) and of an interdendritic phase (α + δ), richer in tin, in an alloy with a relatively low tin content as the alloy CuSn 94-6) is explained by a rapid cooling of the alloy. A short cooling time, in fact, does not allow the complete absorption of the tin in the α structure [2,4]. This structure, containing both α and δ phase, is the most common in cast

bronze [2]. The darker areas in the centre of the dendrites, well visible in Figure 3.2b and 3.2c, represent areas richer in copper, while the edges have a higher tin content.

3.3.2 Electrochemical tests

The corrosion rate was evaluated for all the alloys, with a tin content varying from 3 to 18 %. The solution used for these experiments is a 0.1 M Na_2SO_4 solution. First, chronopotentiometric measurements were carried out. Here the open circuit potential (OCP) was monitored for 2 hours before the linear polarization experiments were carried out in order to verify the equilibrium conditions of the system. The OCP monitoring is presented in Figure 3.3. In the plot the trend of the OCP versus time represents the typical behaviour of a passivating metal [76], consisting in a slow increment of the potential during the monitoring time. A large variability in the OCP values has been encountered, certainly due to the different compositions of the alloys, but also due to differences in the surface condition. Despite the use of a common protocol for the mechanical cleaning of the electrodes, the OCP values measured reflect the presence of the different surface characteristics even on electrodes of the same alloy.

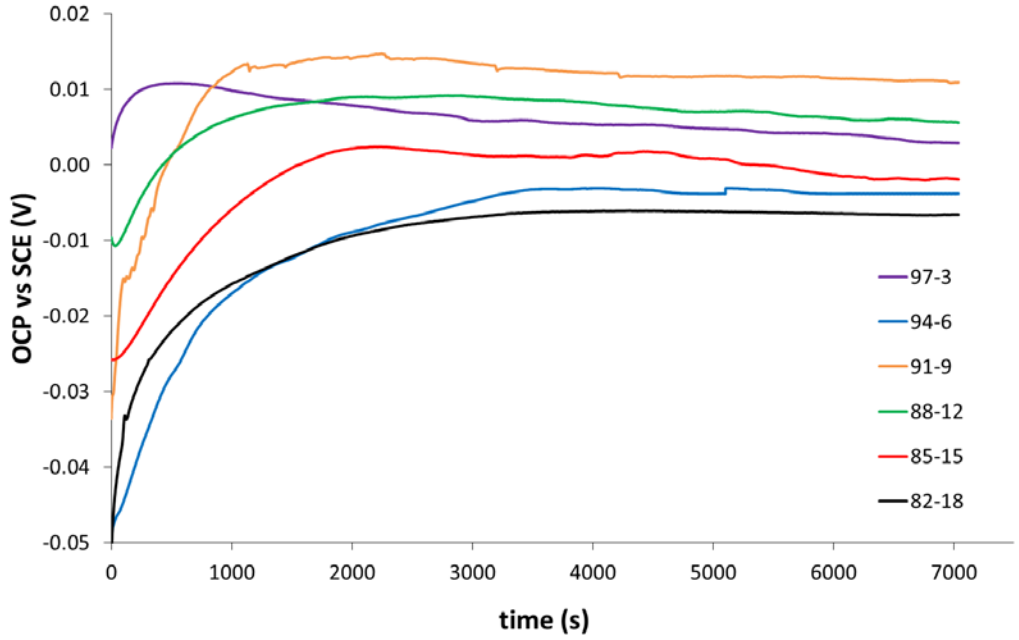

Figure 3.3: OCP trends in 0.1 M Na_2SO_4 for the six alloys.

Polarization experiments were carried out in order to evaluate the polarization resistance (R_p) and the corrosion current density (i_{corr}) of the alloys.

The potentiodynamic curves are presented in Figure 3.4. Large differences can be noticed in the values of the corrosion potential, which vary from -0.08 V to 0.03 V versus the SCE. The potential shift observed does not appear to be connected with the variation of the amount of tin in the alloy, as it can be seen in the chronopotentiometric measurements.

A comparison between the potentiodynamic curves shows that the cathodic curves are very similar to each other and that the percentage of tin in the alloys seems to affect mostly the anodic part of the curve. The slope of the anodic part of the curve for the alloy CuSn 97-3 is characteristic of the absence of passivation phenomena. An increase in tin content from 6 to 15 % causes the slope of the anodic curve to be reduced progressively. The Tafel slope of the anodic curve of alloy CuSn 94-6 is slightly less steep with respect to the 97-3 alloy indicating a slower corrosion rate. A passivation area is clearly visible in the alloys with tin content of 9, 12, 15 and 18 %. In the alloy CuSn 91-9 this region starts around 0.01 V and ends at 0.08 V, where the change in the slope reflects the breakdown of the passivation layer formed.

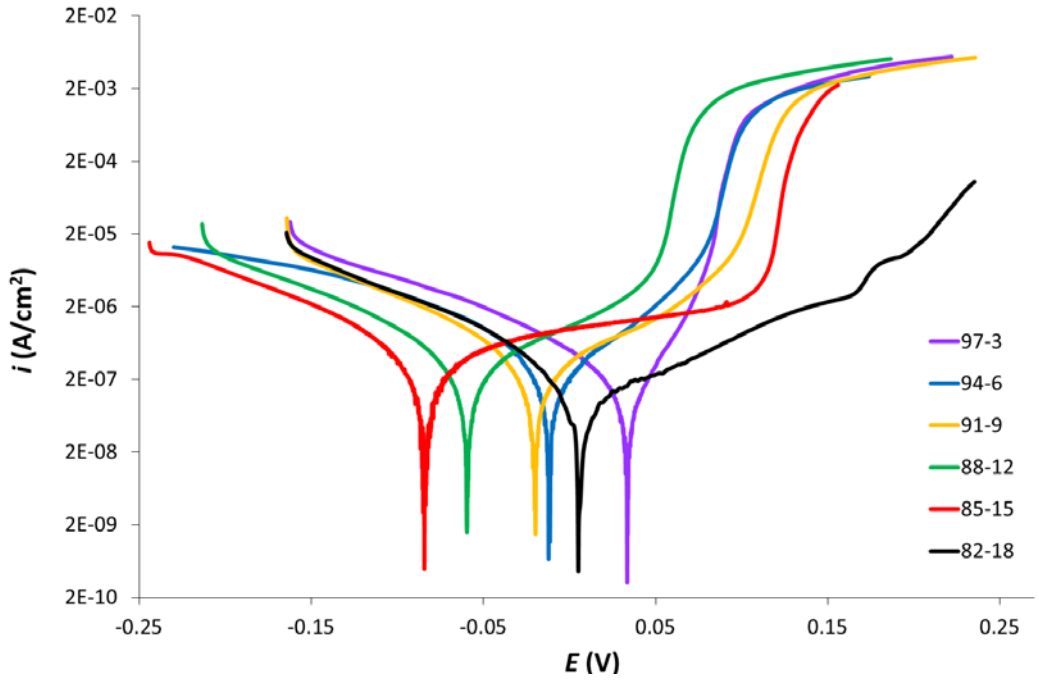

Figure 3.4: Potentiodynamic curves of the six CuSn alloys recorded in 0.1 M Na_2SO_4.

The potential range in which passivation occurs increases with the increase of tin percentage: it changes from 0.07 V of the alloy CuSn 91-9 to 0.15 V of the alloy CuSn 85-15. The Tafel plot of the alloy CuSn 82-18 reflects the presence of passivation phenomena on the surface without evidence of a breakdown potential.

Table 3-IV: II Polarization resistance (R_p) and corrosion current density (i_{corr}) and their respective standard deviation (σ) for the CuSn alloys analysed. For each alloy 6 measurements were performed.

Alloy	R_p (Ω·cm²)	σ	i_{corr} (A/cm²)	σ
97-3	1.2×10^{4}	3.8×10^{3}	5.2×10^{-7}	9.1×10^{-8}
94-6	1.2×10^{4}	2.7×10^{3}	4.8×10^{-7}	5.2×10^{-8}
91-9	1.7×10^{4}	5.9×10^{3}	3.9×10^{-7}	1.3×10^{-7}
88-12	2.1×10^{4}	8.4×10^{3}	3.4×10^{-7}	1.2×10^{-7}
85-15	2.8×10^{4}	1.2×10^{4}	2.1×10^{-7}	7.3×10^{-8}
82-18	3.1×10^{4}	6.7×10^{3}	1.8×10^{-7}	8.3×10^{-8}

The corrosion current density was calculated based on the potentiodynamic measurements and the results are summarized in Table 3.IV. Increasing the amount of tin increases R_p and i_{corr} of the alloys, reducing the corrosion rate. Figure 3.5 illustrates the decreasing trend of i_{corr} as a function of the tin percentage of the alloys. Despite the relatively large error, it is still possible to observe a clear decrease of the corrosion current density as a function of the tin percentage of the alloy.

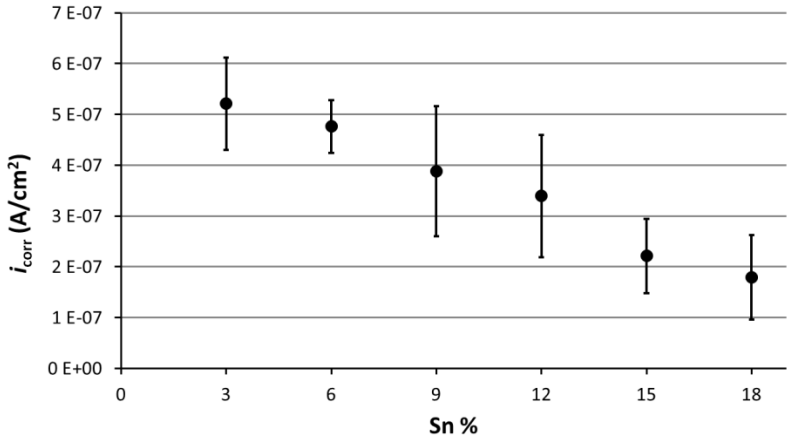

Figure 3.5: Average corrosion current density calculated for the six copper-tin alloys. Error bars are equal to the standard deviation.

The standard deviations, presented in Table 3-IV for R_p and i_{corr}, indicate that the measurements are quite reproducible. The presence of higher standard deviation values for certain alloys can be ascribed to surface differences created by the mechanical cleaning of the bronze coupons before each measurement or by the presence of microcavities. Cast metals, in fact, can present porosity, due to gases dissolved in the melt, or interdendritic holes which have not been filled during the solidification of the alloys [2].

The metallographic analyses previously conducted on the alloy CuSn 94-6 detected the presence of cavities formed during the cooling process by gases dissolved in the smelted mass [74]. The fact that the alloys are characterized by the presence of a biphasic system could also be a source of irreproducibility of the measurements. In Figure 3.2 the presence of the δ phase, increasing with the increase of the tin content in the alloy, was shown. The mechanical cleaning of a bronze coupon, with the removal of its superficial layer, may expose a different pattern every time that each sample is polished. Electrochemical measurements are strictly correlated with the surface properties and a change in the ratio between δ and α phase on the surface can be a cause of change in the electrochemical response and thus of a higher dispersion of R_p and i_{corr} values.

3.3.3 Immersion tests

The alloys CuSn 97-3, CuSn 91-9 and CuSn 85-15, which have been exposed to the corrosive environments, were rinsed with deionized water and were examined by means of optical microscopy.

Figure 3.6 shows the coupons that were immersed in simulated acid rain solution. All of them have developed a brown layer on the surface with darker areas and scattered crystals of a blue-green colour (see magnifications in Figure 3.7). The crystals are not evenly distributed on the surfaces and the also the dark-brown corrosion layer appears to be characterized by colour differences and heterogeneities.

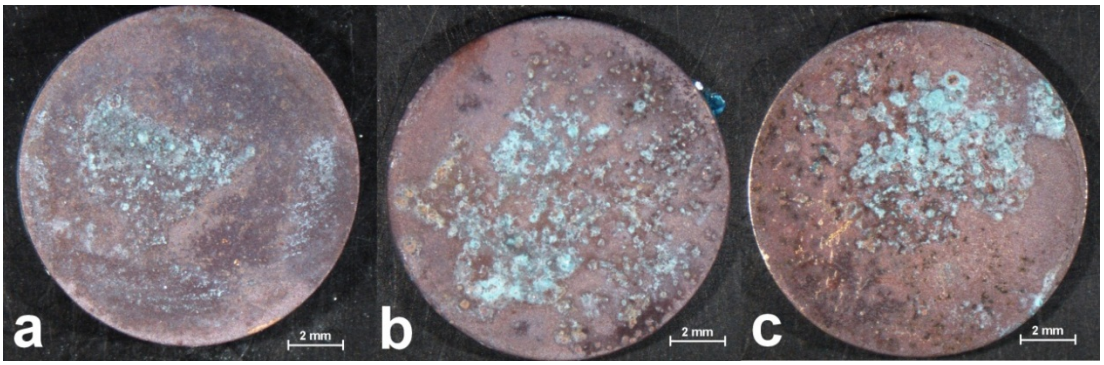

Figure 3.6: Optical micrographs of the bronze coupons immersed in artificial acid rain, Cu-Sn 97-3 (a), Cu-Sn 91-9 (b) and Cu-Sn 85-15 (c). Scale bar is 2 mm.

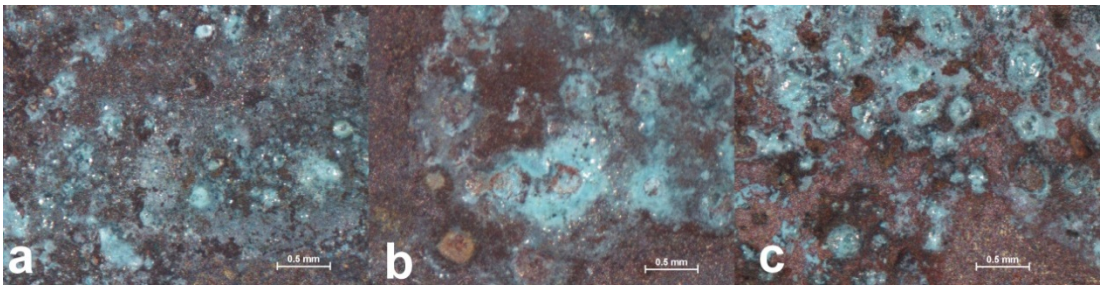

Figure 3.7: Optical micrographs of bronze coupons immersed in artificial acid rain, Cu-Sn 97-3 (a), Cu-Sn 91-9 (b) and Cu-Sn 85-15 (c). Scale bar is 0.5 mm.

The thickness of the corroded layers is summarized in Table 3.V. Results show an average thickness between 9 µm (for the CuSn 97-3 alloy) and 7 µm (CuSn 85-15 alloy).

The bronzes with a higher content of tin (9 and 15 %) are characterized by thinner corroded layers. The alloy CuSn 85-15 presents also small areas free from corrosion products visible in Figure 3.3c in the bottom left part of the coupon.

The high values of standard deviation obtained by the thickness measurements are caused by the heterogeneities present on the surface and the design of the thickness probe. The diameter of the probe is 12 mm, similar to the diameter of the bronze coupons. In order to have reliable results the measurements should be taken far from the edges of the target surface. Considering the small diameter of the samples, all measurements were taken in the centre of the coupons, in the area where scattered crystals are more abundant.

Despite the high standard deviation, it is still possible to observe a decrease of the average thickness of the corrosion layer in the samples with an increased tin content.

Table 3-V: Average thickness of the corroded layer (µm) obtained after exposure to the different corrosive environments: AR (acid rain), SW (seawater) and UE (urban environment).

Corrosive environment	Cu-Sn 97-3	Cu- Sn 91-9	Cu-Sn 85-15
AR	9.4 ± 1.9	7.8 ± 1.6	7.1 ± 1.8
SW	16.1 ± 2.8	11.5 ± 1.3	10.4 ± 1.4
UE	2.1 ± 0.4	1.8 ± 0.6	0.5 ± 0.2
Clean	0.0 ± 0.2	0.0 ± 0.2	0.0 ± 0.1

Figure 3.8 and 3.9 show optical micrographs of the bronze coupons which have been immersed in artificial seawater. The differences in the aesthetic appearance of the corrosion layer between the alloys are more noticeable compared to the samples immersed in simulated acid rain.

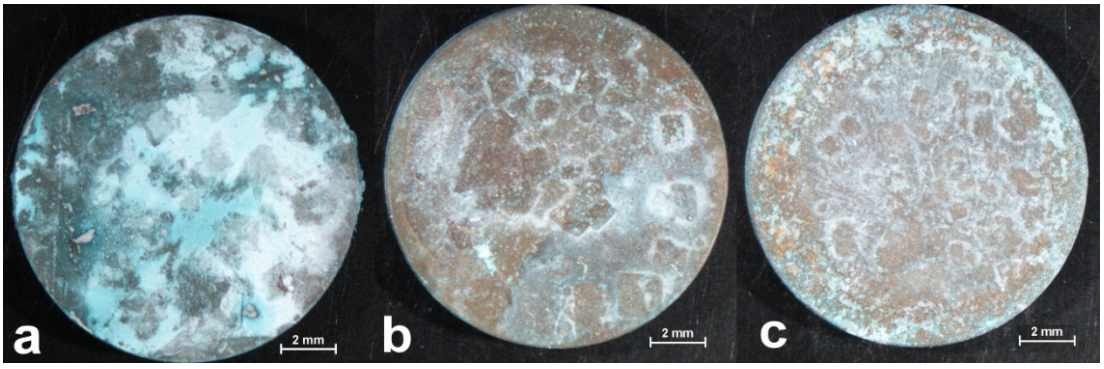

Figure 3.8 Optical micrographs of bronze coupons immersed in artificial seawater, Cu-Sn 97-3 (a), Cu-Sn 91-9 (b) and Cu-Sn 85-15 (c). Scale bar is 2 mm.

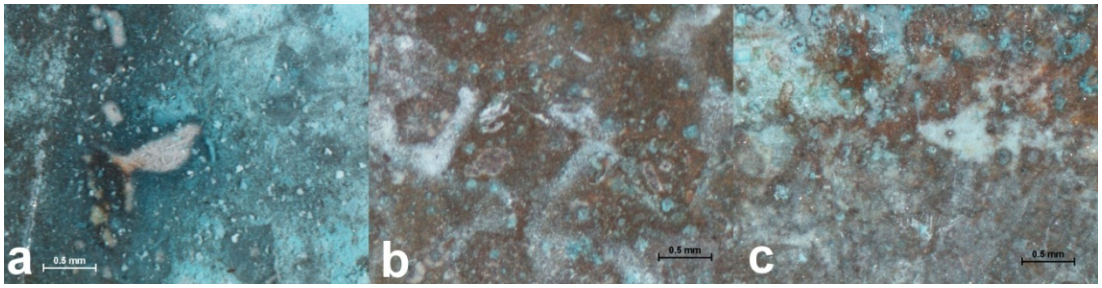

Figure 3.9 Optical micrographs of bronze coupons immersed in artificial seawater, Cu-Sn 97-3 (a), Cu-Sn 91-9 (b) and Cu-Sn 85-15 (c). Scale bar is 0.5 mm.

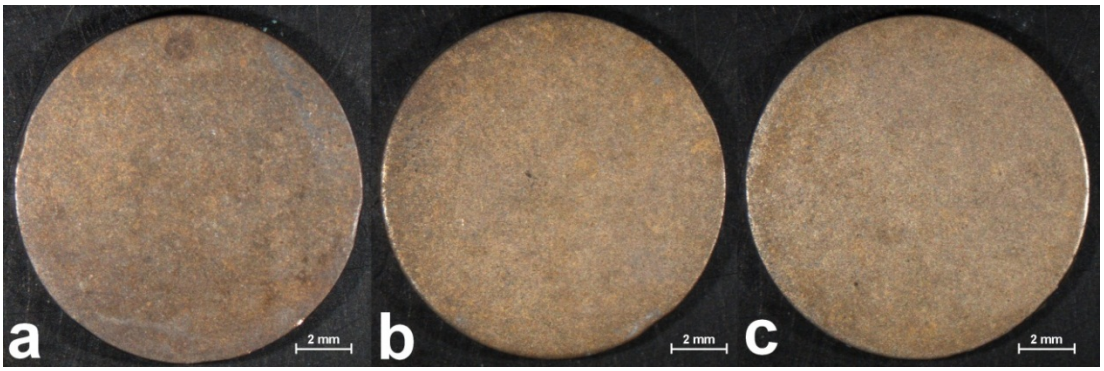

Figure 3.10: Optical micrographs of bronze coupons exposed to an urban environment, Cu-Sn 97-3 (a), Cu-Sn 91-9 (b) and Cu-Sn 85-15 (c). Scale bar is 2 mm.

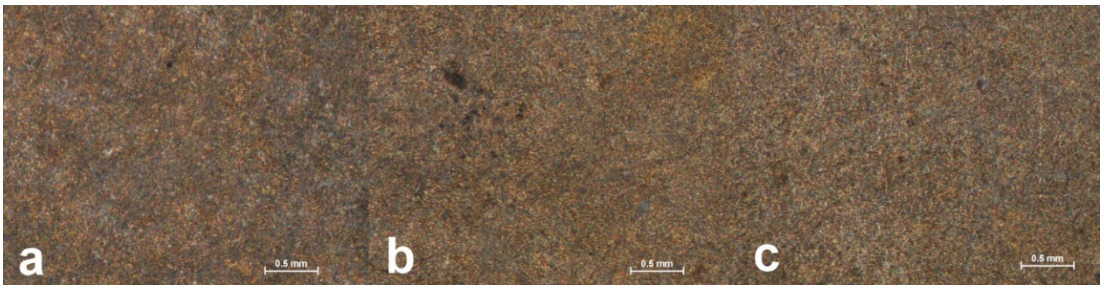

Figure 3.11: Optical micrographs of bronze coupons exposed to an urban environment, Cu-Sn 97-3 (a), Cu-Sn 91-9 (b) and Cu-Sn 85-15 (c). Scale bar is 0.5 mm.

The 3 % tin bronze (Figure 3.8a and 3.9a) shows a blue-green corrosion layer on the entire surface, with some lighter spots due to the presence of white corrosion products, also visible in the magnification of Figure 3.9a. The appearance of the alloys containing 9 and 15 % of tin are very much alike and are characterized by a brown patina covered by a thin and heterogeneous blue-green layer. The thickness of the corrosion layer varies from 16 µm in the CuSn 97-3 alloy to 10 µm in the CuSn 85-15 alloy with a rather high dispersion of the values due to the heterogeneity of the surfaces. Also in this case, when increasing the tin content in the alloy, we observe a reduction in the average thickness of the corrosion layers.

The three samples exposed to an urban environment (Figure 3.10 and 3.11) are characterized in the optical micrographs by a uniform brown-grey superficial layer. The appearance is very similar for the three bronze alloys and the corroded layer formed on CuSn 97-3 and CuSn 91-9 is around 2 µm thick, while CuSn 85-15 has a thinner layer (0.5 µm, in average). The standard deviation of these measurements is

smaller with respect to the analysis on samples immersed in acid rain and seawater because of the homogeneity of the corrosion layers.

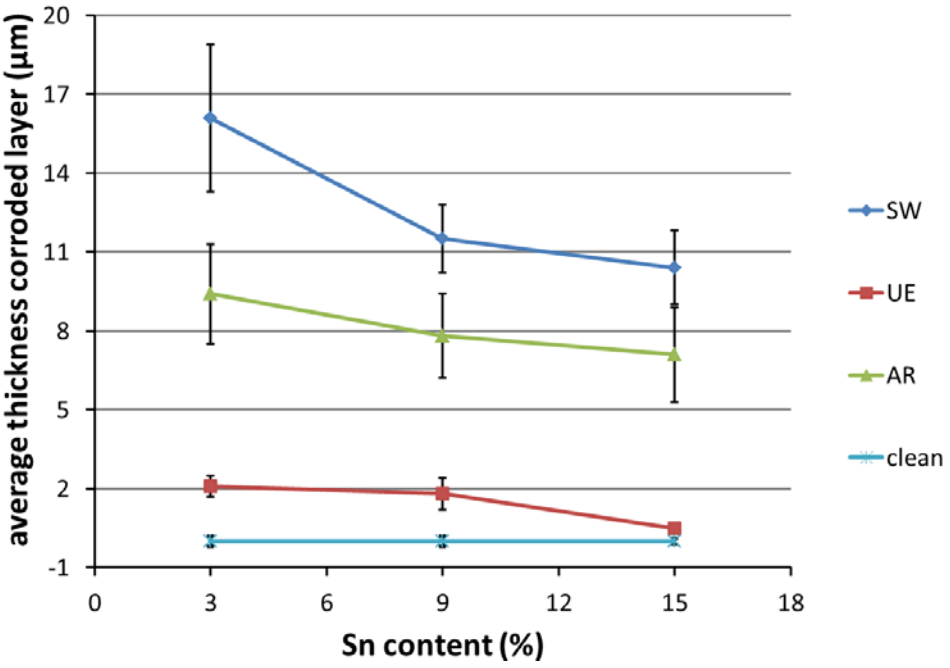

Figure 3.12: Thickness of the corroded layers as a function of the tin content in the bronze alloy and for the three different environments: urban environment (UE), acid rain (AR), seawater (SW).

Overall, the corrosion layer formed on the surfaces is characterized by a variable thickness, depending on the corrosive environment. The measurements show that the corrosion layer formed by atmospheric corrosion is considerably thinner than the one formed by immersion in corrosive solutions.

The samples exposed to an urban environment present in general the thinnest corrosion layers. The bronze coupons immersed in acid rain and seawater have a thicker corrosion layer, characterized by big thickness differences, given by the presence of scattered crystals on the surface. From these data, a general decrease of the corrosion layer thickness can be observed with the increase of tin content in the alloy, independently from the corrosive environment. This trend is illustrated in Figure 3.12, which presents the decrease of corrosion layer thickness in function of tin percentage for all the corrosive environments considered in this study.

3.3.3.1 *XRD evaluation*

The XRD analyses carried out on the corroded samples aimed to investigate the corrosion products formed on the surface. The diffractograms were obtained from the Mar CCD images by using the software esaProject, as described in paragraph 2.8. The patterns have been smoothed using a 3-point running average. Figure 3.13 shows the diffractograms of the samples immersed in synthetic acid rain: the red curve represents the alloy CuSn 97-3, the blue one the alloy CuSn 91-9 and the green one is the alloy CuSn 85-15. In the three diffractograms, the main reflection (peak at 36 degrees) is due to the reflection of cuprite, indicating that this is the main corrosion product present on the surface.

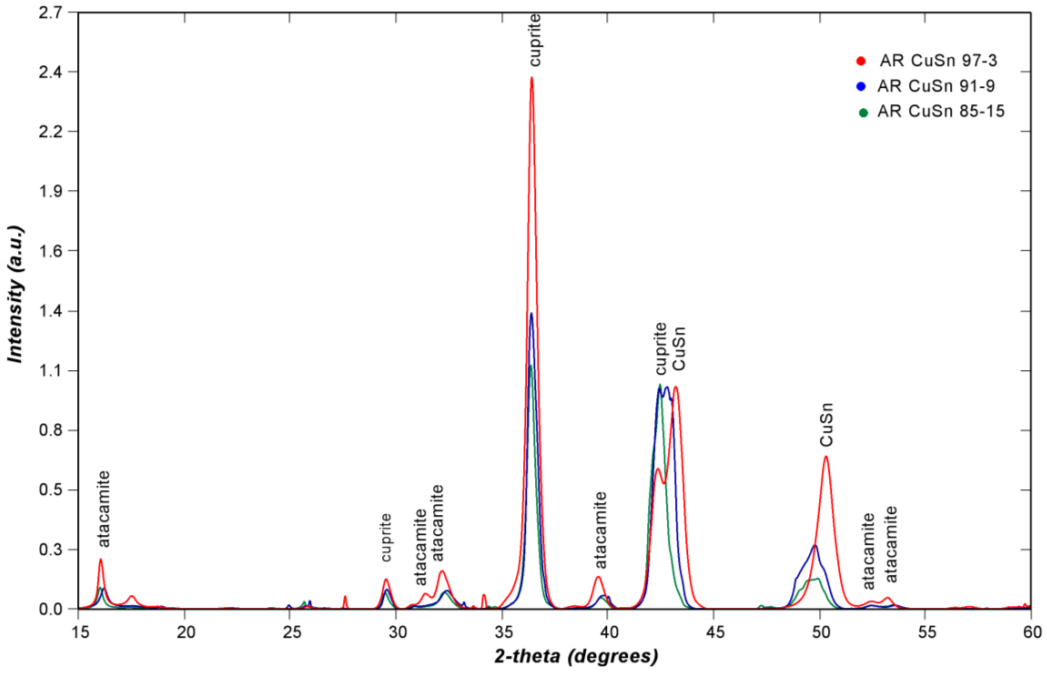

Figure 3.13: XRD diffractograms of the CuSn alloys immersed in artificial acid rain.

The peaks at 43 and 50 degrees represent the main reflections due to the CuSn alloy. Bronze (α and δ phase) have the same crystalline structure of copper (face-centered cubic) [1], but the position of the diffraction peaks does not coincide with the position of the main reflections of copper (respectively at 43.3 and 50.4 degrees) because of the presence of tin atoms that stretch the lattice. The higher the tin content, moreover, the more abundant is the presence of the delta phase [2]. In the

diffractogram this is visible with a progressive shift of the main CuSn reflections towards bigger d-spacing (smaller 2 θ) with the increase of tin content in the alloy [77].

Samples immersed in artificial acid rain are characterized by a thick layer of cuprite. The relative intensities of the cuprite peaks show that the thickness of the oxide layer decreases with the increasing amount of thin in the alloy. As secondary corrosion product, only atacamite is detectable on the sample surfaces.

The immersion in artificial seawater produced the same XRD pattern for the three alloys, presented in Figure 3.14. As is the case for the immersion in acid rain, the surface is characterized by the presence of cuprite. The corrosion layer contains also a mixture of copper hydroxychlorides, with paratacamite being the most relevant. Cassiterite (SnO_2) has also been detected in the three samples.

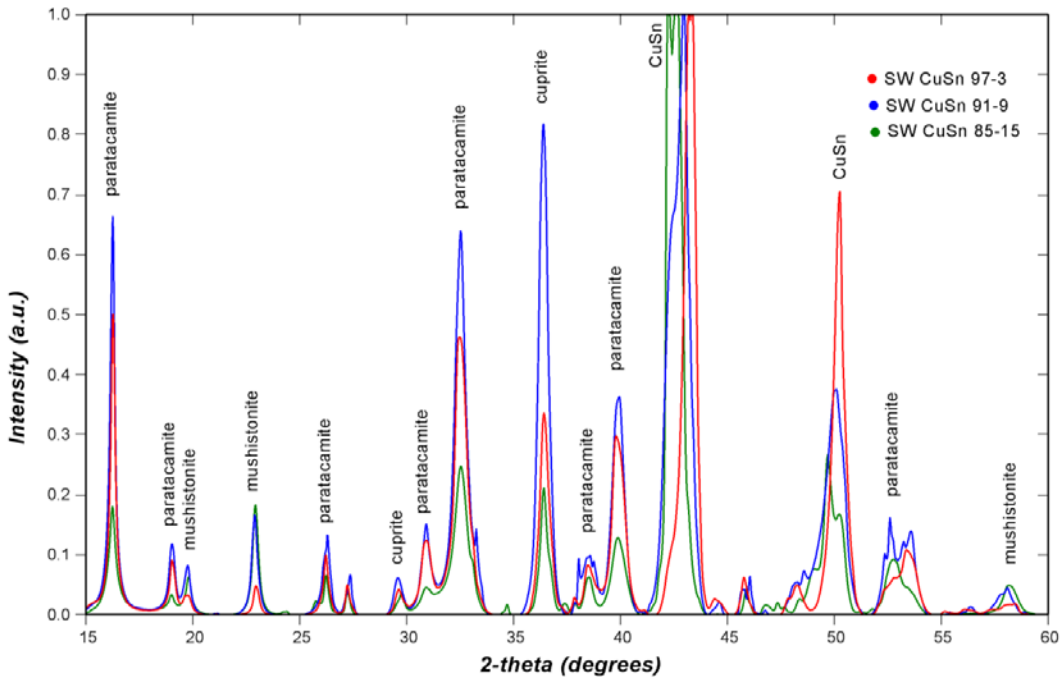

Figure 3.14: XRD diffractograms of the three alloys immersed in artificial seawater.

The diffraction peaks of corrosion products for the samples exposed to an urban environment appear less intense with respect to the relative intensity observed in the other bronze coupons which can be explained by the smaller thickness of the corrosion layer formed on the samples exposed to the atmosphere. Also here the diffractograms (Figure 3.15) show mainly the presence of cuprite and possible traces

of copper hydroxychlorides (paratacamite) and mushistonite ((Cu,Zn,Fe)$SnOH_6$). Considering the low intensity of the XRD reflections, it is difficult to attribute all the diffraction peaks. Nevertheless, in the sample containing 9 and 15 % of tin, peaks of cassiterite (SnO_2) are also visible in the diffractogram, together with possible traces of copper hydrated sulphate, probably chalcantite or brochantite, which is the most common copper hydrated sulphate encountered in bronzes exposed to the urban atmosphere [1,18,28,52,53,78].

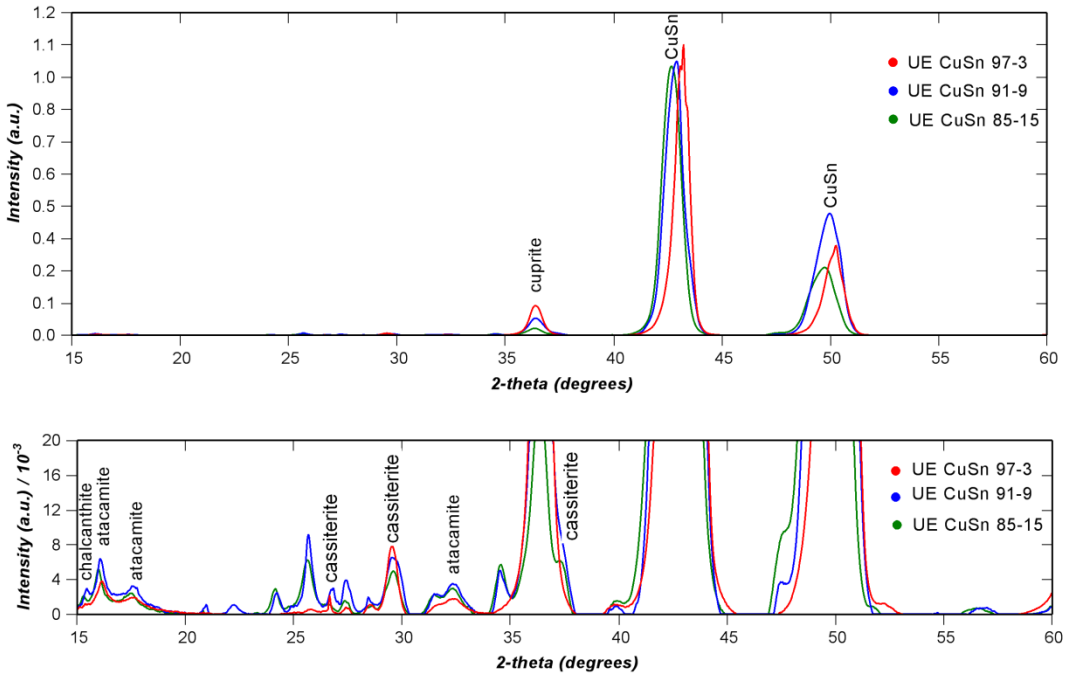

Figure 3.15: XRD diffractograms of the three samples exposed to urban environment (above) and magnification (below).

The thickness of the corroded layer measured and the types of corrosion product identified in bronze coupons exposed to urban environment are consistent with data from literature. In fact, it has been observed that atmospheric corrosion proceeds rather slowly [1,58,79] and that, after cuprite, copper hydroxychlorides are the first copper corrosion products encountered in corrosion layers formed in urban atmosphere [1,79,80].

The comparison between the Mar images collected allows the extraction of more information on the surface characteristics. Figure 3.16 shows the images of the alloy CuSn 91-9 immersed in simulated acid rain (a), simulated seawater (b) and exposed

to an urban environment (c). In all the three images we can distinguish the main reflections given by the alloy at 43, 50 and 74 degrees, indicated by the blue numbers in the figure. Also the main reflections of cuprite are visible in all the samples, indicated by the red numbers, at 36.5, 42.5 and 61 degrees.

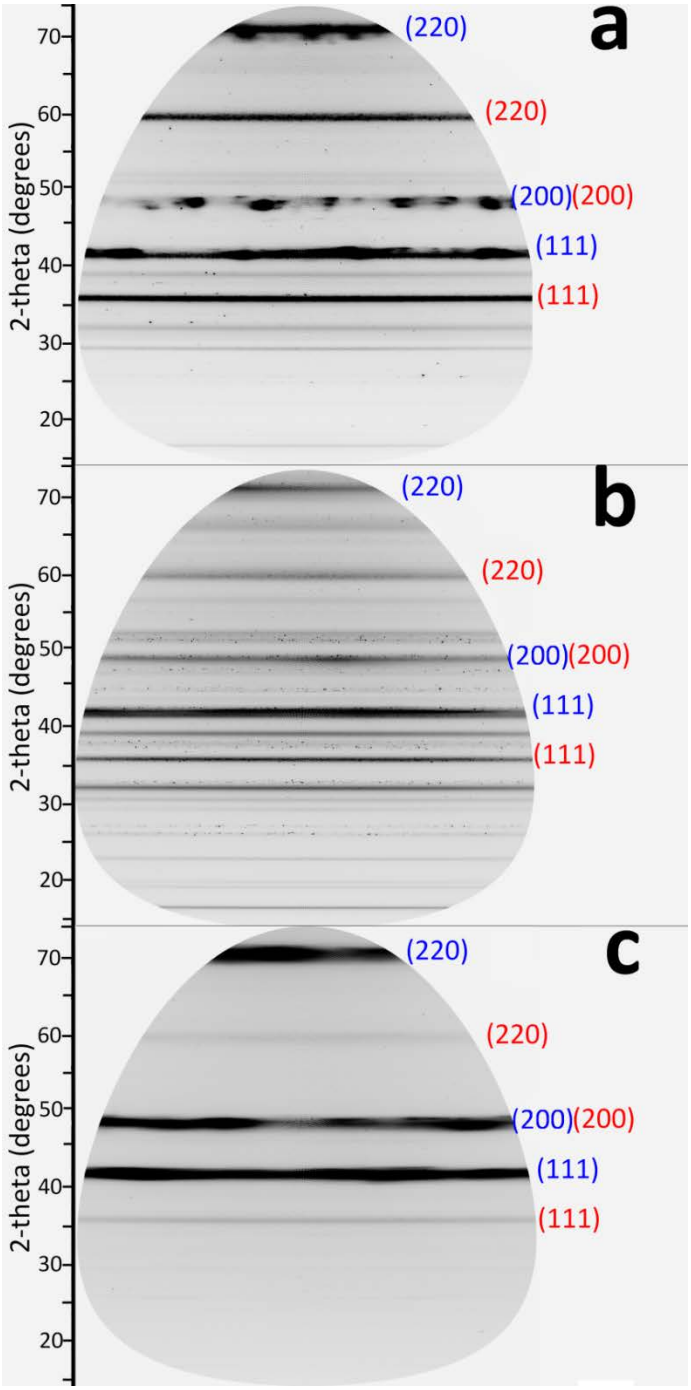

Figure 3.16: XRD images of the alloy CuSn 91-9 immersed in acid rain (a), seawater (b) and exposed to an urban evironment (c). The numbers in blue indicate the main reflections of the CuSn alloy, in red the main reflections of cuprite.

The sample immersed in acid rain present some texture in the rings given by the alloy which is due to the preferred orientation of the crystals on the surface. This effect can be produced by the mechanical polishing carried out to prepare the surface, prior to the immersion in the corrosive solution. This is also observable, but less evident, in the alloy exposed to an urban environment. the reflection bands of the alloy are only slightly visible in the sample immersed in seawater because of the greater thickness of the corroded layer.
The XRD images of samples immersed in a corrosive solution, moreover, present darker spots generated by large crystals. The image of the sample exposed to the atmosphere, on the other hand, only shows continuous diffraction lines, generated by fine and randomly distributed crystals.
Overall the XRD data show that the amount of tin in the alloy affects the growth of the corrosion layer. Higher tin contents are correlated with a thinner corrosion layer, confirmed by the thickness measurements. The composition of the corroded layer, on the other hand, seems to be affected only by the aggressive environments. For a given environment the same minerals have been identified on the surface.

3.3.3.2 XRF evaluation

In the optical examination several irregularities in the surface characteristics have been observed. The XRD analyses aimed to provide information on the minerals present on the bronze surfaces, but it was not possible to correlate the corrosion products with different regions of the surface. The aim of these XRF measurements was to obtain a map of the elemental distribution of the corroded layers in order to correlate the elements (and eventually the minerals detected with the XRD) with particular features of the surface. In particular the distribution of tin needs to be evaluated, considering that the XRD analyses did not reveal a significant presence of tin corrosion products. Tin compounds are often present in archaeological corrosion layers and have an important role in the preservation of bronze objects [5,11,53,54].
For each alloy, a square area of 500 × 500 µm was selected. The latter was done by trying to include zones characterized by different corrosion layers.

In the following paragraphs the XRF maps obtained from the samples are presented and discussed for the three aggressive environments. The results obtained from a selection of samples will be presented here. The entire set of XRF maps is shown in Appendix A.

As was seen in the optical micrographs (Figure 3.6), all the alloys immersed in acid rain present a similar corrosion behaviour, already visible in the types of corrosion product detected with the XRD data. For this reason, only the XRF data obtained from the alloy CuSn 91-9 will be presented here, as a representative sample for this environment. On the surface several elements were detected and they are visible in the sum spectrum of the same area shown in Figure 3.17. Among them, aluminium and silicon must be correlated with the mechanical cleaning of the coupons, done using SiC paper and alumina suspension, and to external contamination (dust). Al and Si, in fact, have been detected on all the bronze samples and their distribution is homogeneous on the entire area analysed and for this reason Al and Si map will not be shown. Si, S, Cl, Cu, Rh and Sn have been also been identified in samples immersed in acid rain and they present differences in the surface distribution. Figure 3.18 presents the XRF maps taken on the alloy CuSn 91-9 immersed in acid rain together with an optical micrograph showing the area selected for the analysis.
As observable in the XRF maps copper is distributed quite homogeneously, except for an area where tin appears slightly more abundant. In the distribution map of sulfur it is also possible to distinguish a small spot characterized by a more elevated number of counts with respect the surrounding region. This may indicate the presence of a tin sulphide or sulphate, which was not detected by the XRD analyses. The low counts of of tin and sulfur, may also explain the absence of tin and sulfur compounds in the diffractogram. Chlorine, on the other hand, seems to be more localized in areas richer in copper, showing the presence of another type of corrosion product, a copper chloride (identified by means of XRD as atacamite).
The signal due to the rhodium (given by scattering from the X-ray tube), must be described separately. As shown in the spectrum in Figure 3.17, the L lines of rhodium are very close and partially overlap the K lines of chlorine. The overlap of these two signals makes the detection of chlorine atoms very difficult, unless it is

very abundant. The separation of the two signals has been done by fitting the spectrum with the AXIL software. The map of the rhodium will be shown for all the samples discussed here together with a map showing the combined signal of chlorine and rhodium. The combination of two signals, in the case of the CuSn 91-9 alloy immersed in acid rain, shows an area with lower counts. This region is partially overlapping with area having higher counts of sulfur and this may indicate the presence of different corrosion products.

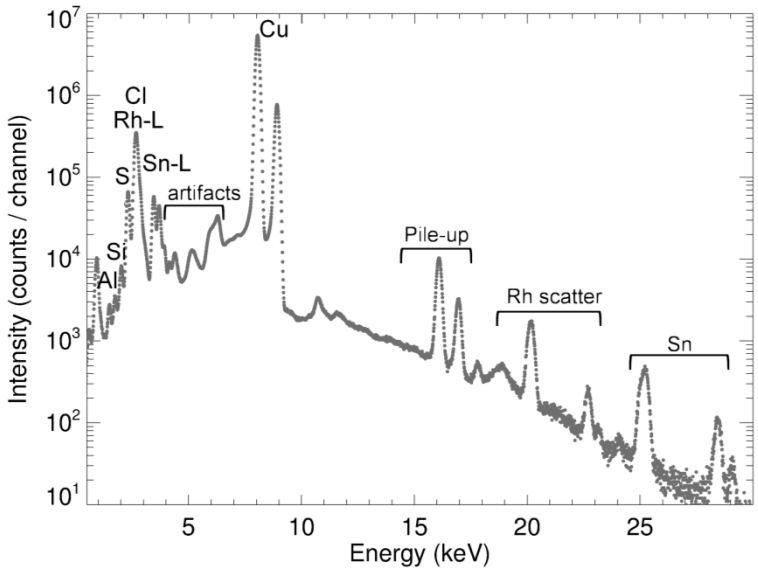

Figure 3.17: XRF sum spectrum of the alloy CuSn 91-9 immersed in acid rain.

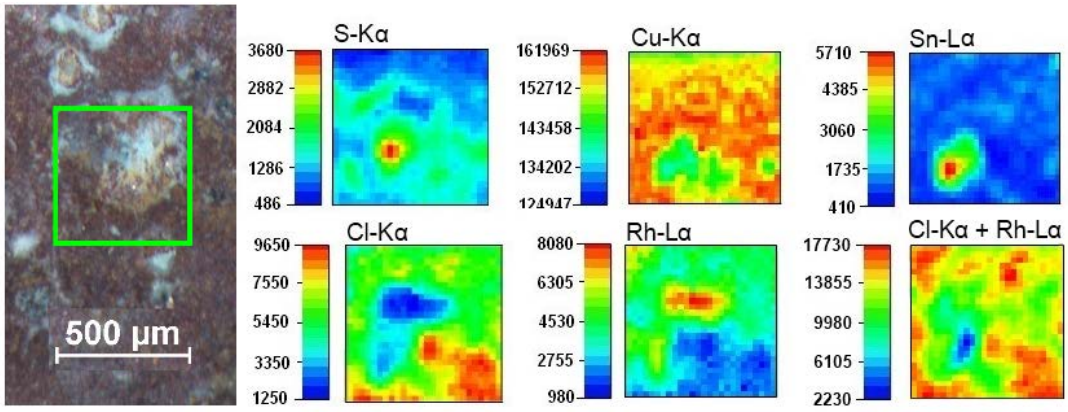

Figure 3.18: Optical micrograph (left) and XRF maps (right) of the CuSn 91-9 alloy, immersed in acid rain. The green square in the optical image indicates the mapped area on the surface. The scale bars indicate the intensity expressed in counts.

It is also interesting to notice that sulfur has been detected on the surface of all the acid rain samples with XRF, while copper and tin sulphates were not identifiable in the XRD spectra. Possible explanations are the use of a different area for the two analyses and the fact that the analyses have been done on a very localized area of the surface: the elemental composition and the diffraction data obtained may be not representative of the entire coupons, especially considering the heterogeneity of the surface characteristics, or the sulphur compounds may be amorphous.

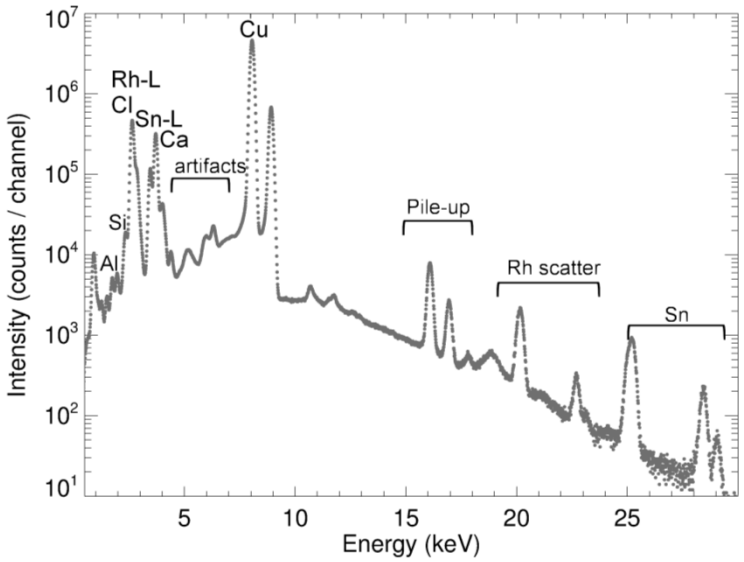

Figure 3.19: XRF sum spectrum of the alloy CuSn 85-15 immersed in seawater.

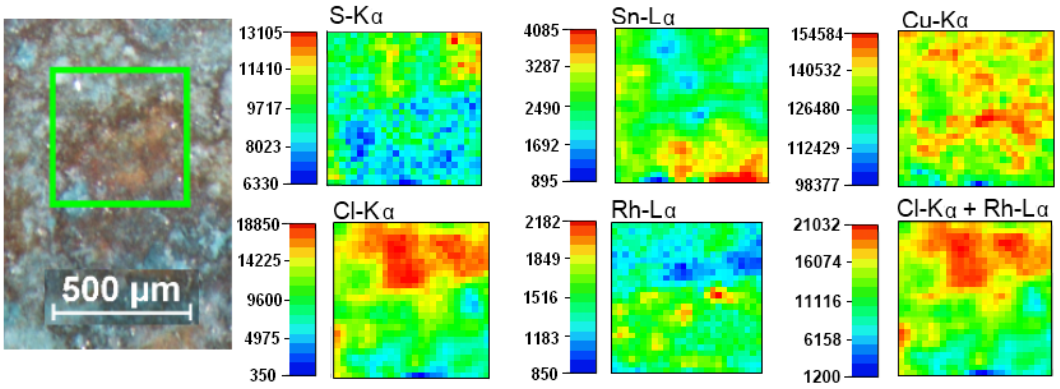

Figure 3.20: Optical micrograph (left) and XRF maps (right) of the CuSn 85-15 sample immersed in artificial seawater. The green square shows the analysed area. The scale bars indicate the intensity expressed in counts.

The immersion in artificial seawater is the treatment that produced the highest difference between the alloys in terms of thickness of the corrosion layer, while the composition of the corroded layer is very similar in the three coupons. The elements detected in these experiments are the same already encountered in samples immersed in acid rain, Al, Si, S, Cl, Ca, Cu, Rh and Sn, as shown in the sum spectra in Figure 3.19. When considering the elemental distribution on the surface, the alloys CuSn 91-9 and CuSn 85-15 present similar results. Figure 3.20 shows the XRF maps of the alloy CuSn 85-15, as an example. The distributions of the elements do not show any noticeable correlation. The distribution of chlorine, on the other hand, appears to be correlated with the areas of light blue colour in the optical micrograph. The combined map of chlorine and rhodium signals is very similar to the chlorine map alone, because of the low counts detected for rhodium.

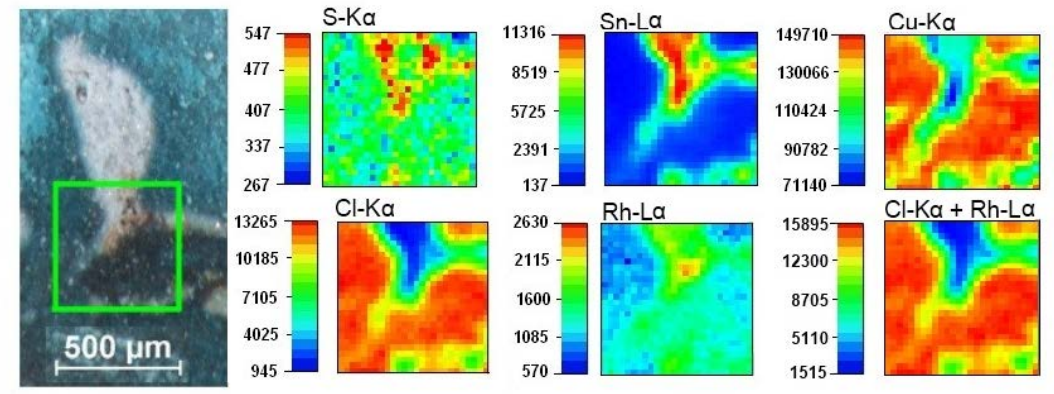

Figure 3.21: Optical micrograph (left) and XRF maps (right) of the CuSn 97-3 sample immersed in artificial seawater. The green square shows the analysed area. The scale bars indicate the intensity expressed in counts.

Some variations in the elemental distribution are visible in the alloy CuSn 97-3, where the thick crust shows more colour differences with respect to the alloys with a higher tin content. The corrosion layer presents blue-green areas (see Figure 3.9), but also small well defined regions characterized by white a colour (Figure 3.21 shows one of this areas). XRF data, which are presented in Figure 3.21, reveal that these portions of the surface are characterized by higher content of tin and sulfur, while the surrounding areas (blue-green) show mostly a copper and chlorine fluorescence. Paratacamite, a copper hydroxychlorides, in fact, has indeed been identified from the diffractogram (shown in Figure 3.14), as being the most

abundant corrosion product on the surface. Because of the low counts from the rhodium, also in this case the combination of chlorine and rhodium signals reflect the information given by the chlorine XRF map. The presence of tin compounds in these samples, on the other hand, was difficult to detect by means of XRD (which with hindsight might have been better acquired with a laboratory diffractometer in this instance), while XRF mapping allowed their detection.

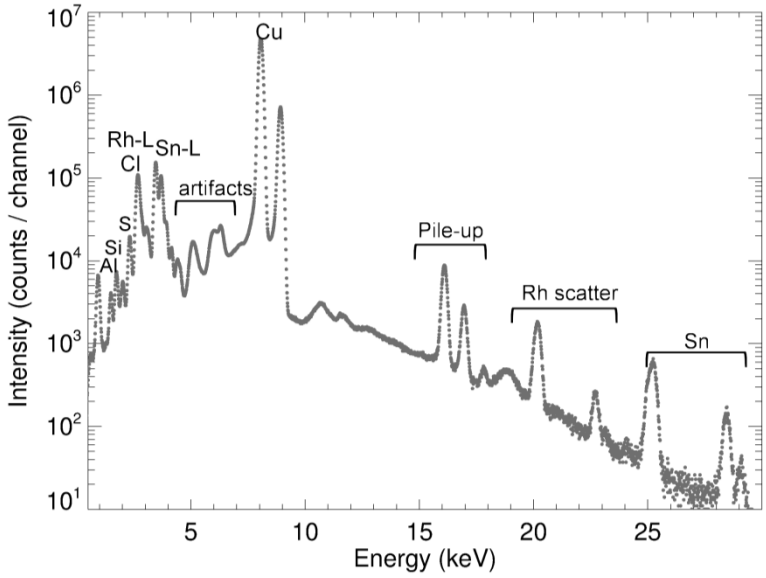

Figure 3.22: XRF sum spectrum of the alloy CuSn 85-15 exposed to urban environment.

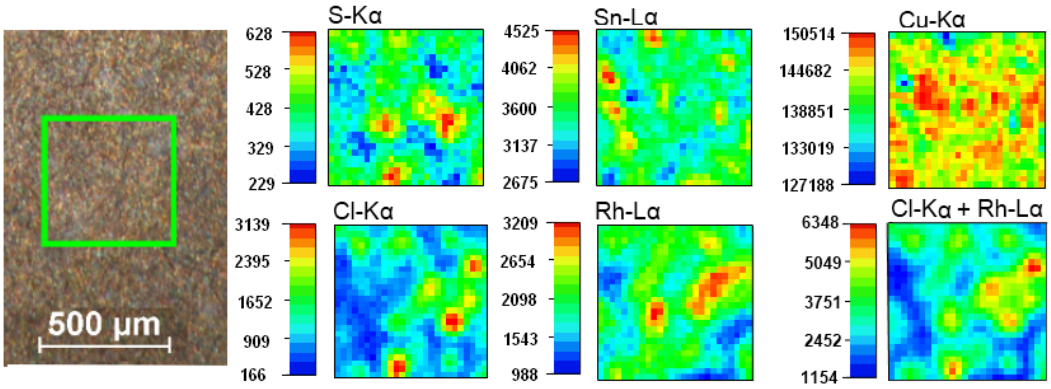

Figure 3.23: Optical micrograph (left) and XRF maps (right) of the CuSn 85-15 sample exposed to urban atmosphere. The green square shows the analysed area. The scale bars indicate the intensity expressed in counts.

Atmospheric corrosion produced thin and uniform corrosion layers on all the alloys. XRF maps taken on the bronze coupons show the presence of the same elements on

the three different alloys. The sum spectrum relative to the sample CuSn 85-15 is presented in Figure 3.22.

The XRF maps of the surface of the alloy CuSn 85-15 exposed to an urban environment are presented in Figure 3.23, together with an optical micrograph showing the area analysed.

Chlorine and sulfur compounds have been detected, confirming the observations made with XRD data which showed the presence of atacamite and brochantite. We observe here that, given the homogeneity of the corroded layer, it is not possible to correlate the distribution of the elements with specific corrosion products. The XRF spectra collected from bronzes CuSn 97-3 and 91-9 exposed to urban environment show the same composition as the alloy CuSn 85-15.

XRF analyses carried out on the corroded bronzes highlight clear differences between the corrosion by exposure to atmosphere and the corrosion by immersion in an aggressive solution. While the bronzes exposed to urban environment show a homogeneous distribution of the elements on the surface, in the samples immersed in synthetic acid rain and artificial seawater the elemental distribution presents visible patterns, which are correlated with the corrosion products detected with XRD measurements.

The interpretation of the XRF maps given here cannot not take into account the effect of the penetration depth of X-rays into the material. The estimation of the penetration depth and its effect is difficult, since a lot of factors would need to considered. The main factors involved are the penetration depth of the incident X-ray beam and the escape depth of the fluorescent X-rays. In general the information obtained from XRF analysis come from a depth varying between few millimetres to few micrometres [81,82]. This depth is related to the beam energy, but it is also strongly influenced by the sample matrix. Elements with a low atomic number, in fact, will produce X-rays with very low energies, and are more difficult to detect even when their signals come from small depths within the sample [6,81-82].

When considering the atomic number of the elements detected in the samples here analysed and the average thickness of the corrosion layers (reported in Table 3.V), it can be deduced that the XRF maps are mostly showing the distribution of the elements in the corrosion layer. This layer, in fact, is constituted by element with a

rather low Z, with the exception of Cu and Sn, which would not be detectable from large sample depths.

On the other hand, the bronzes exposed to an urban environment (like the one showed in Figure 3.22), are characterized by a very thin corrosion layer. The XRF maps, in this case, may contain also information coming from the alloy itself, more than from the corrosion layer.

3.4 Conclusions

This study demonstrated that the variation of the tin content in a binary Cu-Sn alloy influences the corrosion rate. In particular, the electrochemical tests demonstrate that a noticeable decrease of the corrosion current density can be observed with the increase of the tin content in the alloy.

The X-ray diffraction and X-ray fluorescence analyses, coupled with optical microscopy observations, allowed the evaluation of the corrosion layers formed on artificially corroded samples. Three different corrosive environments (artificial acid rain, synthetic seawater and exposure to urban environment) have been tested. The influence of the tin content on the corrosion resistance of the alloys is evident in the thickness of the corroded layer formed on the surface. It was shown that the type of the corrosion products formed was the same, independently from the tin percentage contained in the alloy. An increasing amount of tin appears to slow down the corrosion process, with the effect of having a reduced thickness of the corrosion layers. It must be also pointed out that the limited number of samples prepared affects the interpretation of the results from the point of view of the reproducibility. The use of synthetic acid rain and seawater, moreover, needs to be considered as a necessary simplification in order to simulate real environmental conditions, which differ depending on the location. The results obtained from the immersion tests, nevertheless, are compatible with previous studies conducted on bronzes discussing the composition of natural and artificial patinas.

Besides the identification of corrosion products on the surface, the use of two-dimensional XRD allowed the detection of texture differences between corrosion layers formed in corrosive solutions (acid rain and seawater) and the one formed in

the atmosphere (urban environment). Future corrosion studies, then, should be focused, not only on the characterisation of corroded layers from the point of view of composition and aesthetic appearance, but should also consider crystals dimension and orientation.

References

[1] D.A. Scott, Copper and Bronze in Art – Corrosion, Colorants, Conservation, Getty Publications, Los Angeles, 2002.

[2] D.A. Scott, Metallography and Microstructure of Ancient and Historic Metals, Getty Conservation Institute, Marina del Rey, 1991.

[3] H.J. Leidheiser, The Corrosion of Copper, Tin and their Alloys, John Wiley and Sons, Inc., New York, 1971.

[4] J.R. Davis, Ed., Copper and Copper Alloys, ASM International, 2001.

[5] L. Robbiola, J.-M. Blengino, C. Fiaud, Morphology and mechanisms of formation of natural patinas on archaeological Cu-Sn alloys, Corrosion Science, 40 (1998) 2083–2111.

[6] T. Čechák, M. Hložek, L. Musílek, T. Trojek, X-ray fluorescence in investigations of archaeological finds, Nuclear Instruments and Methods in Physics Research Section B: Beam Interactions with Materials and Atoms, 263 (2007) 54–57.

[7] M. Serghini-Idrissi, M.C. Bernard, F.Z. Harrif, S. Joiret, K. Rahmouni, A. Srhiri, H. Takenouti, V. Vivier, M. Ziani, Electrochemical and spectroscopic characterizations of patinas formed on an archaeological bronze coin, Electrochimica Acta, 50 (2005) 4699–4709.

[8] E. Franceschi, L. Macció, D. Palazzi, L. Rosa, The corrosion of metallic artifacts within different environments. Archaeological objects and laboratory

simulations, in: W. Mourey, L. Robbiola (Eds.), Metal 98: Proceedings of the International Conference on Metals Conservation, Draguignan-Figanières, France, 27-29 May 1998, James & James Ltd, London, 1998: pp. 92–93.

[9] N. Souissi, L. Bousselmi, S. Khosrof, E. Triki, Electrochemical behaviour of an archaeological bronze alloy in various aqueous media: new method for understanding artifacts preservation, Materials and Corrosion, 54 (2003) 318–325.

[10] I. De Ryck, A. Adriaens, F. Adams, Microanalytical metal technology study of ancient near eatern bronzes from Tell Beydar, Archaeometry, 45 (2003) 579–590.

[11] A. Dorigo, C. Fiaud, J.-P. Labbé, L. Robbiola, P. Brunella, H. Böcking, Characterization of the corrosion structures of Roman copper alloys by SEM and EDSX. IMMACO: Improvement of Means of Measurements on Archaeological Copper Alloys for Characterization and Conservation, in: W. Mourey, L. Robbiola (Eds.), Metal 98: Proceedings of the International Conference on Metals Conservation, Draguignan-Figanières, France, 27-29 May 1998, James & James Ltd, 1998: pp. 145–151.

[12] A. Paulin, S. Spaić, A. Zalarb, N. Trampuž-Orelc, Metallographic analysis of 3000-year-old Kanalski Vrh hoard pendant, Materials Characterization, 51 (2003) 205–218.

[13] K.E. Jakielski, M.R. Notis, The metallurgy of Roman medical instruments, Materials Characterization, 45 (2001) 379–389.

[14] E. Figueiredo, P. Valério, M.F. Araújo, J.C. Senna-Martinez, Micro-EDXRF surface analyses of a bronze spear head: Lead content in metal and corrosion layers, Nuclear Instruments and Methods in Physics Research Section A: Accelerators, Spectrometers, Detectors and Associated Equipment, 580 (2007) 725–727.

[15] F. Noli, P. Misaelides, a. Hatzidimitriou, E. Pavlidou, M. Kokkoris, Investigation of artificially produced and natural copper patina layers, Journal of Materials Chemistry, 13 (2003) 114–120.

[16] I.. MacLeod, Identification of corrosion products on non-ferous metal artifacts recovered from shipwrecks, Studies in Conservation, 36 (2011) 222–234.

[17] V. Hayez, V. Costa, J. Guillaume, H. Terryn, A. Hubin, Micro Raman spectroscopy used for the study of corrosion products on copper alloys: study of the chemical composition of artificial patinas used for restoration purposes, The Analyst, 130 (2005) 550–6.

[18] C. Chiavari, K. Rahmouni, H. Takenouti, S. Joiret, P. Vermaut, L. Robbiola, Composition and electrochemical properties of natural patinas of outdoor bronze monuments, Electrochimica Acta, 52 (2007) 7760–7769.

[19] M. Ghoniem, The characterization of a corroded Egyptian bronze statue and a study of the degradation phenomena, International Journal of Conservation Science, 2 (2011) 95–108.

[20] M.A. Crespo, G.P. Cicileo, B.M. Rosales, Electrochemical characterization of patina protectiveness evolution on outdoor bronze sculptures, in: J. Ashton, D. Hallam (Eds.), Metal 04: Proceedings of the International Conference on Metals Conservation, Canberra, Australia, 4 - 8 October 2004, National Museum of Australia, Canberra, 2004: pp. 185–194.

[21] G.P. Cicileo, M.A. Crespo, B.M. Rosales, Comparative study of patinas formed on statuary alloys by means of electrochemical and surface analysis techniques, Corrosion Science, 46 (2004) 929–953.

[22] M.C. Squarcialupi, G.P. Bernardini, V. Faso, A. Atrei, G. Rovida, Characterisation by XPS of the corrosion patina formed on bronze surfaces, Journal of Cultural Heritage, 3 (2002) 199–204.

[23] K. Marušić, H. Otmačić-Ćurković, Š. Horvat-Kurbegović, H. Takenouti, E. Stupnišek-Lisac, Comparative studies of chemical and electrochemical preparation of artificial bronze patinas and their protection by corrosion inhibitor, Electrochimica Acta, 54 (2009) 7106–7113.

[24] J. Virtanen, J. Aromaa, O. Forsén, T. Korpinen, Durability of artificial patina on copper, in: Proceedings of the 15th International Corrosion Congress, Granada 23-27 September 2002, Curran associates Inc., 2007: pp. 697–702.

[25] L. Veleva, P. Quintana, R. Ramanauskas, R. Pomes, L. Maldonado, Mechanism of copper patina formation in marine environments, Electrochimica Acta, 41 (1996) 1641–1646.

[26] B. Rosales, R. Vera, G. Moriena, Evaluation of the protective properties of natural and artificial patinas on copper, Corrosion Science, 41 (1999) 625–651.

[27] D. Šatović, L.V. Žulj, V. Desnica, S. Fazinić, S. Martinez, Corrosion evaluation and surface characterization of the corrosion product layer formed on Cu–6Sn bronze in aqueous Na2SO4 solution, Corrosion Science, 51 (2009) 1596–1603.

[28] E. Bernardi, C. Chiavari, B. Lenza, C. Martini, L. Morselli, F. Ospitali, L. Robbiola, The atmospheric corrosion of quaternary bronzes: The leaching action of acid rain, Corrosion Science. 51 (2009) 159–170.

[29] M.C. Bernard, S. Joiret, Understanding corrosion of ancient metals for the conservation of cultural heritage, Electrochimica Acta, 54 (2009) 5199–5205.

[30] E.S. Friedman, A.J. Brody, M.L. Young, J.D. Almer, C.U. Segre, S.M. Mini, Synchrotron radiation-based x-ray analysis of bronze artifacts from an Iron Age site in the Judean Hills, Journal of Archaeological Science, 35 (2008) 1951–1960.

[31] M.L. Young, F. Casadio, S. Schnepp, J. Almer, D.R. Haeffner, D.C. Dunand, Synchrotron X-ray diffraction and imaging of ancient Chinese bronzes, Applied Physics A, 83 (2006) 163–168.

[32] S. Sánchez Ramos, F. Bosch Reig, J. V Gimeno Adelantado, D.J. Yusá Marco, A. Doménech Carbó, Application of XRF, XRD, thermal analysis, and voltammetric techniques to the study of ancient ceramics., Analytical and Bioanalytical Chemistry, 373 (2002) 893–900.

[33] K. Leyssens, A. Adriaens, C. Degrigny, E. Pantos, Evaluation of corrosion potential measurements as a means to monitor the storage and stabilization processes of archaeological copper-based artifacts, Analytical Chemistry, 78 (2006) 2794–801.

[34] G.M. Ingo, T. de Caro, C. Riccucci, S. Khosroff, Uncommon corrosion phenomena of archaeological bronze alloys, Applied Physics A, 83 (2006) 581–588.

[35] A. Adriaens, Non-destructive analysis and testing of museum objects: An overview of 5 years of research, Spectrochimica Acta Part B: Atomic Spectroscopy. 60 (2005) 1503–1516.

[36] L. Bertrand, L. Robinet, M. Thoury, K. Janssens, S.X. Cohen, S. Schöder, Cultural heritage and archaeology materials studied by synchrotron spectroscopy and imaging, Applied Physics A, 106 (2011) 377–396.

[37] V. Costa, M. Dubus, Impact of the envirnmental conditions on the conservation of metal artifacts: an evaluation using electrochemical techniques, in: T. Padfield, K. Borchersen (Eds.), Museum Microclimates, National Museum of Denmark, Copenhagen, 2007: pp. 63–65.

[38] Bryan Cockrell, Colourful corrosion: black bronze and its enigmatic patina, Papers from the Institute of Archaeology, 19 (2009) 85–90.

[39] A.F. Garbassi, E. Mello, Surface Spectroscopic Studies on Patinas of Ancient Metal Objects, Studies in Conservation, 29 (1984) 172–180.

[40] V. Hayez, a. Franquet, a. Hubin, H. Terryn, XPS study of the atmospheric corrosion of copper alloys of archaeological interest, Surface and Interface Analysis, 36 (2004) 876–879.

[41] C. Debiemme-Chouvy, F. Ammeloot, E.M.M. Sutter, X-ray photoemission investigation of the corrosion film formed on a polished Cu-13Sn alloy in aerated NaCl solution, Applied Surface Science, 174 (2001) 55–61.

[42] F. Ammeloot, C. Fiaud, L. Robbiola, E. Sutter, Some new photoelectrochemical insights into the oxidation mechanisms of a Cu-13Sn alloy in a NaCl aqueous solution with and without 0.1 M BTA, in: W. Mourey, L. Robbiola (Eds.), Metal 98: Proceedings of the International Conference on Metals Conservation, Draguignan-Figanières, France, 27-29 May 1998, James & James Ltd, London, 1998: pp. 229–233.

[43] H. Ling, Z. Qingrong, G. Min, Characterization of corroded bronze Ding from the Yin Ruins of China, Corrosion Science, 49 (2007) 2534–2546.

[44] F. Ospitali, C. Chiavari, C. Martini, E. Bernardi, F. Passarini, L. Robbiola, The characterization of Sn-based corrosion products in ancient bronzes: a Raman approach, Journal of Raman Spectroscopy, 43 (2012) 1596–1603.

[45] P. Ropret, T. Kosec, Raman investigation of artificial patinas on recent bronze - Part I: climatic chamber exposure, Journal of Raman Spectroscopy, 43 (2012) 1578–1586.

[46] T. Kosec, P. Ropret, A. Legat, Raman investigation of artificial patinas on recent bronze-part II: urban rain exposure, Journal of Raman Spectroscopy, 43 (2012) 1587–1595.

[47] M. Kabasakaloglu, T. Kıyak, S. O, A. Asan, Electrochemical behavior of brass in 0 . 1 M NaCl, Applied Surface Science, 193 (2002) 167–174.

[48] N. Souissi, E. Sidot, L. Bousselmi, E. Triki, L. Robbiola, Corrosion behaviour of Cu–10Sn bronze in aerated NaCl aqueous media – Electrochemical investigation, Corrosion Science, 49 (2007) 3333–3347.

[49] E. Sidot, N. Souissi, L. Bousselmi, E. Triki, L. Robbiola, Study of the corrosion behaviour of Cu–10Sn bronze in aerated Na2SO4 aqueous solution, Corrosion Science, 48 (2006) 2241–2257.

[50] G. Kear, B.D. Barker, F.C. Walsh, Electrochemical corrosion of unalloyed copper in chloride media––a critical review, Corrosion Science, 46 (2004) 109–135.

[51] L.M.M. Santos, M.M. Lemos Salta, I.T.E. Fonseca, The electrochemical behaviour of bronze in synthetic seawater, Journal of Solid State Electrochemistry, 11 (2006) 259–266.

[52] C. Chiavari, E. Bernardi, C. Martini, F. Passarini, F. Ospitali, L. Robbiola, The atmospheric corrosion of quaternary bronzes: The action of stagnant rain water, Corrosion Science, 52 (2010) 3002–3010.

[53] L. Robbiola, K. Rahmouni, C. Chiavari, C. Martini, D. Prandstraller, a. Texier, H. Takenouti, P. Vermaut, New insight into the nature and properties of pale green surfaces of outdoor bronze monuments, Applied Physics A, 92 (2008) 161–169.

[54] L. Morselli, E. Bernardi, C. Chiavari, G. Brunoro, Corrosion of 85-5-5-5 bronze in natural and synthetic acid rain, Applied Physics A: Materials Science & Processing, 79 (2004) 363–367.

[55] C. Leygraf, Atmospheric corrosion, in: P. Marcus, J. Oudar (Eds.), Corrosion Mechanisms in Theory and Practice, Marcel Dekker, Inc., New York, 1995: pp. 421–455.

[56] M. Wadsak, I. Constantinides, G. Vittiglio, A. Adriaens, K. Janssens, M. Schreiner, F.C. Adams, P. Brunella, M. Wuttmann, Multianalytical study of patina formed on archaeological metal objects from Bliesbruck-Reinheim, Mikrochimica Acta, 133 (2002) 159–164.

[57] N.W. Farro, L. Veleva, P. Aguilar, Copper Marine Corrosion: I . Corrosion Rates in Atmospheric and Seawater Environments of Peruvian Port, The Open Corrosion Journal, (2009) 130–138.

[58] J. Nairn, K. Fitzgerald, A. Atrens, Atmospheric corrosion of copper, in: I. MacLeod, S.L. Pennec, L. Robboiola (Eds.), Metal 95, Proceedings of the International Conference on Metals Conservation, Semur En Auxois 25-28 September 1995, James & James Ltd, London, 1997: pp. 86–88.

[59] G. Brunoro, A. Frignani, A. Colledan, C. Chiavari, Organic films for protection of copper and bronze against acid rain corrosion, Corrosion Science, 45 (2003) 2219–2231.

[60] L. Campanella, O.C. Alessandri, M. Ferretti, S.H. Plattner, The effect of tin on dezincification of archaeological copper alloys, Corrosion Science, 51 (2009) 2183–2191.

[61] I. Mabille, A. Bertrand, E.M.. Sutter, C. Fiaud, Mechanism of dissolution of a Cu–13Sn alloy in low aggressive conditions, Corrosion Science, 45 (2003) 855–866.

[62] K. Rhattas, Corrosion Inhibition of Copper in 3% NaCl Solution by Derivative of Aminotriazole, Materials Sciences and Applications, 2 (2011) 220–225.

[63] K.F. Khaled, M.N.H. Hamed, K.M. Abdel-Azim, N.S. Abdelshafi, Inhibition of copper corrosion in 3.5% NaCl solutions by a new pyrimidine derivative: electrochemical and computer simulation techniques, Journal of Solid State Electrochemistry, 15 (2010) 663–673.

[64] Y. Feng, K.-S. Siow, W.-K. Teo, K.-L. Tan, A.-K. Hsieh, The corrosion behaviour of copper in neutral tap water. Part I: corrosion mechanisms, Corrosion Science, 38 (1996) 369–385.

[65] Y. Feng, K.-S. Siow, W.-K. Teo, K.-L. Tan, A.-K. Hsieh, The corrosion behaviour of copper in neutral tap water. Part II: determination of corrosion rates, Corrosion Science, 38 (1996) 387–395.

[66] Y. Feng, K.-S. Siow, W.-K. Teo, K.-L. Tan, A.-K. Hsieh, Corrosion mechanisms and products of copper in aqueous solutions at various pH values, Corrosion, 53 (1997) 389–398.

[67] R. Bertholon, R. Bell, J.-M. Blengino, N. Lacoudre, Stabilisation de la corrosion d'un objet archéologique en alliage cuivreux par electrolyse á faible polarization dans le sesquicarbonate de sodium, in: I. MacLeod, S.L. Pennec, L. Robbiola (Eds.), Metal 95, Proceedings of the International Conference on Metals Conservation, Semur En Auxois 25-28 September 1995, James & James Ltd, London, 1997: pp. 209–219.

[68] A. Elia, K. De Wael, M. Dowsett, A. Adriaens, Electrochemical deposition of a copper carboxylate layer on copper as potential corrosion inhibitor, Journal of Solid State Electrochemistry, 16 (2012) 143–148.

[69] W.R. Fischer, B.D. Wagner, H. Siedlarek, B. Fussinger, I. Hanssel, N. von der Bank, The influence of chloride ions and light on the corrosion behavior of copper alloys in aqueous environments with special regard to bronze disease, in: I. MacLeod, S.L. Pennec, L. Robboiola (Eds.), Metal 95, Proceedings of the International Conference on Metals Conservation, Semur En Auxois 25-28 September 1995, James & James Ltd, London, 1997: pp. 89–94.

[70] J. Muller, Etude électrochimique et caractérisation des produits des corrosion formés à la surface des bronzes Cu-Sn en milieu sulfate, PhD Thesis, Université Paris-Est, 2010.

[71] J. Muller, G. Lorang, E. Leroy, B. Laik, I. Guillot, Electrochemically synthesised bronze patina: characterisation and application to the cultural heritage, Corrosion Engineering, Science and Technology, 45 (2010) 322–326.

[72] Liliana Gianni, Corrosion behavior of bronze alloys exposed to urban and marine environment; an innovative approach to corrosion process understanding and to graphical results presentation, PhD Thesis, Sapienza Univesrity of Rome, Ghent University, 2011.

[73] L. Gianni, M. Cavallini, S. Natali, A. Adriaens, Wet and Dry Accelerated Aging Tests in a Spray Chamber to Understand the Effects of Acid Rain Frequencies on Bronze Corrosion, International Journal of Electrochemical Science, 8 (2013) 1822–1838.

[74] L. Linders, De Invloed van het Tingehalte op het Corrosiegedrag van Archeologische Bronzen, Master Thesis, Koninklijke Academie voor Schone Kunsten Antwerpen, 2010.

[75] H. Ding, G.A. Hawthorn, L.H. Hihara, Inhibitive Effect of Seawater on the Corrosion of Particulate-Reinforced Aluminum-Matrix Composites and Monolithic Aluminum Alloy, Journal of The Electrochemical Society, 156 (2009) 352-359.

[76] C. Degrigny, Introduction to the use of electrolytic techniques in conservation, internal report Instituut Collectie Nederland, Amsterdam, 2003.

[77] E. Sidot, A. Kahn-Harari, E. Cesari, L. Robbiola, The lattice parameter of α-bronzes as a function of solute content: application to archaeological materials, Materials Science and Engineering: A, 393 (2005) 147–156.

[78] T.E. Graedel, Corrosion Mechanisms for Silver Exposed to the Atmosphere, Journal of The Electrochemical Society, 139 (1992) 1963–1970.

[79] R. Holm, E. Mattsson, Atmospheric corrosion test of copper and copper alloys in Sweden - 16 year results, in: S.W. Dean, E.C. Rhea (Eds.), Atmospheric Corrosion of Metals. A Symposium, ASTM International, Baltimore, 1982: pp. 85–105.

[80] P. Letardi, Laboratory and field tests on patinas and protective coating systems for outdoor bronze monuments, in: J. Ashton, D. Hallam (Eds.), Metal 04: Proceedings of the International Conference on Metals Conservation, Canberra, Australia, 4 - 8 October 2004, National Museum of Australia, Canberra, 2004: pp. 379–387.

[81] M.S. Shackley, ed., X-ray fluorescence spectrometry (XRF) in geoarchaeology, in: Geoarchaeology, Springer, 2011.

[82] G. Lawes, A.M. James, Scanning Electron Microscopy and X-ray Microanalysis. Analytical Chemistry by Open Learning, J. Wiley & Sons Inc., Chichester, UK, 1987.

4. Characterization of metals and corrosion products using voltammetry of microparticles

4.1 Introduction

Among the different electrochemical methods that have been applied in the field of archaeometry and conservation, the use of voltammetry of microparticles (VMP) has become increasingly significant [1–9].

VMP is based on the mechanical transfer of solid insoluble sample particles onto a solid electrode, followed by the application of a specific polarization technique, such as linear and cyclic voltammetry or square wave voltammetry [10,11]. Because of its versatility, this technique can be used for a wide range of applications.

The amount of sample needed for the analysis is less than 1 µg [9–13]. Thanks to the trace amount of sample required, VMP can be considered a non-invasive and sensitive technique complying with the requirements of non-destructiveness needed for the study of artistic and archaeological objects [3,9]. Apart from the identification of metals and alloys in different fields of research [3,4,8,13–19], voltammetry of microparticles appears to be the most suitable technique for the electrochemical characterization of minerals, also when one deals with a mixture of mineral phases [14,20,21].

In cultural heritage studies, the applications of VMP include the characterization of pigments [6,7,22,23] and organic dyes [24,25] allowing the study of various works of art such as paintings, manuscripts and textiles. Other studies have also been carried out on archaeological ceramic materials, where VMP allows the characterization of ceramic glazes [26–28], thereby demonstrating the versatility of the technique. Also the study of glasses and ceramics has been done because they may contain electroactive species as colourants and opacifier agents [9,27,28].

This work presents the application of VMP in the investigation of historical bronze objects. In first instance the procedure for the electrochemical identification of copper alloys and their corrosion products is examined. This is done using reference

materials. There then follows the study of two historical bronzes, where the metal composition and the corrosion products present were characterized electrochemically. In addition the results have been validated by complementary analyses using XRF and XRD. The application of VMP to the study of heritage artefacts has been developed in recent years [9]. The aim of this work is to show the capability of the technique not only for the analysis of alloys, but in particular for the identification of specific copper minerals. The latter is done, in view of a possible application as a screening technique for the identification of minerals in corrosion layers. As an example, the capability of the technique to detect dangerous corrosion products, such as copper chlorides, can help conservators in the choice of the correct preservation method.

4.2 Experimental

4.2.1 Reference materials

Metal standards (Cu 99.99 %, Sn 99.99 %, Pb 99.95 % and a Cu58-Zn39-Pb3 alloy) were obtained from Goodfellow Cambridge Ltd. (UK). Cuprite (Cu_2O, 99.9 %) and nantokite (CuCl, 99.9 %) powders were purchased from Alfa Aesar GmbH & Co KG (Karlsruhe, Germany), copper acetate ($Cu(CH_3COO)_2$, 98 %) tenorite (CuO, 99.9 %) powders were purchased from Sigma-Aldrich, while malachite ($Cu_2CO_3(OH)_2$) and azurite ($Cu_3(CO_3)_2(OH)_2$), were purchased from Kremer Pigments Inc. (New York). Brochantite ($Cu_4SO_4(OH)_6$), atacamite ($Cu_2(OH)_3Cl$, orthorhombic) and paratacamite ($Cu_2Cl(OH)_3$, hexagonal) were synthesized according to the protocols described below.

Paraffin impregnated electrodes (PIGE) were prepared using graphite rods of 6 mm diameter (Sigma-Aldrich) and paraffin wax (melting temperature 52°C, Sigma-Aldrich) according to the method described below [14].

4.2.2 Synthesis of reference corrosion products

Atacamite, paratacamite and brochantite are not available commercially and they have been synthesized according to protocols described in literature [29–31].

Atacamite was synthesized on a copper plate by using the following procedure [29]. First the polished copper plate was degreased with acetone, pickled in 5 % H_2SO_4, neutralized in 7 % NaOH and rinsed thoroughly with deionized water. The plate was then heated in air up to 250 °C and a 33 % NH_4Cl solution was sprayed on the hot surface four times in a row. Between each application, the plate was left to dry for approximately 20 minutes and then rinsed with distilled water. At the end of the procedure, the surface is covered by an irregular blue-green coloured layer. XRD analysis carried out on the corrosion layer show that is composed of atacamite.

Paratacamite was prepared in two steps [30]. First a polished copper plate was immersed in a saturated copper (II) chloride solution for 2 hours, then rinsed with distilled water and left to dry in air for 24 hours. After that the copper plate was exposed to ~100% RH for 24 hours, by using a desiccator filled with damp K_2SO_4 (which has a relative humidity of 97%). After 24 hours the copper plate was left to dry in air. The surface is covered by a light green layer, which was confirmed to be paratacamite by XRD analyses.

Synthetic brochantite was obtained by adding a 0.1 M NaOH solution drop wise to a 100 mL of a 0.1 M $CuSO_4$ solution, while stirring until the pH of the resulting solution was 8.0 [32]. The precipitate formed, dried in air, was identified as brochantite by means of XRD .

XRD diffractograms are available in appendix B.

4.2.3 Electrode preparation and sampling procedure

Paraffin impregnated graphite electrodes (PIGE) were prepared by immersing graphite rods in liquid paraffin wax, previously melted in an oven at 60 °C, under vacuum (using a water operated vacuum pump) until the impregnation was complete. The impregnation of the graphite rod with paraffin can be considered complete when no more air bubbles are visible in the paraffin.

The modification of the PIGE surface with samples from metallic surfaces is simple and minimally invasive: it is in fact sufficient to rub the PIGE tip on the surface. A simple contact is enough to transfer sufficient microparticles to be detected by VMP.

For the analyses of the archaeological corrosion layers, a few milligrams of crust were sampled with a small scalpel from areas presenting a homogeneous appearance. The latter were located with optical microscopy. The powders, reference and historical samples, were crushed in an agate mortar. The obtained particle size, verified by electron microscopy, was of the order of few microns. The electrode tip was then rubbed across the powders so that the particles stick to the electrode. The measurements were repeated five times and for each measurement the PIGE was rubbed across the same powdered sample.

The sampling procedure must be done with particular care so as not to transfer too much sample onto the solid electrode. The adhesion of a large number of microparticles, in fact, causes the formation of broad oxidation/reduction peaks [20]. In order to verify that the number of particles on the surface is not excessive, it is sufficient to wipe the surface of PIGE gently with a tissue to remove the ill adherent particles. When no more traces of particles are visible on the tissue, all the excess of sample has been removed, leaving only the necessary amount of sample on the PIGE. Practice in the manipulation of the PIGE and the sampling procedure is essential in order to achieve reproducible results.

As there are no guidelines for the correct sampling procedure from archaeological artefacts, it was decided to take a sample from each artefact after a careful examination of the object under the optical microscopy, in the attempt of selecting a sampling area which is representative for the corrosion layer considered. The choice of the sampling area remains, thus, very subjective. The VMP analyses carried out on corrosion products, and presented in this work, have the objective of highlighting the effectiveness of the technique for the identification of copper minerals, being aware that a unique sample taken from the corrosion layer unlikely can fully describe the complex composition of an archaeological crust.

4.2.4 Reagents and experiments

VMP analyses were performed using square wave voltammetry with an amplitude of 15 mV and a frequency of 8 Hz. The reference electrode was a saturated calomel electrode and a platinum grid was used as a counter electrode. Prior to the

measurements, the solution was deoxygenated for 20 minutes with a nitrogen flux. The electrolytes used were 0.1 M NaOH, 0.1 M oxalic acid and 0.1 M NH_4Cl for the identification of the metals in the alloys, and a 0.5 M potassium phosphate buffer (pH 7.0) for the characterization of copper corrosion products. All chemicals were purchased from Merck. The analyses in different electrolytes, selected on the basis of literature data [8,15,36,37], are necessary in order to create a database of oxidation peaks to be kept as reference for further analyses objects of unknown composition.
The XRF measurements on the Danish coffin decoration were performed using a micro-XRF instrument developed in the department of Analytical Chemistry at Ghent University. The beam size was 120 µm horizontally by 46 µm vertically. XRF mapping on the artefact labelled Tonn07-204 was carried out with the Eagle-III microprobe (see paragraph 2.6 for the description of the instruments). An area of 500 µm by 1400 µm was mapped. The step size used was 25 µm and the counting tome was 1000 s/step.

4.2.5 Archaeological samples

Several historical bronze objects were analysed. The artefact, which has been dated to the XVIIth century AD (Figure 4.1), is part of a set of small bronze ornaments from a coffin that has been located in the crypt under Sabro Church (near Aarhus, Denmark). These little ornamented nail heads were usually used in rows (and large amounts) to fix leather or textile bands on a coffin-edge [33].

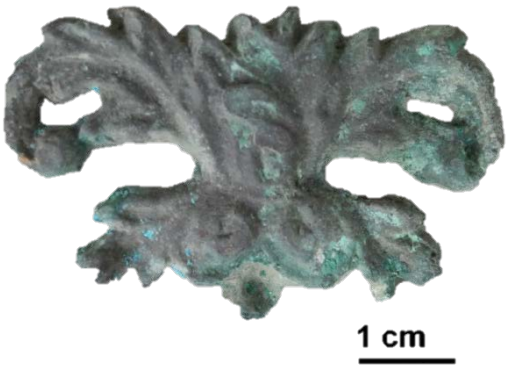

Figure 4.1: Photograph of a bronze coffin decoration (Denmark, XVIIth century).

The rest of the archaeological samples are part of the collection of the Flemish Heritage Institute (Onroerend Erfgoed – OE). They consist of bronze artefacts from archaeological excavations in Oudenburg and Tongeren, Belgium.

4.2.5.1 Oudenburg (Belgium)

The site of Oudenburg, on the Belgian coast near Ostend, was excavated between 2001 and 2005. In this area parts of a Roman "castellum" (fort) have been found. The site presents evidence of different occupation phases including a sequence of three wooden and two stone castella. The duration of the occupancy went from the III century AD to the end of the V century AD [34]. The list of samples from Oudenburg that have been analysed are listed in Table 4.I

Table 4-I: List of artefacts analysed from the site Oudenburg together with their excavation number.

Label	Object
OS 2000A	ring
OS 2000E	bracelet (fragments)
OS 2000G-A	piercer
OS 2000G (M.KL.2.14) -2	bracelet (fragments)
OS 2023-2	ring
OS 44248	nut
OS 4906	plate
OS 4949	fragments
OS 5.2.86	ring
OS 7904	fragments
OS 7907	sieve (fragment)
OS 7624 C	coins (agglomerate)
OS 7966 C	fibula
OS 80050 KL113	fragments
OS 8956	stud

Figures 4.2 to 4.5 present some of the objects excavated in Oudenburg. They all have a thick crust that makes the interpretation of the shape in certain cases difficult. The photographs of all the artefacts analysed are presented in appendix C (in the scale bar, each square is 1 cm wide).

Figure 4.2: Photograph of a nut (OS 44248).

Figure 4.3: Photograph of a ring (OS 2000A).

Figure 4.5: Photograph of a sieve fragment (OS 7907).

Figure 4.4: Photograph of a piercer (OS 2000G-A)

4.2.5.2 Tongeren (Belgium)

Tongeren, one of the oldest cities in Belgium, was conquered by Julius Cesar in 54 BC and since then became the capital of the Roman administrative district of *Civitas Tungrorum*, a wide region that covers the eastern Belgium and the southern part of the Netherlands. The city became later a Christian diocese in the middle age and the area has never been abandoned until the present time.

Figure 4.6: Photograph of a fragment of a fibula (TONN07-612).

Figure 4.7: Photograph of a coin (TONN07-0522).

Figure 4.8: Photograph of a pin head (TONN07-0494).

Figure 4.9: Photograph of a coin (TONN07-0664).

The archaeological objects studied in this work come from two different archaeological excavations within the city. On the site called "Tongeren Busstelplaats", the excavation started on 26 November 2007 and continued until 8 December 2007. The site is situated between the Novemberwal and the Sacramentstraat. The objects are Roman and date between the 1st and 4th century AD.

A selection of objects from this site is presented in Figures 4.6 to 4.9. In contrast to the artefacts found in Oudenburg their corrosion crust is thinner, making the identification of the original surface easier. Most of the objects are coins from different periods, indicating the intensive use of the site and the importance of the city during roman period. The list of artefacts analysed is shown in Table 4-II.

Table 4-II: List of artefacts analysed from the site Tongeren Busstelplaats together with their excavation number.

Label	Object
TONN07-0494	pin head
TONN07-0522	coin
TONN07-0610	coin (fragments)
TONN07-612	fibula (fragments)
TONN07-0661	coin
TONN07-0664	coin
TONN07-0669	plate (fragments)
TONN07-0692	fibula (fragments)
TONN07-0716	coin
TONN07-0907	coin
TONN07-0984	coin
TONN07-204	mirror (fragments)
TONN07-351	ear scoop
TONN07-432 A	plate (fragment)
TONN07-996 B	fibula (fragment)

Table 4-III: List of artefacts analysed from the site Tongeren Momberstraat together with their excavation and OE numbers.

Label	OE number	Object
TO-05-MO-005	VIOE 0916.1	plate
-	VIOE 0916.2	pendant
TO-05-MO-16	VIOE 0916.3	fragments
TO-05-MO-009	VIOE 0916.5	pin head
TO-05-MO-004	VIOE 0916.6	bracelet (fragments)
TO-05-MO-15	VIOE 0916.7	coin

The second site considered in this study is called "Tongeren Momberstraat", were a small scale rescue excavation was undertaken between March and May 2005. The objects recovered are Roman and date back to the middle of the 1st century AD [35].

Examples of the artefacts analysed are shown in Figures 4.10 to 4.13. The table 4-III lists the objects analysed in this study.

Figure 4.7: Photograph of fragments of a pendant (VIOE 0916.2).

Figure 4.6: Photograph of fragments of a plate (VIOE 0916.1).

Figure 4.8: Photograph of a coin (VIOE 0916.7).

Figure 4.9: Photograph of a bracelet (VIOE 0916.6).

4.3 Results and discussion

4.3.1 The analysis of metals and alloys

4.3.1.1 Reference materials

In order to show the presence of microparticles on the PIGE surface after sampling, backscattered electron images were obtained of the electrode surface (Figure 4.14). The surface of a clean electrode (Figure 4.14a) appears smooth and homogenous. After rubbing the tip on a metallic copper plate, it is possible to observe the

presence of copper microparticles on the surface (Figure 4.14b). These are characterized by a lighter colour with respect to the background colour. Figure 4.14c shows the electrode surface modified with lead particles. The number of lead particles is clearly larger than in the case of copper because the metal is softer and there is a very thin tarnished layer (made of very finely dispersed oxide particles) present on the lead plate [38].

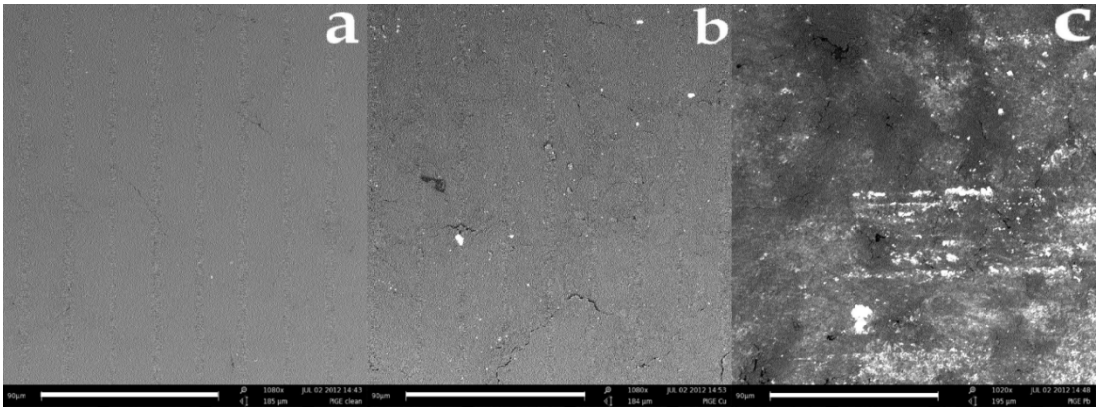

Figure 4.10: Backscattered electron micrograph of the surface of PIGE electrodes clean (a) and after sampling on a Cu plate (b) and a Pb plate (c).

The choice of the electrolyte for the electrochemical characterization of the microparticles is fundamental to the separation of the voltammetric peaks of the different elements [8,14,20]. Voltammetric peaks of different metals may occur in the same potential region, causing difficulties in the correct identification of the metal. An example is presented in Figure 4.15, which shows the voltammograms obtained from Cu, Sn and Pb particles, sampled from the respective metallic plates, analysed in 0.1 M oxalic acid (a), 0.1 M NaOH (b) and 0.1 M NH_4Cl (c). The intensity of the current peak is related to the amount of material present on the electrode surface [20].

In a 0.1 M oxalic acid solution only one current peak was observed for copper and tin. The peak is related to the oxidation of Cu (0.07 V) and the oxidation of Sn (-0.57 V) to form Cu(II)-oxalate and Sn(II)-oxalate complexes respectively [13,18]. In the case of lead we observe two oxidation peaks (-0.52 and -0.44 V), due to the formation of Pb(II) and Pb(IV) species [39]. It is important to notice that the

oxidation peaks of Sn and Pb overlap, leading to the impossibility of distinguishing the two signals when analysing an alloy containing the two metals.

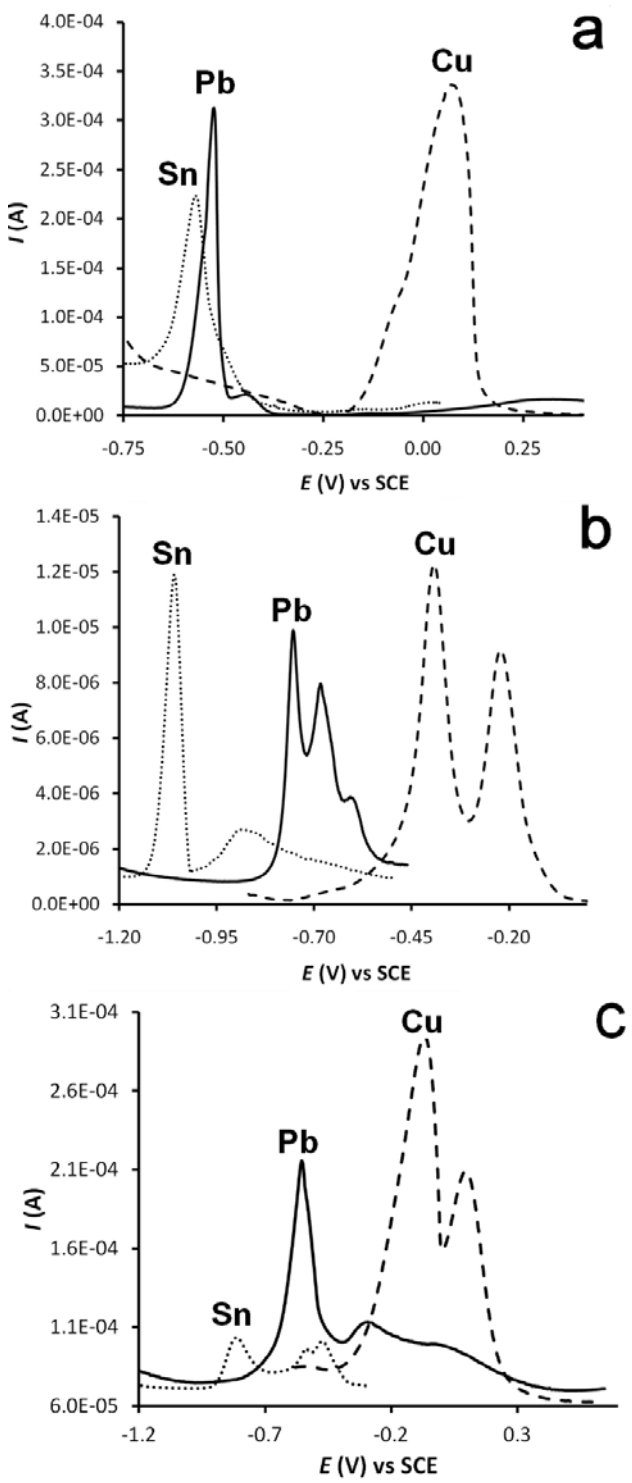

Figure 4.11: Square wave voltammogram of Cu, Pb and Sn in 0.1 M oxalic acid (a) and 0.1 M NaOH (b) and 0.1 M NH_4Cl (c).

When performing the same experiment in a 0.1 M NaOH solution we can observe a clear separation of the different voltammetric peaks. Sn presents a double peak (-1.1 and -0.9 V) which refers to the oxidation of Sn to Sn^{2+} and of Sn^{2+} to Sn^{4+} [40]. The copper signal is also characterized by the presence of a double peak (0.43 and -0.23 V), representing the oxidation to Cu^{+} and Cu^{2+} [41], while the signal of Pb is more complex due to the formation of Pb^{2+}, Pb^{4+}, but also of other intermediate oxides [42].

In 0.1 M NH_4Cl, the voltammogram of copper shows two oxidation peaks, at -0.08 V and 0.08 V. They are related to the formation of Cu(I) and Cu(II) species [43]. The signal given by the lead oxidation presents a characteristic sharp peak at -0.55 V volt, due to the oxidation to Pb (II), and a sequence of less intense peaks due to the formation of Pb(IV) complexes [44]. The tin signal is characterized by the presence of peaks due to the formation of Sn (II) and Sn (IV) species. It must be noticed, nevertheless, that the oxidation peak of Sn(IV) overlaps with the oxidation peak of Pb (II). This partial overlap makes NH_4Cl a suitable electrolyte for detecting the presence of Cu, Sn and Pb. However, for a correct and precise determination of the signal of lead and tin, the use of NaOH as electrolyte is preferable.

The reproducibility of the VMP measurements is connected to the number of microparticles that are present on the PIGE surface. Some practice is required in order to ensure the sampling of the same amount of powder and obtain a reproducible curve [21]. Another possible source of lack of reproducibility is the inhomogeneity of the sample. This issue is particularly important in the case of complex samples, such as archaeological corrosion layers, and can be solved only by selecting single crystals for the VMP analysis by using an optical microscope.

4.3.1.2 Coffin ornament from Denmark

The sampling of the coffin ornament from Denmark was done by rubbing the PIGE on an area that was free from corrosion layers. The metallic surface is clearly visible in Figure 4.16 (indicated by an arrow). Figure 4.17 shows the square wave voltammograms obtained in 0.1 M NH_4Cl from this archaeological object (full line) and from a standard Cu-Zn-Pb alloy (dashed line) as a comparison. The analysis of

a reference alloy containing copper, zinc and lead has been carried out since the comparison of the data obtained did not match the voltammogram of reference alloys containing copper, tin and lead.

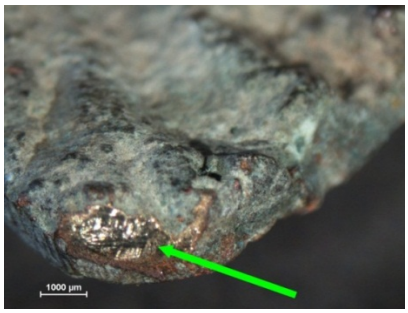

Figure 4.12: Optical micrograph of the sampling point (indicated by the green arrow) on the Danish bronze artefact.

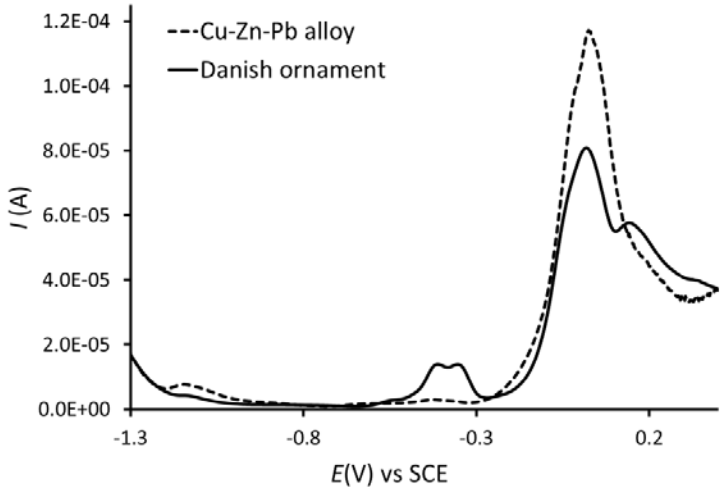

Figure 4.13: Square wave voltammogram of the Danish artefact. The full line is the Danish artefact, the dotted line is the voltammogram of a Cu-Zn-Pb alloy.

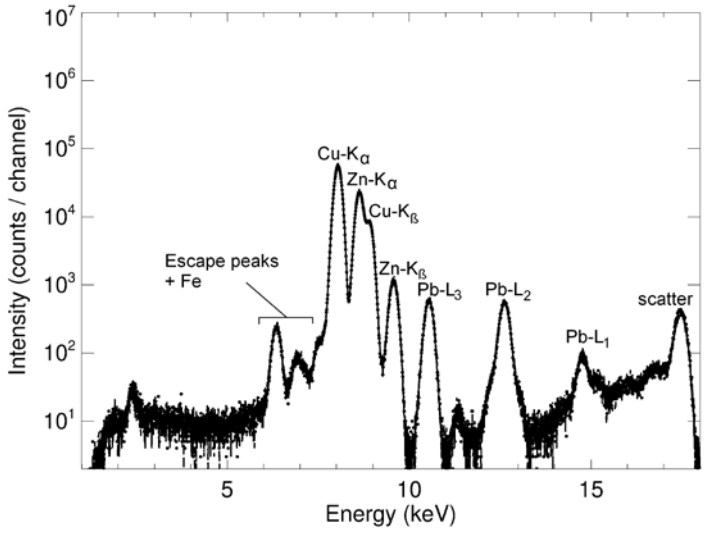

Figure 4.14: XRF spectrum taken on the Danish artefact (sampling spot is visible in figure 4.16).

NH_4Cl has been chosen for this measurement because it provides a good separation between the Cu, Zn, Pb and Sn oxidation peaks. In the case of the Danish coffin ornament, the use of NH_4Cl was sufficient to identify the elements constituent the alloy. The composition of the archaeological object can thus be identified as a leaded brass, based on the presence of the oxidation peaks of Zn, Pb and Cu. The electrochemical data collected are in good agreement with the XRF spectrum collected on the same area of the object (Figure 4.18). Quantitative information has been obtained from the XRF measurements: the composition is reported in Table 4.IV. The presence of iron in the artefact can be due from impurities in the raw materials used for the casting.

The detection limits of VMP analysis with PIGE electrodes are difficult to establish because of the sampling method. Even if the amount of sample attached to the PIGE surface can be made reproducible with some practice, it is always difficult to determine the exact quantity present on the electrode. For this reason quantitative results with PIGE electrode are not possible.

Table 4-IV: composition of the alloy of the Danish coffin ornament obtained from XRF measurements.

Element	Percentage
Cu	73.00 ± 1.9
Zn	24.36 ± 0.39
Pb	2.46 ± 0.25
Fe	0.18 ± 0.01

4.3.1.3 Tonn07-204

The case of the sample labelled Tonn07-204 (Figure 4.19) is unique because of the presence of a fragment characterized by an area free from corrosion (indicated in figure 4.20), which is different from the other fragments from the same objects and from all the other artefacts investigated in this study. The object is fragmented and it was not possible to determine the original shape.

Figure 4.15: Photograph of Tonn07-204. The artefact is fragmented into six pieces.

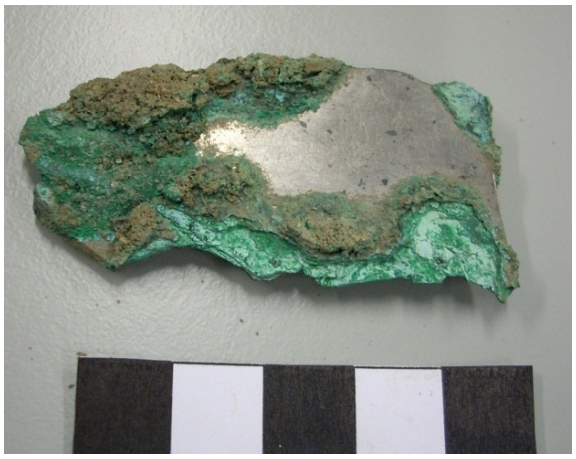

Figure 4.16: Photograph of a fragment of the artefact labelled Tonn07-204. On the top right, the original metallic surface of the object is visible.

The object Tonn07-204 has been analysed because it is the only artefact, among the ones investigated, which still presents a metallic surface. The rest of the artefacts studied, from all the excavation sites, are heavily corroded and the original metallic surface is not visible.

VMP analysis has been performed in 0.1 M NaOH after rubbing the electrode on the clean area of the surface. NaOH was selected instead of NH_4Cl because of the peculiarity of the object. This is, in fact, characterized by a shiny silver-like aspect, characteristic of high-tin bronzes [45–49]. The voltammogram in Figure 4.21 shows the oxidation peaks of Cu, Pb and Sn, indicating that the object is made of a high-tin leaded bronze.

The analysis, performed with XRF (spectrum in Figure 4.22), confirms the presence of these three metals. Minor elements (Fe, Al, Si) are also present and attributable to impurities in the alloy (e.g. Fe) or to the contamination of the surface due to the dirt present on the sample crust. The tin percentage, in particular, seems rather high (around 30 %), compatible with the composition of a mirror [45,50]. High percentages of tin on the surface may also be due to the occurrence of decuprification phenomena, which lead to the selective dissolution of copper from the alloy, and thus an enrichment in the tin content [45,46,51]. In order to exclude that this high percentage of tin is only due to decuprification, it was decided to cut a

slice from the bronze fragment and analyse the cross section to verify the bulk composition of the alloy.

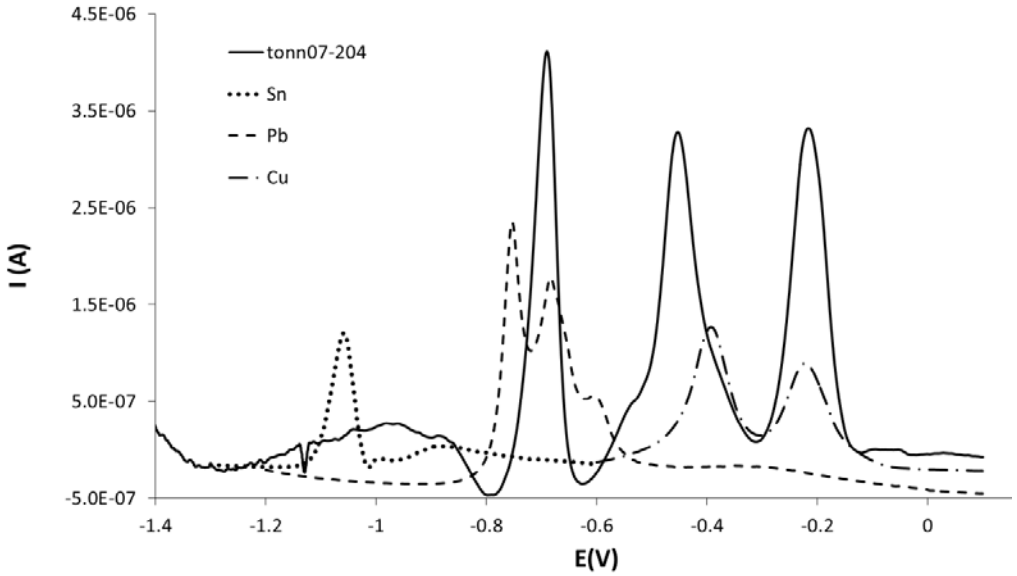

Figure 4.17: Voltammograms of the sample TONN07-204 (analyses of metal) and the metals Sn, Pb and Cu.

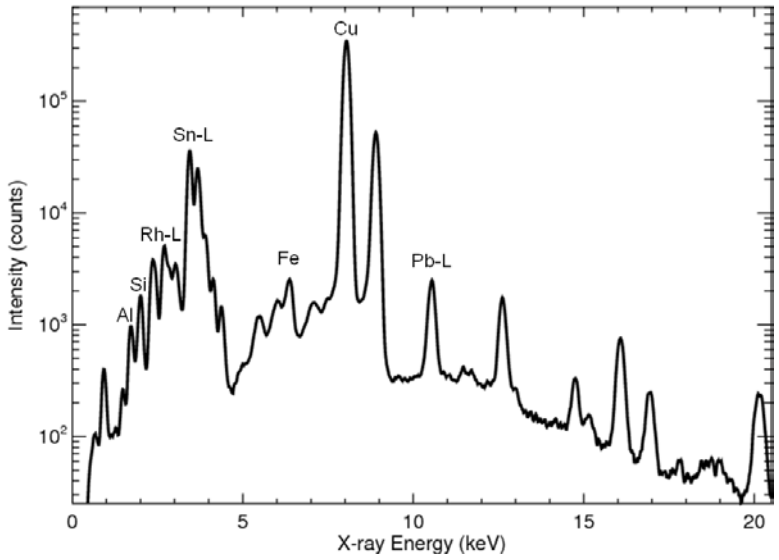

Figure 4.18: XRF spectrum of sample TONN07-204. The sampling area is indicated in figure 4.24.

XRF mapping was performed in order to verify the homogeneity of the tin and copper distribution in the bulk. The analysed area is highlighted in green in the optical micrograph, shown in Figure 4.23. The XRF maps presented in Figure 4.24 show the signals of copper, tin and lead. The distribution of copper and tin along

the cross section of the sample is uniform. The signals detected on the upper and lower edge of the sample, which appear to show a lower concentration, are due to the dispersion of particles in the embedding resin. The XRF map of lead shows the presence of few spots richer in lead, due to the insolubility of lead in the copper matrix at room temperature.

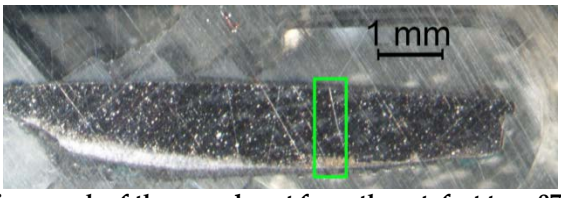

Figure 4.19: Optical micrograph of the sample cut from the artefact tonn07-204 and embedded in resin. The green area has been mapped by means of XRF.

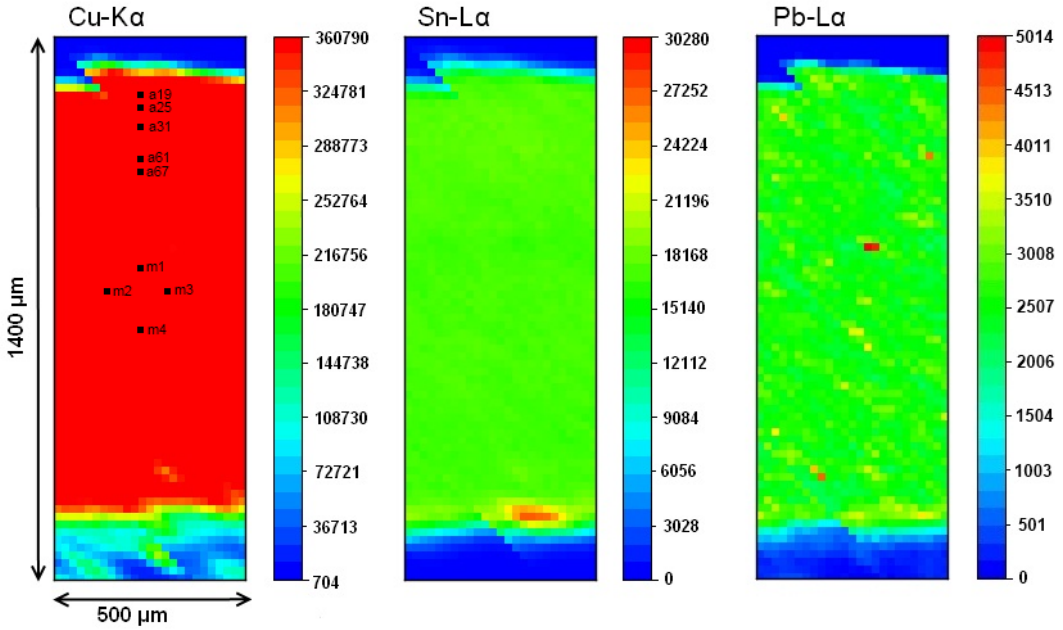

Figure 4.20: XRF maps of copper (left) and tin (right) in the cross section (figure 4.23). the black dots indicate the location of the spot measurements. The scale bars indicate the intensity expressed in counts.

Quantitative data on the bulk alloy composition have been collected in few selected spots (in black in Figure 4.24). They are presented in Table 4.V.

The compositional analyses confirm the high amount of tin present in the alloy and the fact that it is homogeneously distributed. The results allow us to exclude the hypothesis that the high concentration of tin on the surface is only due to

decuprification phenomena, seen that also in the bulk of the object high tin percentage have been detected.

Table 4-IV: Elemental composition and percentage error obtained by means of XRF analyses of the alloy of tonn07-204 for several measurements spot (indicated in figure 4.24).

Spot	% wt Cu	% wt Sn	% wt Pb
a19	73.08 ± 0.08	21.50 ± 0.06	5.41 ± 0.04
a25	70.08 ± 0.08	23.86 ± 0.06	6.05 ± 0.04
a31	69.24 ± 0.08	24.67 ± 0.06	6.09 ± 0.04
a61	68.84 ± 0.08	25.31 ± 0.06	5.85 ± 0.04
a67	69.47 ± 0.08	25.21 ± 0.06	5.32 ± 0.04
m1	68.57 ± 0.08	26.44 ± 0.08	4.99 ± 0.05
m2	67.83 ± 0.08	26.28 ± 0.07	5.89 ± 0.05
m3	68.18 ± 0.08	26.34 ± 0.07	5.47 ± 0.05
m4	66.47 ± 0.08	26.42 ± 0.07	7.10 ± 0.05
Average	**69.08**	**25.11**	**5.80**

The elemental composition and the average percentage of tin are consistent with literature data with respect to mirrors of the Roman period. Roman bronze mirrors were in fact made either by using low-tin alloys (tinned on the surface to obtain the a reflective appearance) or they were produced using high-tin alloys containing 20-24% of tin and a variable amount of lead (ranging from 5 to 12 %) [45]. It is therefore logical to assume that the fragment analysed was part of a bronze mirror.

4.3.2 The analysis of copper corrosion products

The characterization of the corrosion products follows the same principle as the identification of metals and is based on the presence of voltammetric peaks. Here, the electrochemical reduction process produces cathodic peaks that can be used for the identification. The copper corrosion products can be differentiated easily by

their peak potential (E_{peak}) in a given electrolyte and for fixed electrochemical conditions [6,7,9,20,52].

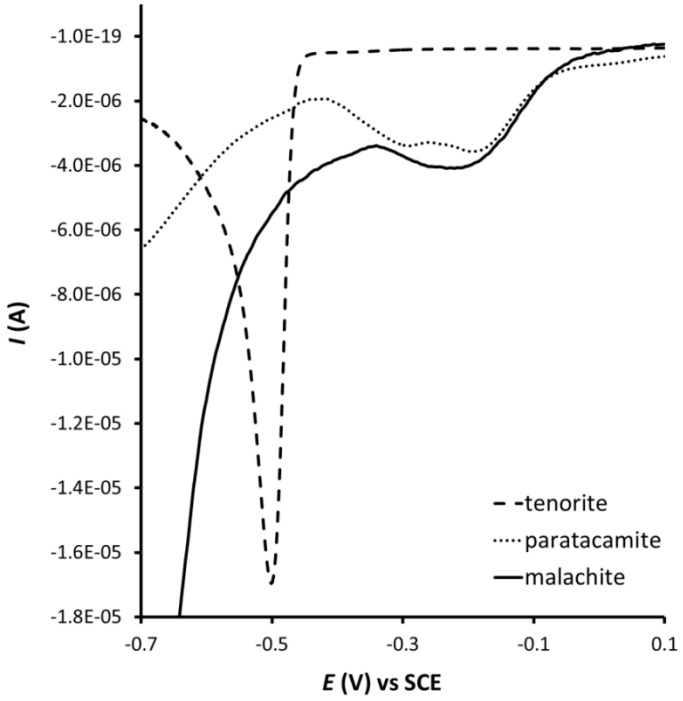

Figure 4.21: Voltammograms of different copper corrosion products: tenorite (dashed line), malachite (full line) and paratacamite (dotted line).

This is the case for the reference materials cuprite, nantokite and tenorite. Analyses were done in a 0.5 M K-phosphate buffer (pH 7), whose choice was made based on literature data [52]. This pH value prevents copper dissolution in the electrolyte observable when a lower pH is used. Using a pH 7 solution, the electrochemical response will mainly be due to the reduction of the mineral [52]. In addition preliminary tests in other electrolytes (NH_4Cl, NaOH, $NaNO_3$, oxalic acid) did not provide any improvement to the separation of copper reduction peaks of the different minerals. As shown in Figure 4.25, tenorite presents a very sharp and intense reduction peak at -0.5 V .

Most of the copper (II) compounds, however, present overlapping reduction peaks, thus necessitating the use of other electrochemical parameters. In the case of minerals, shape-dependent parameters can be derived from the Tafel analysis of the voltammetric signals, as described by Domenech [6,7,9,52–54].

When considering the rising portion (highlighted in green in Figure 4.26) of the voltammetric peak relative to the reduction of copper species, it is observed that the logarithm of the normalized current (ln i/i_p, where i_p is the peak current) plotted vs the potential (E) shows a linear behaviour, as presented in Figure 4.27. From this plot, the slope and the intercept on the y-axis at the origin can be calculated for each compound analysed [6,7,9].

The slope (from now on called Tafel slope or Tafel SL) and the y-intercept (Tafel Ordinate at the Origin or Tafel OO) depend on the phase of the mineral analysed and the electrochemical conditions used for the measurements (i.e. scan rate, frequency and amplitude of the square wave). [6,7,9,52].

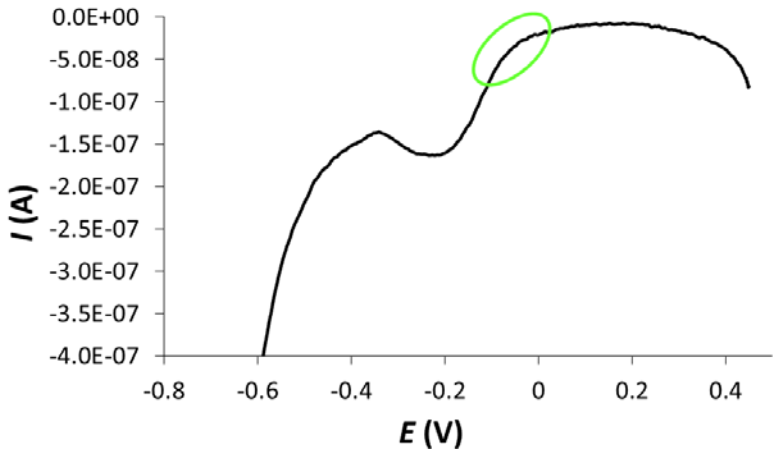

Figure 4.22: Square wave voltammogram of malachite. The Tafel region is highlighted in green.

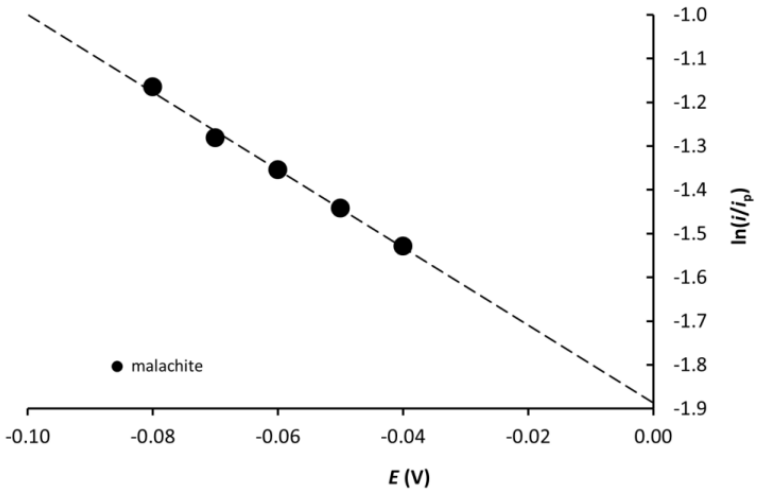

Figure 4.23: Normalized current in the Tafel region plotted vs the potential for malachite. From the extrapolation line (dotted line) the slope (-8.87 V^{-1}) and the y-intercept (-1.88) for this sample are calculated.

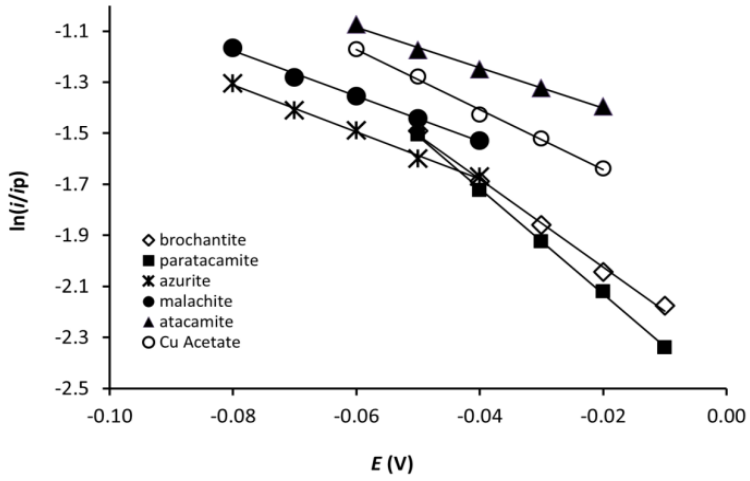

Figure 4.24: Normalized current in the Tafel region plotted vs the potential for the reference copper minerals analysed.

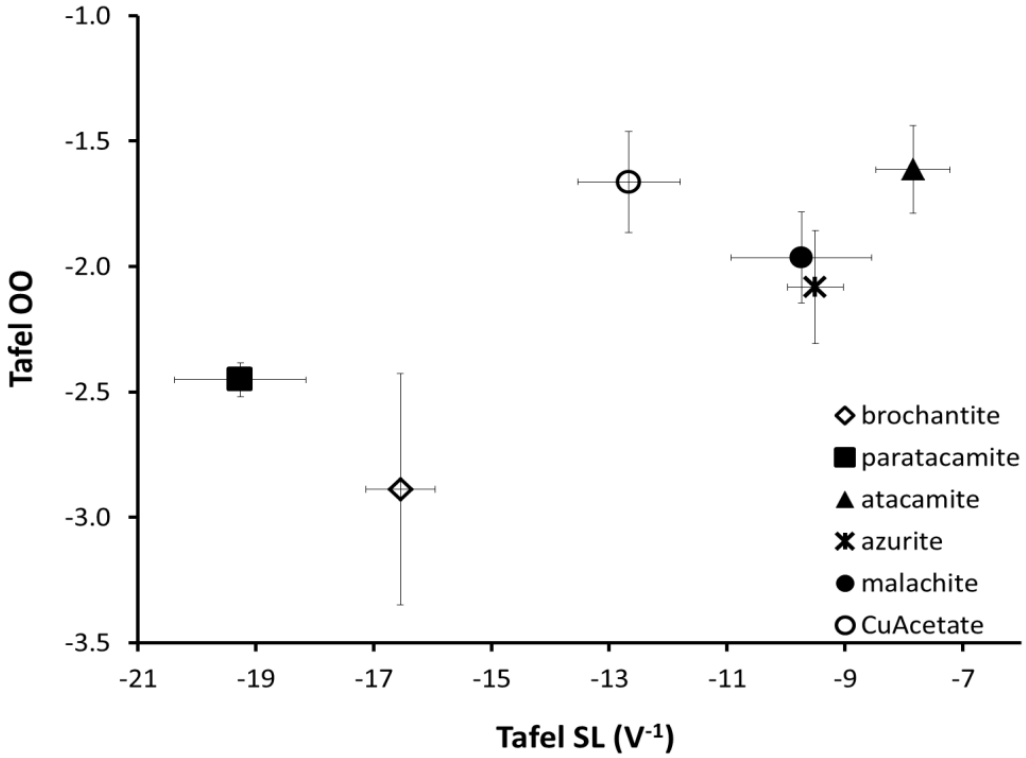

Figure 4.25: Tafel SL vs Tafel OO plot of reference corrosion products.

The initial stage of the research entailed the creation of log i/i_p vs E plots. Figure 4.27 shows the log i/i_p vs E plot obtained from a malachite sample (which voltammogram is reported in Figure 4.26). Figure 4.28 shows the plots for the most

common copper corrosion products found in archaeological objects [46]. The slope and the y-intercept for each different product appear different. These parameters are plotted in Figure 4.29 for each reference corrosion product analysed. The plot shows that the combined use of Tafel SL and Tafel OO can separate compounds like copper chlorides, while copper carbonates such as azurite and malachite present very similar behaviour and are almost impossible to separate with this method.

4.3.3 Analysis of copper minerals on historical bronze objects

4.3.3.1 Denmark

A small amount of corrosion crust was taken on the back side of the Danish coffin ornament (labelled "Denmark10"). VMP analysis (Figure 4.30) shows the presence of two copper minerals. Their Tafel parameters have intermediate values between the Tafel parameters characteristics for paratacamite ($Cu_2Cl(OH)_3$) and copper acetate ($Cu(CH_3COO)_2$). Intermediate values of the Tafel parameters occur in the presence of mixtures of different copper corrosion products [52].

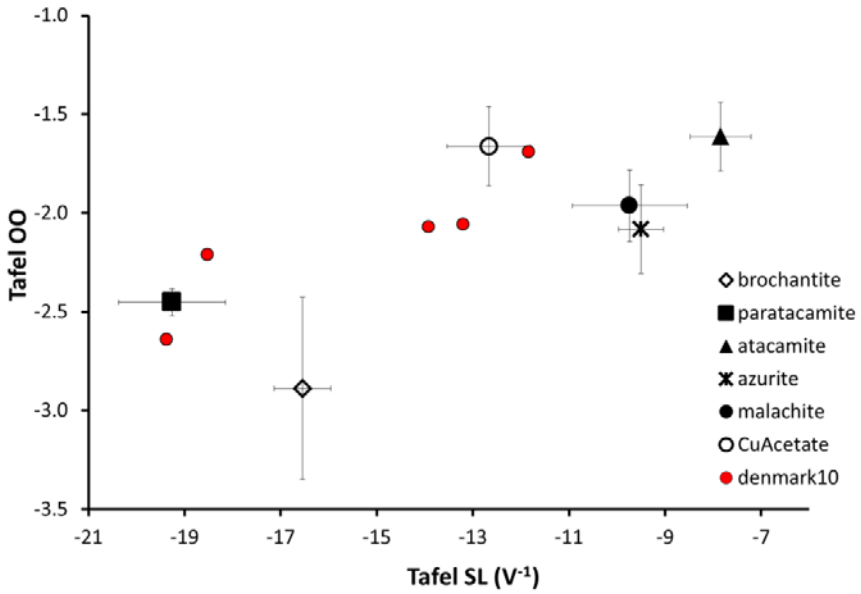

Figure 4.26: Tafel SL vs Tafel OO plot showing the copper minerals found on the Danish copper artefact (labelled Denmark_10).

The high dispersion of the data points in the plot reflects the heterogeneity of the sample. The XRD analysis performed on the powder sample (not presented here)

confirm the identification of the copper minerals done by VMP, showing diffraction peaks of copper acetate and paratacamite. The presence of copper acetate, uncommon in archaeological samples, can be explained by the use of the object as decoration of a wooden coffin. The emission of acetic acid and other volatile organic compounds (VOCs) from the wood of the coffin may have favoured the formation of organic corrosion products on the bronze object [55].

4.3.3.2 Oudenburg

Powder samples were taken from the surface of the objects. The sampling area was selected by observation under the optical microscope and a few micrograms of the corrosion crust were taken in an area presenting a homogenous colour and appearance.
Figure 4.31 shows the sampling point on the object labelled os2000G-A.

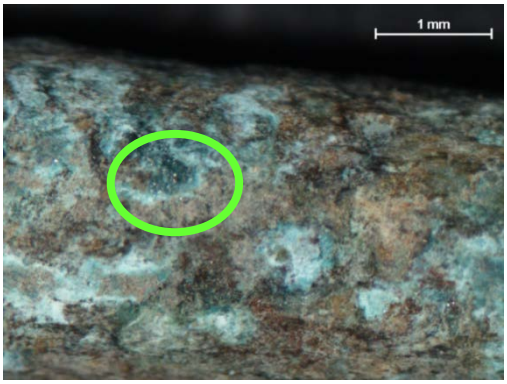

Figure 4.27: In the green circle, the sampling point for the artefact labelled os2000G-A.

VMP analyses were done in the K-phosphate buffer 0.5 M at pH 7 buffer. The data were processed and, as described above (see paragraph 4.3.2), E_{peak}, Tafel SL and Tafel OO have been extrapolated, from the voltammetric curves. These parameters have been used to identify the main copper corrosion product present. The identification has been done by comparison of the electrochemical parameters of the analysed samples with the reference data obtained previously and shown in figure 4.28. The plot in figure 4.32 presents the results of repeated measurements on the objects, each of which is represented by a different coloured symbol. In contrast to the reference compounds, it is not possible to estimate the error on the Tafel

parameters because of the potential heterogeneity of the material. Considering the complexity of the composition of an archaeological corrosion layer and considering the very small amount of powder that is attached to the PIGE during the sampling, it is reasonable to consider each repetition of the measurement as if it were done on different samples.

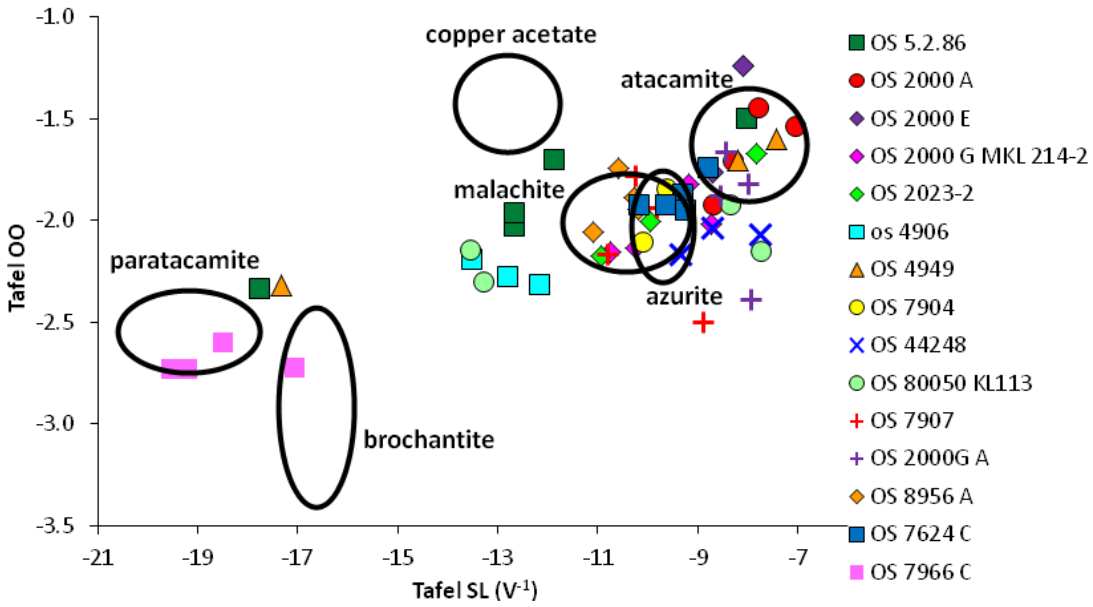

Figure 4.28: Tafel SL vs Tafel OO plot for artefacts of the site Oudenburg. The ellipses represent the area corresponding to the reference compounds.

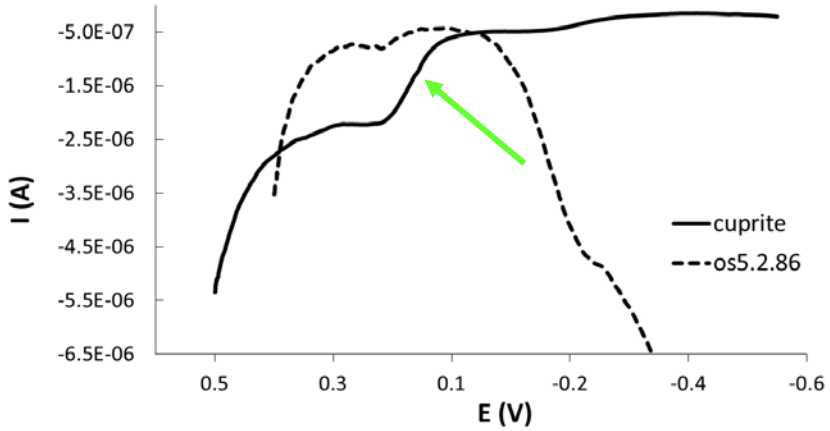

Figure 4.29: Voltammogram of sample labelled OS 5.2.86 (dashed line) and of cuprite reference powder. The peak at 0.165 V shows the presence of cuprite (indicated by the green arrow).

Cuprite has been detected only in one sample form this archaeological site (labelled OS 5.2.86). The presence of copper(I)oxides is characterized by a voltammetric peak

at 0.165 V, hence it can be identified easily without the Tafel analysis. The voltammogram of sample OS 5.2.86 is shown in figure 4.33, together with the voltammogram obtained from the analyses of a reference sample of cuprite. From the comparison of the two voltammograms the presence of cuprite in the sample OS 5.2.86 is confirmed. The identification of cuprite only in a limited number of samples should not be surprising. Copper (I) oxide is the first copper corrosion formed during the aging of a copper surface and it is normally localized at the interface with the metal core. The sampling for the VMP analyses, on the other hand, has been carried out on the outer layer of the corrosion layer, presumably containing mostly copper (II) corrosion products.

Table 4-VI: Copper minerals identified in artefacts from the site Oudenburg.

Label	Object	Cu product identified
OS 2000A	ring	atacamite + malachite
OS 2000E	bracelet (fragments)	atacamite + cuprite
OS 2000G A	piercer	atacamite
OS2000G (M.KL.2.14)	fragments	malachite
OS 2023-2	ring	malachite
OS 44248	nut	malachite + atacamite
OS 4906	plate	atacamite+ paratacamite
OS 4949	fragments	atacamite+ paratacamite
OS 5.2.86	ring	atacamite + paratacamite + cuprite
OS 7904	fragments	malachite
OS 7907	sieve (fragment)	malachite + atacamite
OS 7624 C	coins (agglomerate)	malachite + atacamite
OS 7966 C	fibula	paratacamite
OS 80050 KL113	fragments	atacamite + paratacamite
OS 8956	stud	malachite

The copper compounds identified in the bronze objects are summarized in table 4-VI and it can be observed that most of the corrosion layers contain mainly atacamite or malachite. Some measurements gave results characterized by intermediate values, indicating the co-presence of two (or more) copper compounds.

4.3.3.3 Tongeren

The objects recovered for the excavation in Tongeren have been analysed with the same procedure used for objects from Oudenburg. Also in this case, the presence of cuprite has been detected in only a few samples. The results of the Tafel analyses for the identification of copper (II) corrosion products are presented in figure 4.34 for the site Tongeren Busstelplaats (label tonn07) and 4.35 for the site Tongeren Momberstraat (label to-05-mo). The list of copper minerals identified in the artefacts is presented in table 4-VII (tonn07) and table 4-VIII (to-05-mo).

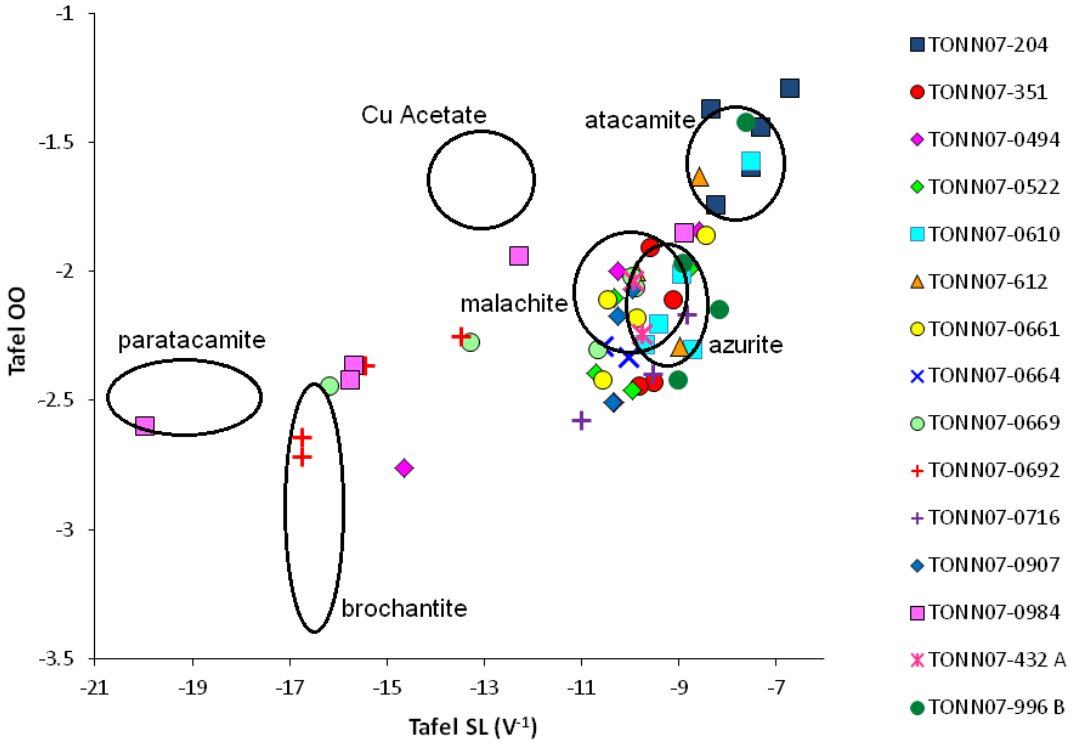

Figure 4.30: Tafel SL vs Tafel OO plot for artifacts of the site Tongeren Busstelplaats. The ellipses represent the area corresponding to the reference compounds.

As in the case of Oudenburg, the main copper corrosion products found in the corrosion layer are malachite and copper hydroxychlorides (paratacamite and atacamite). With respect to the coastal site, the number of samples containing copper carbonate is higher, which may be due to lower levels of chlorides in the environment.

Several objects contain brochantite. Copper sulphates are common corrosion products in outdoor bronzes, being produced by the interaction of bronze surfaces

with polluted wet air, rich in SO_2. It is rarely found on buried bronzes, but it has been observed in the case of bronze objects recovered from acidic soil [56].

Table 4-VI: Copper minerals identified in artefacts from the site Tongeren Busstelplaats.

Label	Object	Cu product identified
TONN07-0494	pin head	brochantite
TONN07-0522	coin	malachite
TONN07-0610	coin (fragments)	atacamite + paratacamite
TONN07-612	fibula (fragments)	malachite + atacamite
TONN07-0661	coin	atacamite
TONN07-0664	coin	malachite
TONN07-0669	fragments	malachite + brochantite
TONN07-0692	fibula (fragments)	atacamite
TONN07-0716	coin	malachite
TONN07-0907	coin	malachite
TONN07-0984	coin	atacamite + paratacamite + cuprite
TONN07-204	mirror (fragments)	atacamite
TONN07-351	ear scoop	malachite + cuprite
TONN07-432 A	plate (fragments)	malachite
TONN07-996 B	fibula (fragment)	atacamite + paratacamite

Table 4-VII: Copper minerals identified in artefacts from the site Tongeren Momberstraat.

OE nr	Label	Object	Cu product identified
VIOE 0916.1	TO-05-MO-005	plate	malachite + atacamite + cuprite
VIOE 0916.2	-	pendant	atacamite
VIOE 0916.3	TO-05-MO-16	fragments	atacamite + paratacamite
VIOE 0916.5	TO-05-MO-009	pin head	atacamite+ paratacamite + cuprite
VIOE 0916.6	TO-05-MO-004	bracelet (fragments)	atacamite + paratacamite
VIOE 0916.7	TO-05-MO-15	coin	paratacamite

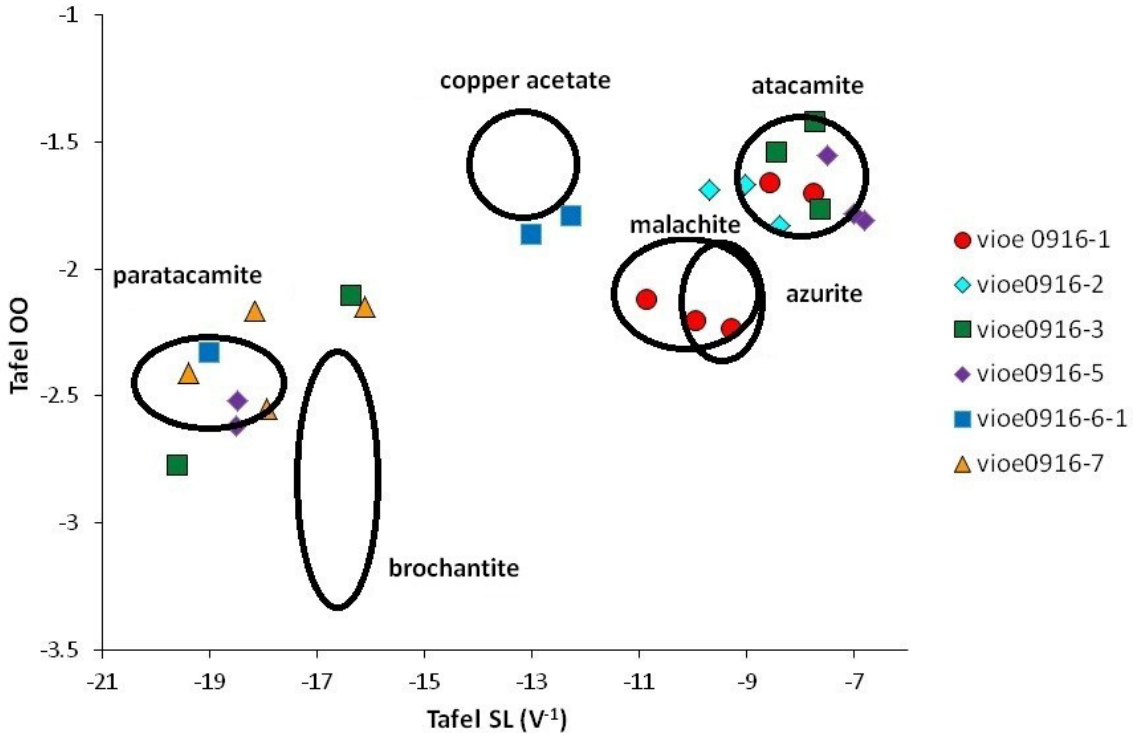

Figure 4.31: Tafel SL vs Tafel OO plot for artifacts of the site Tongeren Momberstraat. The ellipses represent the area corresponding to the reference compounds.

4.4 VMP vs XRD

The results obtained by the VMP analyses are in good agreement with XRD analyses performed on the powder samples taken from the corrosion layer. Among the XRD data collected (shown in appendix B) the diffractogram of the sample labelled OS 2000G-A is presented, as an example, in figure 4.36, where the peaks belonging to atacamite are highlighted.

The sample contains also traces of SiO_2, due to the presence of soil on the surface. The case presented shows how VMP should not be considered as an alternative to XRD analyses. X-ray diffraction, in fact, provides information on crystalline structures present in the sample. This means that it provides general information, since the diffractograms contain peaks coming from different compounds and creating, in some cases, a pattern of peaks whose interpretation is difficult. Thanks to its specificity, VMP allows us to discriminate, in such complex system, the

presence of a certain element (copper in this case) and to identify specific minerals (i.e. copper compounds). In this regards, it must be emphasized the complementarity of the two techniques, considering the contribution that VMP can give in the interpretation of XRD data.

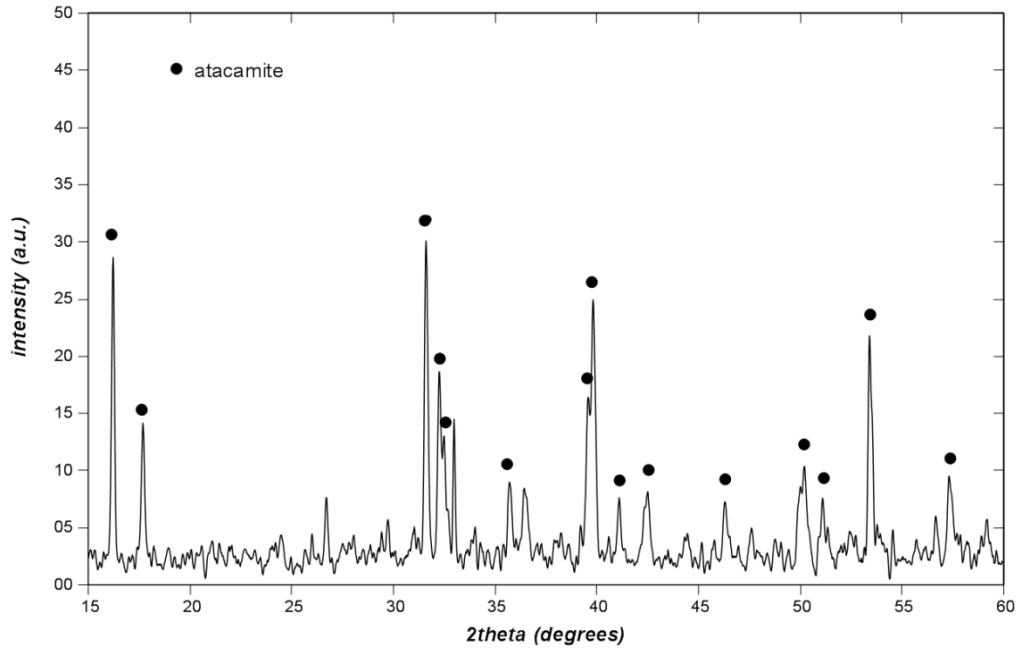

Figure 4.32: XRD diffractogram of the sample labelled OS 2000G-A. The sample contains mainly atacamite (the diffraction peaks from atacamite are highlighted with a black dot).

4.5 Conclusions and perspectives

This chapter has presented the application of voltammetry of microparticles to the analysis of heritage bronze objects. The metal constituent of a Danish coffin decoration was identified as a copper alloy containing lead and zinc, while the main copper corrosion products present on its surface are paratacamite and copper acetate. The analysis of the corrosion crust on Roman archaeological objects showed the prevalence of malachite and atacamite in the superficial layer, compatible with archaeological provenance of the objects. The presence of a copper sulphate in the sites of the city of Tongeren is to be correlated with a more acidic soil respect to the site of Oudenburg.

From the point of view of the conservative aspect, the results confirm the presence of copper(II) hydroxychlorides on several objects. These compounds may indicate the existence of active corrosion underneath the surface [46]. particular care, then, should be taken in the choice of appropriate conservation treatment of these objects.
Overall, the low amount of material needed for the analyses and the characteristics of the technique make VMP an attractive tool for restorers and restoration ateliers in museums. The use of a paraffin impregnated graphite electrode makes the sampling procedure simple and minimally destructive. The technique allows an easy and effective identification of the alloy constituents and the characterization of the copper minerals present in the corrosion crust. The results presented here summarize the capability of VMP in the field of archaeological conservation. The analysis of several archaeological Roman artefacts excavated in Flanders showed the possibility of using VMP as a screening technique for detecting the presence of copper chlorides, particularly dangerous for the preservation of copper artefacts. The knowledge acquired on the presence of specific copper minerals can thus facilitate the choice of the correct conservation procedure.
Future development of this field of application may include the extension of the range of reference minerals used for the identification of copper corrosion products. The list of reference materials may possibly contain corrosion products of other metals (such as tin, lead and zinc) frequently present in archaeological bronze objects. Other electrolytes should also be investigated in order to arrive to the simultaneous identification of corrosion products of different metals. While the discovery of a universal electrolyte appears quite unlikely, it can be certainly encouraged the investigation of a propaedeutic electrolyte, able to discriminate between copper, tin, lead and zinc minerals. As NH_4Cl can be used for preliminary analyses on metals and alloys containing Cu, Sn, Pb and Zn, an electrolyte with a similar properties should be investigated for the analyses of their corrosion products.

References

[1] A. Doménech-Carbó, M.T. Doménech-Carbó, M.A. Peiró-Ronda, "One-touch" voltammetry of microparticles for the identification of corrosion products in archaeological lead, Electroanalysis, 23 (2011) 1391–1400.

[2] A. Doménech-Carbó, Electrochemistry for conservation science, Journal of Solid State Electrochemistry, 14 (2009) 349–351.

[3] V. Costa, K. Leyssens, A. Adriaens, N. Richard, F. Scholz, Electrochemistry reveals archaeological materials, Journal of Solid State Electrochemistry, 14 (2009) 449–451.

[4] A. Doménech-Carbó, Voltammetric methods applied to identification, speciation, and quantification of analytes from works of art: an overview, Journal of Solid State Electrochemistry, 14 (2009) 363–379.

[5] A. Doménech, M.T. Doménech-Carbó, I. Martínez-Lázaro, Layer-by-layer identification of copper alteration products in metallic works of art using the voltammetry of microparticles, Analytica Chimica Acta, 680 (2010) 1–9.

[6] A. Doménech, M.T. Doménech-Carbó, H.G.M. Edwards, Quantitation from Tafel analysis in solid-state voltammetry. Application to the study of cobalt and copper pigments in severely damaged frescoes, Analytical Chemistry, 80 (2008) 2704–16.

[7] A. Doménech-Carbó, M.T. Doménech-Carbó, J. V Gimeno-Adelantado, F. Bosch-Reig, M.C. Saurí-Peris, M.J. Casas-Catalán, Electrochemical analysis of the alterations in copper pigments using charge transfer coefficient/peak potential diagrams. Application to microsamples of baroque wall paintings attached to polymer film electrodes., Fresenius' Journal of Analytical Chemistry, 369 (2001) 576–81.

[8] F. Arjmand, A. Adriaens, Electrochemical quantification of copper-based alloys using voltammetry of microparticles: optimization of the experimental conditions, Journal of Solid State Electrochemistry, 16 (2011) 535–543.

[9] A. Doménech-Carbó, M.T. Doménech-Carbó, V. Costa, Electrochemical Methods in Archaeometry, Conservation and Restoration, Springer, Berlin, 2009.

[10] F. Scholz, L. Nitschke, G. Henrion, A new procedure for fast electrochemical analysis of solid materials, Naturwissenschaften, 76 (1989) 71–72.

[11] F. Scholz, L. Nitschke, G. Henrion, A technique to study the electrochemistry of minerals, Naturwissenschaften, 76 (1989) 167–168.

[12] F. Scholz, B. Lange, Abrasive stripping voltammetry — an electrochemical solid state spectroscopy of wide applicability, TrAC Trends in Analytical Chemistry, 11 (1992) 359–367.

[13] F. Scholz, F. Rabi, W.-D. Müller, The anodic dissolution of dental amalgams studied with abrasive stripping voltammetry, Electroanalysis, 4 (1992) 339–346.

[14] F. Scholz, L. Nitschke, G. Henrion, Abrasive stripping voltammetric analysis of tin-bismuth, Electroanalysis, 2 (1990) 85–87.

[15] F. Arjmand, A. Adriaens, Quantification of Tin and Lead in Binary Alloys Using Voltammetry of Immobilized Microparticles, Electroanalysis, 23 (2011) 1941–1947.

[16] I.H.M. Van Oorschot, T. Grygar, M.J. Dekkers, Detection of low concentrations of fine-grained iron oxides by voltammetry of microparticles, Earth and Planetary Science Letters, 193 (2001) 631–642.

[17] G. Cepriá, E. Bolea, F. Laborda, J.R. Castillo, Quick, easy, and inexpensive way to detect small metallic particles in suspension using voltammetry of immobilized microparticles, Analytical Letters, 36 (2003) 923–931.

[18] G. Cepriá, O. Abadías, J. Pérez-Arantegui, J.R. Castillo, Electrochemical behavior of silver-copper alloys in voltammetry of microparticles: a simple method for screening purposes, Electroanalysis, 13 (2001) 477–483.

[19] G. Cepriá, C. Aranda, J. Pe, F. Lacueva, J.R. Castillo, Voltammetry of immobilised microparticles: a powerful analytical technique to study the physical and chemical composition of brass, Journal of Electroanalytical Chemistry, 513 (2001) 52–58.

[20] A.M. Bond, F. Scholz, Field-based identification of minerals using a battery-operated electrochemical measuring system with mechanical transfer of the solid to a graphite electrode, Journal of Geochemical Exploration, 42 (1992) 227–235.

[21] F. Scholz, U. Schröder, R. Gulaboski, Electrochemistry of Immobilized Particles and Droplets, Springer, Berlin, 2005.

[22] A. Doménech-Carbó, F.J. Torres, J. Alarcén, Electrochemical characterization of cobalt cordierites attached to paraffin-impregnated graphite electrodes, Journal of Solid State Electrochemistry, 8 (2004) 127–137.

[23] A. Doménech-Carbó, M.. Doménech-Carbó, M. Moya-Moreno, J.. Gimeno-Adelantado, F. Bosch-Reig, Identification of inorganic pigments from paintings and polychromed sculptures immobilized into polymer film electrodes by stripping differential pulse voltammetry, Analytica Chimica Acta, 407 (2000) 275–289.

[24] A. Doménech-Carbó, M.T. Doménech-Carbó, M. Calisti, V. Maiolo, Sequential identification of organic dyes using the voltammetry of microparticles approach., Talanta, 81 (2010) 404–11.

[25] A. Doménech-Carbó, T. Doménech-Carbó, C. Saurí-Peris, J.V. Gimeno-Adelantado, F. Bosch-Reig, Identification of curcuma and safflower dyes by voltammetry of microparticles using paraffin-impregnated graphite electrodes, Microchimica Acta, 152 (2005) 75–84.

[26] S. Sánchez Ramos, F. Bosch Reig, J. V Gimeno Adelantado, D.J. Yusá Marco, A. Doménech Carbó, Application of XRF, XRD, thermal analysis, and voltammetric techniques to the study of ancient ceramics., Analytical and Bioanalytical Chemistry, 373 (2002) 893–900.

[27] A. Doménech-Carbó, M.T. Doménech-Carbó, J. V Gimeno-Adelantado, M. Moya-Moreno, F. Bosch-Reig, Voltammetric identification of lead (II) and (IV) in mediaeval glazes in abrasion-modified carbon paste and polymer film electrodes. Application to the study of alterations in archaeological ceramic, Electroanalysis, 12 (2000) 120–127.

[28] A. Doménech-Carbó, M.T. Doménech-Carbó, L. Osete-Cortina, J. V Gimeno-Adelantado, F. Bosch-Reig, R. Mateo-Castro, Electrochemical identification of metal ions in archaeological ceramic glazes by stripping voltammetry at graphite/polyester composite electrodes, Talanta, 56 (2002) 161–74.

[29] K. Marušić, H. Otmačić-Ćurković, Š. Horvat-Kurbegović, H. Takenouti, E. Stupnišek-Lisac, Comparative studies of chemical and electrochemical preparation of artificial bronze patinas and their protection by corrosion inhibitor, Electrochimica Acta, 54 (2009) 7106–7113.

[30] R.B. Faltermeier, A corrosion inhibitor test for copper-based artifacts, Studies in Conservation, 44 (1998) 121–128.

[31] S.V.S. Prasad, V. Sitakara Rao, Thermal analysis, X-ray diffraction and infrared spectroscopic study of synthetic brochantite, Journal of Thermal Analysis, 30 (1985) 603–609.

[32] N. Koga, J.M. Criado, H. Tanaka, Reaction pathway and kinetics of the thermal decomposition of synthetic brochantite, Journal of Thermal Analysis, 49 (1997) 1467–1475.

[33] Personal communication with K. Stemann Petersen, National Museum of Denmark.

[34] Personal communication with L. Linders (OE).

[35] A. Vanderhoeven, G. Vynckier, B. Cooremans, A. Ervynck, A. Lentacker, W. Van Neer, et al., Het oudheidkundig bodemonderzoek aan de Mombersstraat te Tongeren (prov . Limburg). Eindverslag 2005, Relicta, 3 (2005) 93–158.

[36] V. Costa, Characterisation of cultural artefacts using electrochemical techniques, in: J.H. Townsend, L. Toniolo, F. Cappitelli (Eds.), Conservation Science 2007: Paper from the Conference Held in Milano, Italy 10-11 May 2007, Archetype, London, 2007: pp. 209–211.

[37] V. Costa, Electrochemistry as a conservation tool: an overview, in: J. Townsend, K. Eremin, A. Adriaens (Eds.), Conservation Science 2002: Papers from the Conference Held in Edinburgh, Scotland 22-24 May 2002, Archetype, London, 2003: pp. 88–95.

[38] S.D. Cramer, B.S. Covino Jr, eds., ASM Handbook, Volume 13A. Corrosion: Fundamentals, Testing and Protection, ASM International, 2003.

[39] I. Šestáková, J.J. Dytrtová, M. Jakl, T. Navrátil, Assessment of cadmium and lead mobility in the rhizosphere using voltammetry and electrospray ionization mass spectroscopy, International Journal of Energy and Environment, 5 (2011) 347–355.

[40] B. Bozzini, G. Giovannelli, S. Natali, M. Serra, A. Fanigliulo, Electrodeposition of Au – Sn alloys from alkaline baths, Journal of Applied Electrochemistry, (2002) 165–171.

[41] F.H. Assaf, A.M. Zaky, S.S. Abd El-Rehim, Cyclic voltammetric studies of the electrochemical behaviour of copper–silver alloys in NaOH solution, Applied Surface Science, 187 (2002) 18–27.

[42] A.A. Montaser, P. Veluchamy, H. Minoura, Structure, morphology and photoelectrochemical responses of anodic PbO films formed on Pb electrodes in various concentrations of alkaline solution, Journal of Electroanalytical Chemistry, 419 (1996) 47–53.

[43] C. Nila, I. González, The role of pH and Cu(II) concentration in the electrodeposition of Cu(II) in NH4Cl solutions, Journal of Electroanalytical Chemistry, 401 (1996) 171–182.

[44] N. Blagojević, V. Kastratović, R. Zejnilović, Ž. Blečić, Determination of lead in an Sb-Pb alloy by anodic linear scan voltammetry, Fresenius' Journal of Analytical Chemistry, 371 (2001) 1023–1027.

[45] D.A. Scott, Metallography and Microstructure of Ancient and Historic Metals, Getty Conservation Institute, Marina del Rey, 1991.

[46] D.A. Scott, Copper and Bronze in Art – Corrosion, Colorants, Conservation, Getty Publications, Los Angeles, 2002.

[47] C. Giardino, I Metalli nel Mondo Antico. Introduzione all'Archeometallurgia, Editori Laterza, Roma, 2002.

[48] D. Dungworth, Roman copper alloys: analysis of artefacts from Northern Britain, Journal of Archaeological Science, 24 (1997) 901–910.

[49] Bryan Cockrell, Colourful corrosion: black bronze and its enigmatic patina, Papers from the Institute of Archaeology, 19 (2009) 85–90.

[50] R.F. Tylecote, A History of Metallurgy, Institute of Materials, London, 2002.

[51] L. Robbiola, N. Pereira, K. Thaury, C. Fiaud, J.-P. Labbé, Decuprification phenomenon of Cu-Sn alloys in aqueous solution in nearly neutral pH conditions, in: W. Mourey, L. Robbiola (Eds.), Metal 98: Proceedings of the International Conference on Metals Conservation, Draguignan-Figanières, France, 27-29 May 1998, James & James Ltd, London, 1998: pp. 136–144.

[52] A. Doménech-Carbó, M. Doménech-Carbó, I. Martínez-Lázaro, Electrochemical identification of bronze corrosion products in archaeological artefacts. A case study, Microchimica Acta, 162 (2007) 351–359.

[53] A. Doménech-Carbó, M.T. Doménech-Carbó, M. a. Peiró-Ronda, L. Osete-Cortina, Electrochemistry and authentication of archaeological lead using voltammetry of microparticles: application to the Tossal de Sant Miquel Iberian plate, Archaeometry. 53 (2011) 1193–1211.

[54] A. Doménech, M.T. Doménech-Carbó, T. Pasies, M.C. Bouzas, Application of modified Tafel Analysis to the Identification of corrosion products on archaeological metals using voltammetry of microparticles, Electroanalysis, 23 (2011) 2803–2812.

[55] L.T. Gibson, C.M. Watt, Acetic and formic acids emitted from wood samples and their effect on selected materials in museum environments, Corrosion Science, 52 (2010) 172–178.

[56] A.G. Nord, E. Mattsson, K. Tronner, Factors influencing the long-term corrosion of bronze artefacts in soil, Protection of Metals, 41 (2005) 309–316.

5. Electrochemical deposition of a copper carboxylate layer

5.1 Introduction

Historical copper-based objects are often preferred in the corroded state, not only because of the aesthetically pleasing colours, but also because the presence of corrosion products provides evidence of past times past, thereby adding extra value to the object. However, corrosion may also become a problem, especially when specific corrosion products (such as cuprous chlorides) are in contact with the metal core. Under certain conditions, the deterioration of the underlying metal will continue and will lead to the destruction of the object [1].

The use of corrosion inhibitors and protective coatings is thus necessary in order to preserve the characteristics of the material. Inorganic ions, such as CrO_4^{2-} and $B_4O_7^{2-}$, form a passivating layer of metal oxide on the copper surface, but their used is limited due to the high toxicity [2,3]. Organic coating and inhibitors are one of the most important ways of protecting metal against corrosive agents and they have been used since antiquity. Wax and oils for instance were commonly used by ancient Greek craftsmen to protect copper and bronze objects [1]. More recently copper corrosion inhibitors include a large variety of organic compounds, such as azoles and amines [3,4], thiourea and triazole derivatives [4,5], amino acids (and their derivatives) and sodium salts of saturated carboxylic acids [6–17]. A significant problem with presently available treatments is that products for protective coatings and corrosion inhibitors are dangerous for conservators: 1,2,3-benzotriazole, for example, is very efficient against copper corrosion, but it is extremely toxic with a possible carcinogenic effect [18,19].

Saturated monocarboxylic chains have been tested as corrosion inhibitors for various metals, including copper. They are environmentally friendly in comparison with other possibilities (such as benzotriazole) as they do not contain sulfur, aromatic rings or nitrogen, and have been extensively tested in cosmetics and

foodstuffs. The effectiveness of carboxylic acids and sodium-carboxylates as aqueous corrosion inhibitors has been discussed in various studies [7,9–16] not only as a general corrosion inhibitor, but specifically in the framework of treating cultural artefacts [7–13]. Moreover, crystalline layers of metal carboxylate formed by immersion of the metal in the aqueous solution containing the corresponding carboxylic acid have been described as effective inhibitors against lead and iron corrosion [6,8,9,12,20]. Previous studies have shown that the length of the carboxylic chain, in particular, is very important: longer chains provide better protection against aggressive agents [9–11]. In general these compounds act via adsorption on the metal surface and the formation of complexes [3]. With regard to copper protection, there are only few studies which investigate the formation of layers of copper carboxylates from aqueous [9] solutions.

This chapter deals with the study of the deposition of a copper carboxylate layer by means of electrochemical methods. The electrochemical deposition of carboxylate layers on a metal surface allows controlling the deposition process of the copper carboxylates onto the electrode. The same procedure has already been applied to lead electrodes, leading to the formation of a lead carboxylate layer effective against corrosion in an aggressive environment [6].

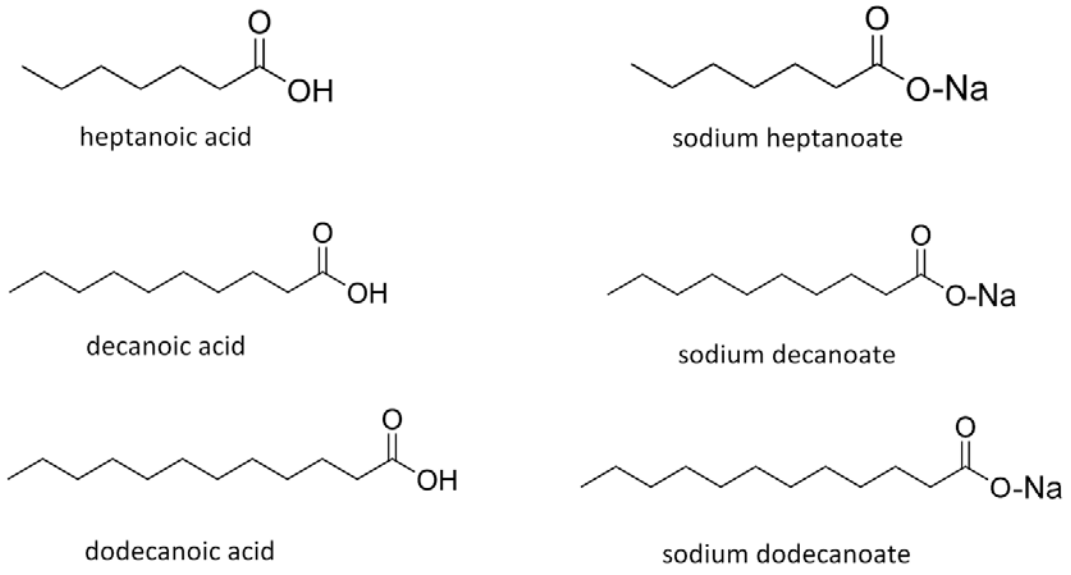

Figure 5.1: Structures of the carboxylic acids and the respective sodium carboxylates used in this study.

For this study, three types of carboxylic acids were studied and compared: heptanoic acid, decanoic acid and dodecanoic acid. The deposition was performed using the respective sodium carboxylates (NaC_n) as they tend to have a better solubility in water than the related carboxylic acid [21] The structure of the three carboxylic acids and their sodium carboxylates are shown in figure 5.1.

The modified electrodes were characterized using attenuated total reflectance - Fourier transform infrared spectroscopy (FTIR-ATR). In addition polarization and Tafel plot experiments were performed to evaluate the inhibition effect of the three carboxylate layers.

5.2 Experimental

Three different sodium carboxylate solutions were used for the experiments: sodium heptanoate (NaC_7), sodium decanoate (NaC_{10}) and sodium dodecanoate (NaC_{12}) with each a concentration of 0.025 M. The solutions were prepared by neutralizing the respective carboxylic acid with sodium hydroxide (NaOH). For 100 mL of deionized water the following quantities were weighed: heptanoic acid (HC_7, purity > 97 %) 0.325 g, decanoic acid (HC_{10}, purity ≥ 98%) 0.431 g and dodecanoic acid (HC_{12}, purity 98 %) 0.501 g. A reference solution was also prepared by dissolving the same quantity of NaOH in water used to neutralize the carboxylic acids. A NaOH solution with the concentration of 0.025 M was obtained. The sodium carboxylate and reference solutions were purged with nitrogen for 15 minutes before each experiment. All chemical products used for the experiments were purchased from Sigma Aldrich.

Experiments were carried out using a saturated calomel electrode (SCE) as a reference electrode (Radiometer Analytical, France) and a carbon rod as a counter electrode. The working electrode was a pure copper rod (diameter 2 mm, purity 99.99% purchased from Goodfellow) embedded in epoxy resin.

Prior to each experiment the electrode was mechanically cleaned with silicon carbide (SiC) paper of P1200 grit to obtain a fresh surface. The surface was subsequently polished using a polishing cloth and an alumina (Al_2O_3) water

suspension (1 µm particle size). To remove any adhering Al_2O_3 particles, the electrode was rinsed with deionized water and ultrasonically cleaned in ethanol for 15 minutes.

The modification of the copper electrode by carboxylate was performed by recording successive cyclic voltammetric scans (100 scans) in a potential window from −1.1 to 0.6 V vs SCE with a scan rate of 50 mV/s. After each modification procedure, the electrode was rinsed with deionized water.

The electrochemical properties of the modified electrode were then evaluated by means of linear sweep voltammetry (LSV) in a 0.1 M Na_2SO_4 solution. The polarization resistance (R_p) was measured in a range of ± 20 mV with respect to the open circuit potential (OCP) at a scan rate of 1 mV/s. The corrosion current was calculated via the Tafel extrapolation from the LSV curve recorded in a range of ± 250 mV vs OCP with a scan rate of 0.2 mV/s.

Infrared spectroscopic analyses were performed in order to obtain qualitative proof of the deposition of a copper carboxylate layer. The spectra were recorded in reflectance mode in the range 4000-600 cm^{-1}.

5.3 Results and discussion

5.3.1 Deposition of the copper carboxylate layer

Figure 5.2 represents the potentiodynamic curve of a copper electrode in the 0.025 M NaOH reference solution to which no corrosion inhibitors had yet been added. Three anodic peaks are clearly visible showing the oxidation to different copper species.

Peaks A1 (–0.35 V) and A2 (–0.14 V) are related to the oxidation to Cu_2O and CuO respectively, as described in previous studies [22–25]. They can be explained using the following reactions:

$$2\ Cu\ +\ 2\ OH^- \longrightarrow Cu_2O\ +\ H_2O \quad \text{(peak A1)} \tag{5.1}$$

$$Cu_2O\ +\ 2\ OH^- \longrightarrow 2\ CuO\ +\ H_2O \quad \text{(peak A2)} \tag{5.2}$$

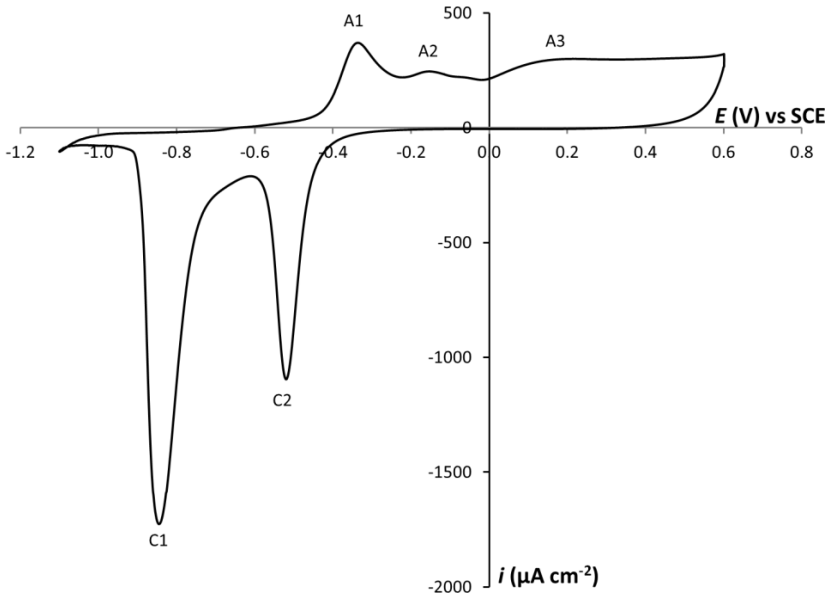

Fig. 5.2: The current density vs potential behaviour of a copper electrode in a 0.025 M NaOH solution.

The broad shape of peak A3 (in the potential region between 0.01 and 0.46 V) can be attributed to the formation of a $Cu(OH)_2$ layer from the hydration of the cupric oxide layer [22].

In the cathodic curve, peaks C1 (–0.86 V) and C2 (–0.49 V) are associated with the reduction processes of copper oxides and hydroxides formed during the oxidation according to the following reactions:

$$2\ CuO\ +\ H_2O \longrightarrow Cu_2O\ +\ 2\ OH^-\ \text{(peak C1)} \tag{5.3}$$

$$Cu_2O\ +\ H_2O \longrightarrow 2\ Cu\ +\ 2\ OH^-\ \text{(peak C2)} \tag{5.4}$$

Figure 5.3 shows the electrochemical behaviour of the copper electrode in the three different sodium carboxylate solutions, NaC_7, NaC_{10} and NaC_{12}, after 100 cycles. In the three curves presented, there are no clear peaks identifiable which are related to the oxidation processes observed before in Figure 5.2. Moreover compared to the copper electrode in the NaOH solution, the current density range is significantly smaller. The total current density is the largest in the voltammogram of copper in NaC_7 solution, while it is progressively reduced in the NaC_{10} and NaC_{12} solutions. NaC_{12} produces the most evident reduction in the total current density.

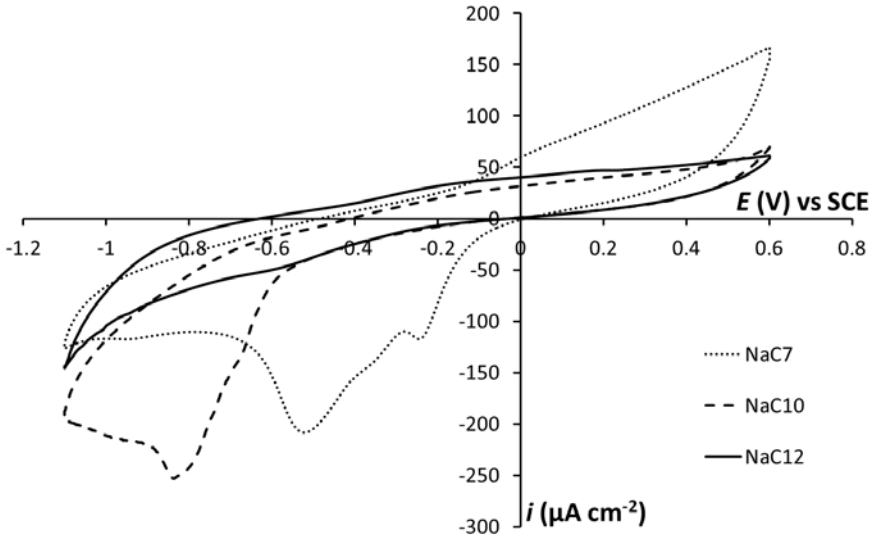

Fig. 5.3: Potentiodynamic curves of a copper electrode in NaC_7, NaC_{10} and NaC_{12} (0.025 M).

This decrease can be explained by an inhibition effect of the carboxylate in the solution and the progressive deposition of a copper carboxylate layer on the electrode surface, according to the reaction

$$Cu + 2C_n^- \rightarrow Cu(C_n)_2 \qquad (5.5)$$

where C_n is the carboxylate chain and n represents the number of carbon atoms in the carboxylate chain (7, 10 or 12).

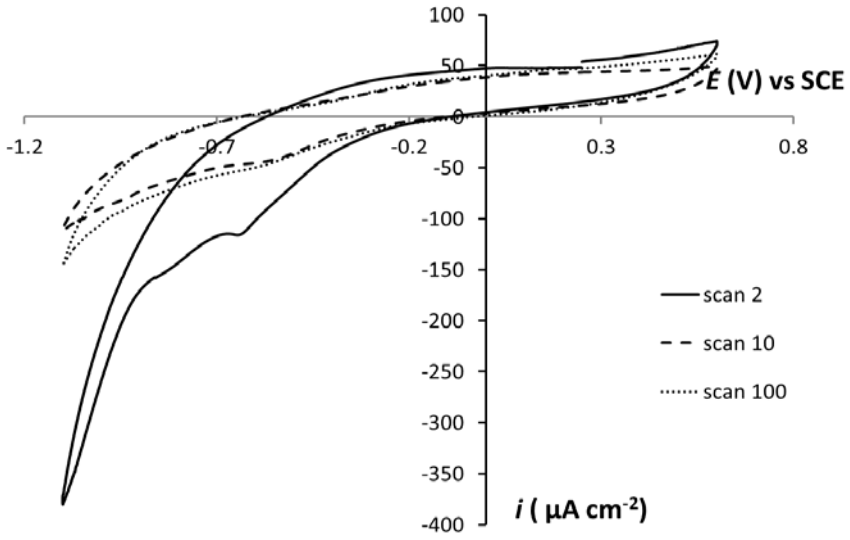

Fig. 5.4: Voltammetric scans of a copper electrode in a 0.025 M NaC_{12} solution (scan 2, 10 and 100).

Figure 5.4 shows three voltammograms (scan 2, 10 and 100) obtained from a copper electrode in a NaC_{12} solution (0.025 M). The decrease of the total current density is visible comparing successive cycles, and the signal is already stable after the 10^{th} scan, indicating a progressive deposition of a layer of copper carboxylate.
For all sodium carboxylates used, the electrode modification was stopped after 100 cycles.

5.3.2 Evaluation of the copper carboxylate layer

Copper carboxylates typically show a blue-green colour [17,26,27], but observations of the electrodes carried out with the optical microscope did not show any difference between the surface appearance before and after the modification, as expected in the case of a very thin layer. Nevertheless, FTIR-ATR analyses on electrodes modified using NaC_{10} and NaC_{12} confirm the deposition of copper carboxylates on the surface. On the copper electrode treated with NaC_7 it was not possible to observe the presence of a copper heptanoate ($Cu(C_7)_2$) layer with infrared analyses. Here we assume that the copper heptanoate layer was too thin to be detected by FTIR-ATR. A thicker layer could be achieved by increasing the number of cycles, but it was decided to not proceed with this, since NaC_{10} and NaC_{12} were providing good results already after 100 cycles.
In Figure 5.5, the FTIR-ATR spectrum of a copper electrode after 100 cycles in a 0.025 M NaC_{10} solution is compared to the spectrum of a bare copper electrode. The spectrum of the copper electrode modified with NaC_{10} shows two absorption peaks at 2849 and 2917 cm^{-1}, which are related to the symmetric and asymmetric stretching vibrations of CH bonding [28–30]. The frequencies of the absorption bands of the carbonyl group (symmetric and asymmetric stretching) are in the region of 1350–1750 cm^{-1}. In the same spectrum presented, the asymmetric COO- stretching of copper decanoate ($Cu(C_{10})_2$) is visible at 1588 cm^{-1}. The absorption frequency of the COO- stretching is highly sensitive to the structure of the carboxylate group and the identity of the metal ion [28–30] and allows us to distinguish between carboxylic acid, sodium carboxylate and copper carboxylate [28].

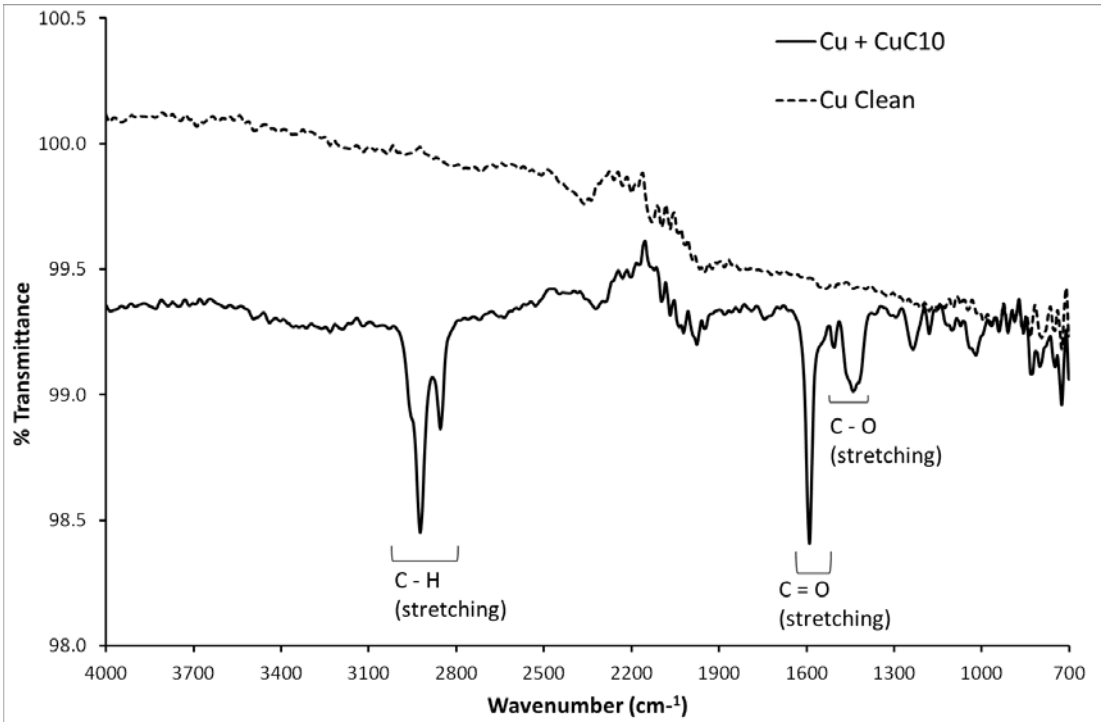

Fig. 5.5: FTIR-ATR spectra of a bare Cu electrode and a Cu electrode after 100 cycles in 0.025M NaC_{10} solution.

The comparison of the infrared analyses with literature data [29] confirm the attribution of the carbonyl absorption frequencies to copper compounds. Absorption bands characteristic of copper carboxylates were present in all the electrodes modified with NaC_{10} and NaC_{12}. The infrared spectra obtained from these electrodes are shown in appendix D.

Finally, the corrosion resistance of the copper caboxylate layer was evaluated using polarization techniques. Figure 5.6 presents the polarization curves of the electrodes modified using carboxylates of different chain length. Samples treated with NaC_{10} and NaC_{12} show a lower slope. This is an indication of the protective effect of the carboxylate layer deposited on the surface. The increase of the polarization resistance is related to the chain length: longer aliphatic chains provide better protection, while in the case of copper heptanoate it is not possible to observe a protective effect.

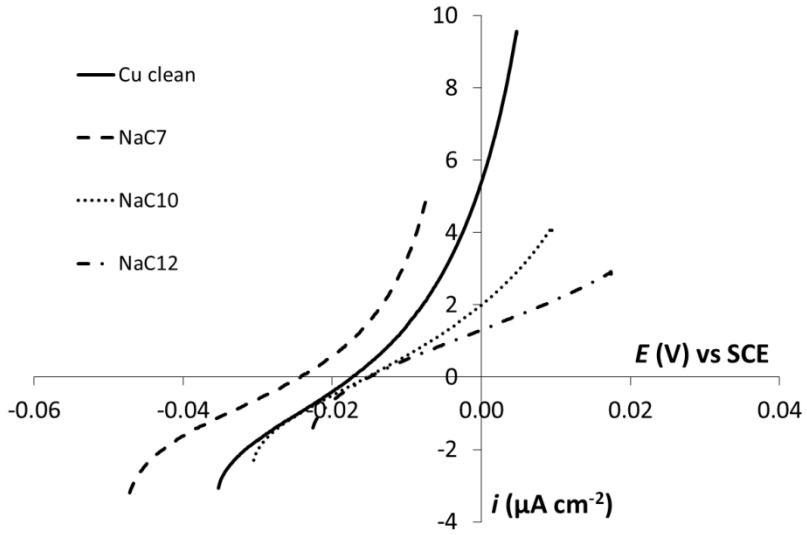

Fig. 5.6: Polarization curves for a copper electrode modified with different carboxylates. The electrolyte is 0.1 M Na_2SO_4.

Table 5-I shows the average of four experiments and their standard deviation (σ) of polarization resistance values obtained from the polarization curves. The analyses reveal the absence of a deposited layer of copper heptanoate on the electrode (as suspected from the FTIR-ATR data) as the polarization resistance of the electrode modified with NaC_7, in fact, is very close to the value of polarization resistance (R_p) of clean copper. Given the results obtained from optical microscopy, FTIR-ATR and polarization techniques, it was decided to discard the electrodes modified with $Cu(C_7)_2$ in the subsequent polarization experiments.

The deposition of a copper decanoate ($Cu(C_{10})_2$) and copper dodecanoate ($Cu(C_{12})_2$) coating, on the other hand, increases the polarization resistance of the electrode.

Table 5-I: Polarization resistance (R_p) and standard deviation (σ) of the modified electrodes in 0.1 M Na_2SO_4. The values are the averages of four measurements.

Cu carboxylate	R_p (Ω mm²)	σ
Uncoated copper	1.5×10^5	5.4×10^4
$Cu(C_7)_2$	2.4×10^5	6.9×10^4
$Cu(C_{10})_2$	3.8×10^5	1.6×10^5
$Cu(C_{12})_2$	1.1×10^6	6.2×10^5

The Tafel extrapolation of the linear polarization curves is presented in Figure 5.6. The presence of a $Cu(C_{10})_2$ and $Cu(C_{12})_2$ layer on the electrode surface produces a shift of the corrosion potential towards more negative values and reduces clearly the corrosion current density. The decrease of the corrosion current density is more evident in case of the presence of $Cu(C_{12})_2$ layer which gives a better protection against corrosion.

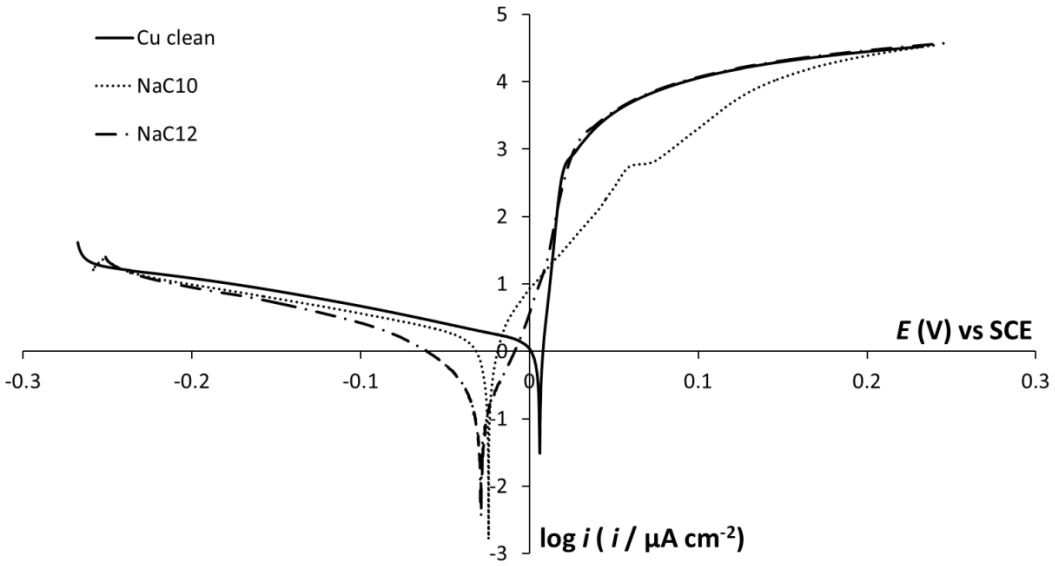

Fig. 5.7: Polarization curves (logarithmic scale) of a copper electrode modified with different carboxylates. The electrolyte is 0.1 M Na_2SO_4.

Table 5-II presents the average value for the corrosion current density (i_{corr}) obtained from these experiments. The inhibition efficiency (*IE*) can be calculated using the formula [17]

$$IE\ (\%) = \frac{i_{(clean)} - i_{(coated)}}{i_{(clean)}} \times 100 \qquad (5.6)$$

This parameter is useful to compare the decrease in corrosion current produced by different coatings. The corrosion current density and the inhibition efficiency values are consistent and confirm the results of the polarization resistance experiment. The copper carboxylates $Cu(C_{12})_2$ and $Cu(C_{10})_2$ reduce the corrosion current and $Cu(C_{12})_2$

deposited on the electrode surface is more effective than $Cu(C_{10})_2$ in inhibiting the corrosion process.

Table 5-II: Corrosion current density (i_{corr}), standard deviation (σ) and inhibition efficiency of the modified electrodes in 0.1 M Na_2SO_4. The values are the averages of four measurements.

Cu carboxylate	i_{corr} (A mm^{-2})	σ	*IE* (%)
Uncoated copper	1.4 x 10^{8}	8.3 x 10^{9}	-
$Cu(C_{10})_2$	1.1 x 10^{8}	3.2 x 10^{9}	21
$Cu(C_{12})_2$	8.0 x 10^{9}	7.9 x 10^{9}	41

As a negative point it must be noticed that the standard deviation is very high, indicating that a large variability of i_{corr} values has been encountered. This could be due to varying layer thicknesses for the copper carboxylate on the surface or to heterogeneity of the layer. Other causes may be the softness of carboxylate soaps and their consequent susceptibility to mechanical damage, or differing amounts of hydration of the layers themselves permitting some ion transfer. Further investigation is required here because of the implications for both aqueous and atmospheric corrosion protection. Another source of error may also be the cleaning method chosen for the electrode. Different cleaning protocols may be tested, such as chemical cleaning or mechanical cleaning with abrasive powders other than Al_2O_3, in order to verify the effect of the electrode preparation on the deposition of a carboxylate layer and the consequent inhibition efficiency.

5.4 Conclusions

This chapter describes the deposition of copper carboxylate layers for the protection of copper surfaces. It was shown that it is possible to apply a layer of copper decanoate and copper dodecanoate by electrochemical means using aqueous solution of sodium carboxylates (more soluble in water than carboxylic acids). The effective deposition was confirmed using infrared spectroscopy and the modified electrodes are visually indistinguishable from pure copper.

Although the polarization resistance of the copper electrode modified with $Cu(C_{10})_2$ and $Cu(C_{12})_2$ is increased by the coating deposition, the analyses of i_{corr} show a high standard deviation. More research is indeed needed to better understand the formation of the copper carboxylate layer by means of electrochemical deposition and to improve the reproducibility of the process.

References

[1] D.A. Scott, Copper and Bronze in Art – Corrosion, Colorants, Conservation, Getty Publications, Los Angeles, 2002.

[2] A.I. Muñoz, J.G. Antón, J.L. Guiñón, V.P. Herranz, Comparison of inorganic inhibitors of copper, nickel and copper–nickels in aqueous lithium bromide solution, Electrochimica Acta, 50 (2004) 957–966.

[3] M.M. Antonijević, S.C. Alagić, M.B. Petrović, M.B. Radovanović, A.T. Stamenković, The influence of pH on electrochemical behavior of copper in presence of chloride ions, International Journal of Electrochemical Science, 4 (2009) 516–524.

[4] D.M. Bastidas, E. Cano, E.M. Mora, Volatile corrosion inhibitors: a review, Anti-Corrosion Methods and Materials, 52 (2005) 71–77.

[5] D.M. Bastidas, M. Criado, S. Fajardo, V.M. La Iglesia, E. Cano, J.M. Bastidas, Copper deterioration: causes, diagnosis and risk minimisation, International Materials Reviews, 55 (2010) 99–127.

[6] K. De Wael, M. Keersmaecker, M. Dowsett, D. Walker, P. a. Thomas, A. Adriaens, Electrochemical deposition of dodecanoate on lead in view of an environmentally safe corrosion inhibition, Journal of Solid State Electrochemistry, 14 (2009) 407–413.

[7] S. Hollner, F. Mirambet, A. Texier, E. Rocca, J. Steinmetz, L. De Chimie, et al., Development of new non-toxic corrosion inhibitors for cultural property

made of iron and copper alloys, in: V. Argyropoulos, A. Hein, M. Abdel Harith (Eds.), Proceedings of International Conference on Conservation Strategies for Saving Indoor Metallic Collections, Cairo 25 February – 1 March 2007, TEI of Athens, Athens, 2007: pp. 156–161.

[8] M. Dowsett, A. Adriaens, B. Schotte, G. Jones, L. Bouchenoire, Real time spectroelectrochemical growth and corrosion resistance monitoring of lead carboxylate coatings in an environmental cell (eCell), in: C. Degrigny, R. van Langh, I. Joosten, B. Ankersmit (Eds.), Metal 07: Proceedings of the International Conference on Metals Conservation, Amsterdam 17-21 September 2007, Rijksmuseum Amsterdam, Amsterdam, 2007: pp. 26–31.

[9] S. Hollner, F. Mirambet, E. Rocca, J. Steinmetz, Environmentally-friendly treatments for the protection of iron artefacts of the cultural heritage against atmospheric corrosion, in: C. Degrigny, R. Van Langh, I. Joosten, B. Ankersmit (Eds.), Metall 07: Proceedings of the International Conference on Metals Conservation. Amsterdam 17-21 September 2007, Rijksmuseum Amsterdam, Amsterdam, 2007: pp. 64–70.

[10] E. Rocca, J. Steinmetz, Inhibition of lead corrosion with saturated linear aliphatic chain monocarboxylates of sodium, Corrosion Science, 43 (2001) 891–902.

[11] E. Rocca, C. Rapin, F. Mirambet, Inhibition treatment of the corrosion of lead artefacts in atmospheric conditions and by acetic acid vapour: use of sodium decanoate, Corrosion Science, 46 (2004) 653–665.

[12] A. Adriaens, F. De Bisschop, M. Dowsett, B. Schotte, Growth and real time corrosion resistance monitoring of lead decanoate coatings, Applied Surface Science, 254 (2008) 7351–7355.

[13] C. Georges, E. Rocca, P. Steinmetz, Synergistic effect of tolutriazol and sodium carboxylates on zinc corrosion in atmospheric conditions, Electrochimica Acta, 53 (2008) 4839–4845.

[14] N. Stein, L. Johann, C. Rapin, J.M. Lecuire, In-situ ellipsometric study of copper passivation by copper heptanoate through electrochemical oxidation, Electrochimica Acta, 43 (1998) 3227–3234.

[15] E. Rocca, G. Bertrand, C. Rapin, J.C. Labrune, Inhibition of copper aqueous corrosion by non-toxic linear sodium heptanoate: mechanism and ECAFM study, Journal of Electroanalytical Chemistry, 503 (2001) 133–140.

[16] G. Bertrand, E. Rocca, C. Savall, C. Rapin, J.-C. Labrune, P. Steinmetz, In-situ electrochemical atomic force microscopy studies of aqueous corrosion and inhibition of copper, Journal of Electroanalytical Chemistry, 489 (2000) 38–45.

[17] I. Milošev, T. Kosec, M. Bele, The formation of hydrophobic and corrosion resistant surfaces on copper and bronze by treatment in myristic acid, Journal of Applied Electrochemistry, 40 (2010) 1317–1323.

[18] M. Finšgar, I. Milošev, Inhibition of copper corrosion by 1,2,3-benzotriazole: A review, Corrosion Science, 52 (2010) 2737–2749.

[19] Health Council of the Netherlands, 1,2,3-Benzotriazole. Health-based recommended occupational exposure limit, http://www.gezondheidsraad.nl/en/publications/123-benzotriazole-health-based-recommended-occupational-exposure-limit (2002), (accessed 23/08/2010).

[20] A. Denker, A. Adriaens, M. Dowsett, A. Giumlia-Mair, eds., Cost Action G8. Non-Destructive Testing and Analyses of Museum Objects, Fraunhofer IRB Verlag, München, 2006.

[21] G.H. Aylward, T. Findlay, SI Chemical Data Book, 4th ed., J. Wiley & Sons Inc., Brisbane, 1998.

[22] R. Babić, M. Metikoš-Huković, A. Jukić, A Study of Copper Passivity by Electrochemical Impedance Spectroscopy, Journal of The Electrochemical Society, 148 (2001) B146.

[23] F.H. Assaf, A.M. Zaky, S.S. Abd El-Rehim, Cyclic voltammetric studies of the electrochemical behaviour of copper–silver alloys in NaOH solution, Applied Surface Science, 187 (2002) 18–27.

[24] R. Bogdanowicz, J. Ryl, K. Darowicki, B.B. Kosmowski, Ellipsometric study of oxide formation on Cu electrode in 0.1 M NaOH, Journal of Solid State Electrochemistry, 13 (2008) 1639–1644.

[25] R. Procaccini, M. Vázquez, S. Ceré, Copper and brass aged at open circuit potential in slightly alkaline solutions, Electrochimica Acta, 54 (2009) 7324–7329.

[26] B. Zacharie, A. Ezzitouni, J.-S. Duceppe, C. Penney, A simple and efficient large-scale synthesis of metal salts of medium-chain fatty acids, Organic Process Research & Development, 13 (2009) 581–583.

[27] C.H. Yoder, W.D. Smith, V.L. Katolik, K.R. Hess, M.W. Thomsen, C.S. Yoder, et al., The synthesis and analysis of copper (II) carboxylates, Journal of Chemical Education, 72 (1995) 267–269.

[28] S.K. Papageorgiou, E.P. Kouvelos, E.P. Favvas, A. a Sapalidis, G.E. Romanos, F.K. Katsaros, Metal-carboxylate interactions in metal-alginate complexes studied with FTIR spectroscopy, Carbohydrate Research, 345 (2010) 469–73.

[29] E.G. Palacios, A.J. Monhemius, Infrared spectroscopy of metal carboxylates I. Determination of free acid in solution, Hydrometallurgy, 62 (2001) 135–143.

[30] K. Nakamoto, Infrared and Raman spectra of Inorganic and Coordination Compounds, 3rd edition, Wiley Interscience, New York, 1978.

6. Copper carboxylate coating deposition from ethanolic solutions

6.1 Introduction

The electrochemical deposition treatment described in the previous chapter is based on the use of aqueous solutions. Water, however, can accelerate the corrosion process, especially in the case of copper alloys attacked by nantokite (CuCl). Under some circumstances moisture promotes the conversion from nantokite to copper hydroxychlorides (such as atacamite and paratacamite) producing fragmentation of the surface and developing further corrosion until the metal is completely destroyed [1–3]. Another drawback of an aqueous solution is the limited solubility of higher molecular carboxylic weight carboxylic acids (i.e. dodecanoate – octadeconate). Longer carboxylic chains give better inhibition [4], but their insolubility in water prevents their use for the preparation of aqueous coating solutions [5]. Carboxylic acids, on the other hand, are highly soluble in alcohols such as ethanol and propanol [6]. The use of ethanol, therefore, allows extending the range of lengths of carboxylic chains for the preparation of the coating solutions.

The principal aim of this study is to describe the deposition of a layer of metal carboxylates simply achieved by soaking the metal in alcoholic solutions of carboxylic acids from heptanoic acid (HC_7) to dodecanoic acid (HC_{12}), or a sodium carboxylate in the same range, as a function of different concentrations and times of immersion. The main objective is to have a practical and easy method for producing protective and corrosion inhibiting layers for copper and copper alloys. The development of these nontoxic coatings should also comply with the specific requirements of heritage preservation, such as the preservation of surface characteristics and the reversibility, but also freedom from exposure to water-based treatments.

The carboxylate layers deposited on the surface of copper coupons were characterized by XRD and electrochemical polarization tests. In addition, the layers

and the growth mechanism were characterized in-situ on the UK CRG beam line XMaS at ESRF.

6.2 Experimental

6.2.1 Coating solutions

Carboxylic acids with different carbon chain lengths, heptanoic acid (HC_7) decanoic acid (HC_{10}) and dodecanoic acid (HC_{12}) (Sigma-Aldrich), were dissolved in ethanol (99 % analytical grade). Different concentrations were prepared: 0.05 M, 0.1 M and 0.15 M.

In addition, sodium and potassium carboxylate solutions were prepared by adding respectively sodium hydroxide (0.5 M in deionized water since NaOH is insoluble in ethanol) and potassium hydroxide (0.5 M in ethanol) to the above-mentioned carboxylic acid solutions in order to raise the pH to an apparent level of 7 to provide a reproducible reference point whilst remaining aware that the concept of pH is in this medium differs considerably from that in an aqueous solution [7].

6.2.2 Sample preparation

Experiments were carried out on copper coupons (Goodfellow), 2 mm thick, 99.9 % pure and 12.6 mm diameter. The coupons were mechanically cleaned with P1200 grit SiC abrasive paper to expose a fresh surface. The surfaces were subsequently polished using a polishing cloth and Al_2O_3 water suspension (1 µm particle size). To remove any adherent Al_2O_3 particles, coupons were rinsed with deionized water and cleaned in ethanol in an ultrasonic bath for 15 minutes.

Copper samples were treated simply by immersion in the solutions for 1, 6 or 24 hours; after the immersion, samples (not rinsed) were dried by exposure to air for 2 hours.

After the treatment, the copper coupon surfaces were characterized by optical and electron microscopy. In addition, polarization measurements were carried out in a 0.1 M Na_2SO_4 solution. The reference electrode was a mercury mercurous sulphate

K_2SO_4 saturated electrode (MSE), the counter electrode a platinum grid. All the potentials given are referred to the MSE reference electrode. The polarization resistance was measured using a linear polarization in a range of ± 20 mV versus the open circuit potential (OCP) with a scan rate of 1 mV/s. The corrosion current density was calculated using linear polarization (± 250 mV vs OCP, scan rate 0.2 mV/s) and via the Tafel extrapolation.

6.2.3 Preparation of artificially corroded samples

In order to verify the effect of copper carboxylate deposition on corroded objects, artificially corroded copper coupons were prepared according to protocols described in literature [8]. The corrosion products produced included cuprite (Cu_2O), nantokite (CuCl), paratacamite $Cu_2Cl(OH)_3$ and a mixture of copper chlorinated compounds.

The cuprite layer was obtained by polarizing the copper coupon at -0.360 V in a 0.1 M Na_2SO_4 solution for 16 hours.

The nantokite layer was produced by immersing the copper sample in a $CuCl_2 \cdot 2H_2O$ saturated solution for half an hour. After that, the sample was rinsed with deionized water (which is necessary to remove residual $CuCl_2$, but also produces some cuprite [9]) and let dry in air for 24 hours.

In order to produce paratacamite a corrosive solution was first prepared by dissolving 10 g of $Cu(NO_3)_2 \cdot H_2O$ and 10 g of NaCl in 100 mL of deionized water. The copper coupon was wetted twice a day with the corrosive solution for five consecutive days.

The same protocol was followed for the preparation of the mixture of copper chlorinated compounds using a different corrosive solution, made by dissolving 15 g of $(NH_4)_2CO_3$ and 10 g of NH_4Cl in 100 mL of deionized water.

6.2.4 Synchrotron-XRD

The deposition process has been studied by means of SR-XRD at the UK CRG beam line XMaS. For this experiment a special environmental cell (eCell [10], described in

paragraph 2.8) was used, in which the sample can be analysed whilst permanently in solution.

The cell was filled with an ethanolic solution of dodecanoic acid (0.15 M), with the apparent pH was adjusted to 7 as described above by adding a 0.5 M aqueous solution of sodium hydroxide. This experiment was carried on only with the solution of sodium dodecanoate because, among the carboxylates tested, this provided the highest reduction of the corrosion current density when used for treating a copper surface. Sequences of XRD images were taken using a Mar CCD camera in order to obtain time-lapse information on the deposition. This approach was previously used to investigate the growth of lead decanoate from aqueous solutions of sodium decanoate [11,12]. The camera was positioned in plane with its axis at an angle of 40° to the incoming beam which was incident at 10° to the sample surface. The acquisition time was 10 s per image and stacks of several hundred images were acquired with a 2 minute interval between images.). The X-ray wavelength was 1.55 Å. Figure 6.1 shows the eCell filled with the ethanolic solution, with the copper coupon clearly visible at the centre. A stepper motor controls the distance of the sample from an X-ray transparent window. The coupon is moved every two minutes to within 100 µm of the window where it remains for a few seconds whilst XRD data is collected. Most of the time the coupon is >3 mm away to facilitate the surface reaction with the solution. The images have been processed using esaProject©, specially developed for this purpose [12] and described in paragraph 2.8.

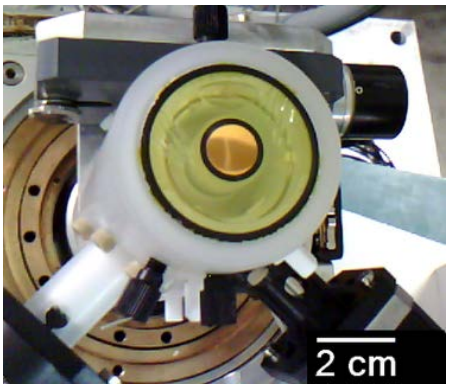

Figure 6.1: eCell mounted on the beamline BM28 at the ESRF. In the centre the copper coupon is visible.

6.3 Results and discussion

6.3.1 Ethanolic solutions of carboxylic acids

Copper coupons were immersed in ethanolic solutions of heptanoic, decanoic and dodecanoic acid, testing different times of immersion and concentrations. None of the solutions provided a homogeneous coating. Figure 6.2, for example, shows an optical micrograph of a copper coupon immersed for 24 hours in a 0.1 M heptanoic acid solution, which illustrates the deposition of blue-green crystals consistent with the formation of copper heptanoate [13].

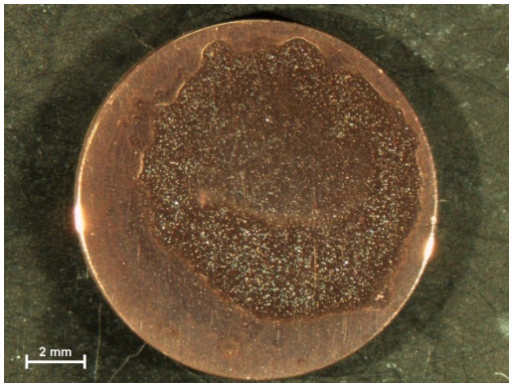

Figure 6.2: Optical micrograph of a copper coupon treated for 24h in a 0.1 M HC_7 ethanolic solution.

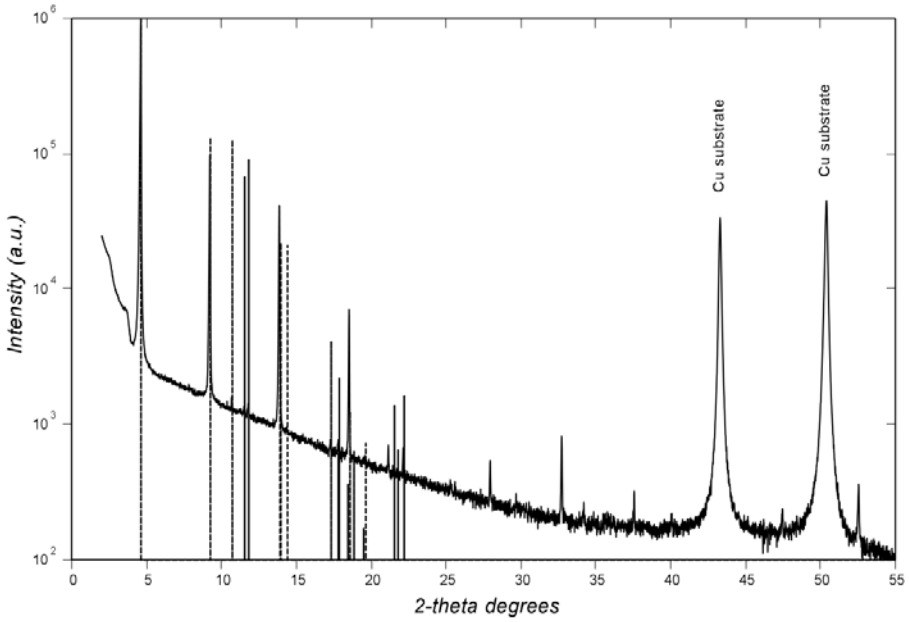

Figure 6.3: XRD diffractogram (log-lin plot) of copper treated for 24 h in a 0.1 M HC_7 solution (thick continuous line) and the reference spectrum of Cu-heptanoate obtained by [12].

The XRD diffractogram of the sample is presented in Figure 6.3. The comparison of the diffractogram with references in the ICDD PDF2 database [14] could not find a match and further examination showed that the latter does not contain reference spectra for copper heptanoate. The XRD diffractogram collected, nevertheless, showed a good agreement with the structural information given by Ghermani et al [13].

Figure 6.4 (a) shows a backscattered (BS) electron image of the same sample. Here darker areas represent the copper carboxylate crystals (characterized by a low average Z elements, such as carbon and hydrogen), while the metallic copper surface (higher Z) appears as a lighter colour. The secondary electron (SE) image (Figure 6.4b) presents the topography of the sample surface in the same region. Figure 6.4c is a magnification of image (b) and zooms into one of the copper carboxylate crystals and shows that copper-carboxylate growth starts from needle-shaped crystals (6.4c). The coverage of the sample surface given by the carboxylate is not complete, as it can be verified by the backscattered electron image.

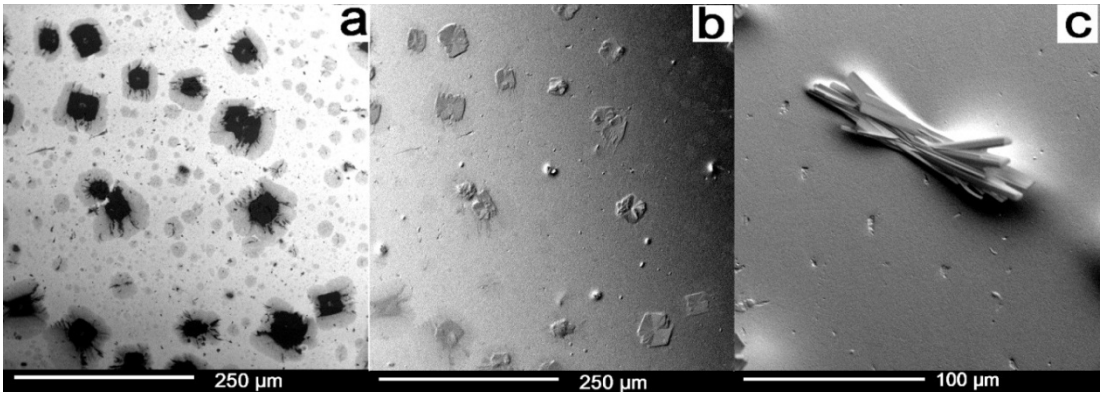

Figure 6.4: SEM images of copper treated for 24 h in a 0.1 M HC_7 ethanolic solution. Backscattered electron (BS) image (a), secondary electron (SE) images (b and c).

Longer carboxylic chains, such as decanoic (HC_{10}) and dodecanoic acid (HC_{12}) in an ethanolic solution give similar results, with the formation of similar crystals dispersed on the copper surface. An example is the optical image presented in Figure 6.5, where crystals of copper dodecanoate are clearly visible. In general, longer immersion times and higher concentrations lead to an increase in the number of crystals.

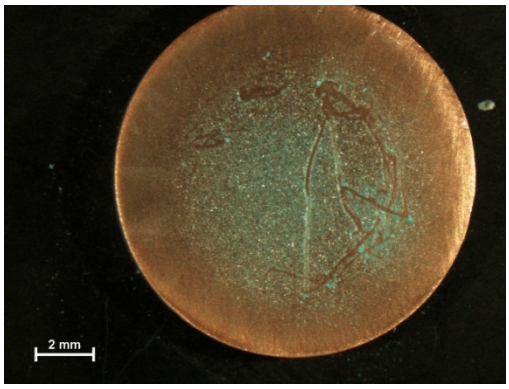

Figure 6.5: Optical micrograph of a copper coupon treated for 24 h in a 0.1 M HC_{12} ethanolic solution.

6.3.2 Sodium carboxylate solutions

In a second set of experiments, copper coupons were immersed in a sodium carboxylate (NaC_n) ethanolic solution. With the NaC_7 solution (concentration equal to, or higher than 0.1 M), after 24 hours of immersion, samples show a good coverage of the surface.

Figure 6.7a shows an optical micrograph of this sample. The surface is covered by a whitish translucent layer. In the SEM images, we observe the presence of a sort of net formed by crystals (Figure 6.6b and c). In the backscattered electron image (Figure 6.6b) the crystals appear darker respect to the background, indicating that they are composed of lighter elements than copper. The layer formed could be then formed either by copper carboxylates or by sodium carboxylates.

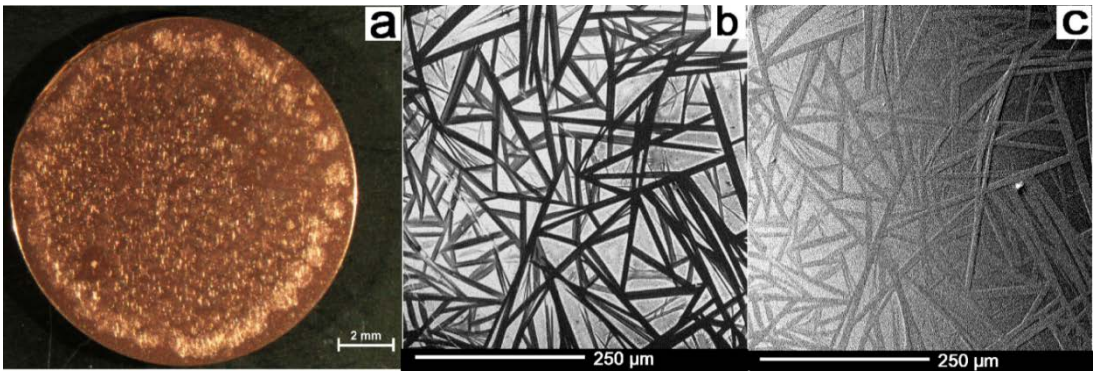

Figure 6.6: Copper coupon treated for 24 h in a 0.1 M NaC_7 ethanolic solution: optical image (a), BS (b) and SE (c) images.

In order to better understand the composition of this layer, XRD analyses were performed and the diffractogram is presented in Figure 6.7. Copper heptanoate

reflections are clearly visible combined with a second sequence, attributable to the presence of sodium carboxylate. A common feature in XRD patterns collected from layers grown from sodium carboxylates in alcohol, is a diffraction peak at 13.3° which is likely to be a reflection from copper hydroxide ($Cu(OH)_2.H_2O$). This is not present on depositions from carboxylic acids alone. The coating formed by immersing copper coupons in ethanolic sodium carboxylate solutions appear to be formed by a mixture of copper and sodium carboxylate.

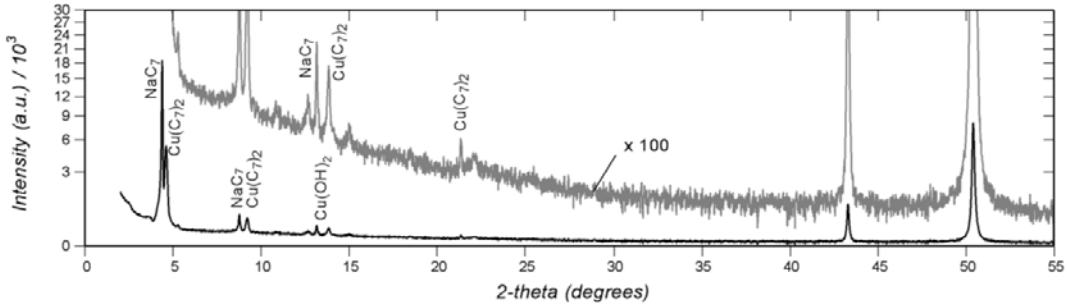

Figure 6.7: XRD diffractogram (square root intensity plot) of a copper coupon immersed in a 0.1 M NaC_7 ethanolic solution. The grey spectrum is a magnification (100x).

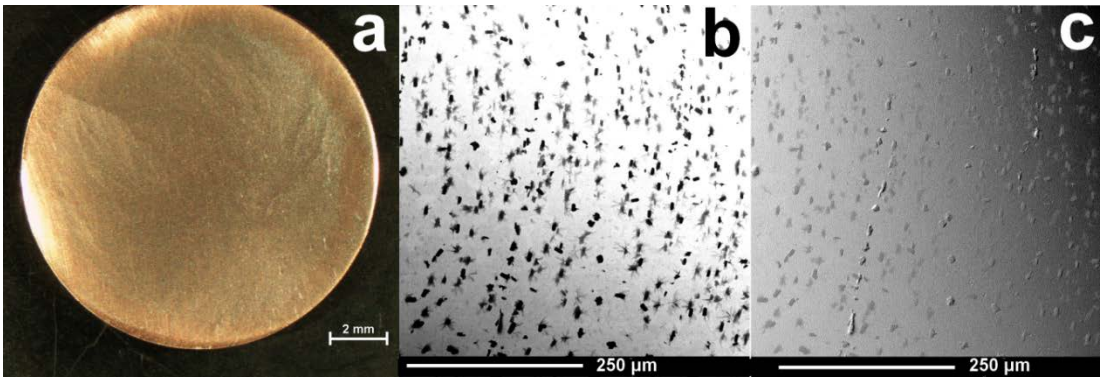

Figure 6.8: Sample treated for 24h in 0.15 M HC_{10}, optical image (a), BS (b) and SE (c) images.

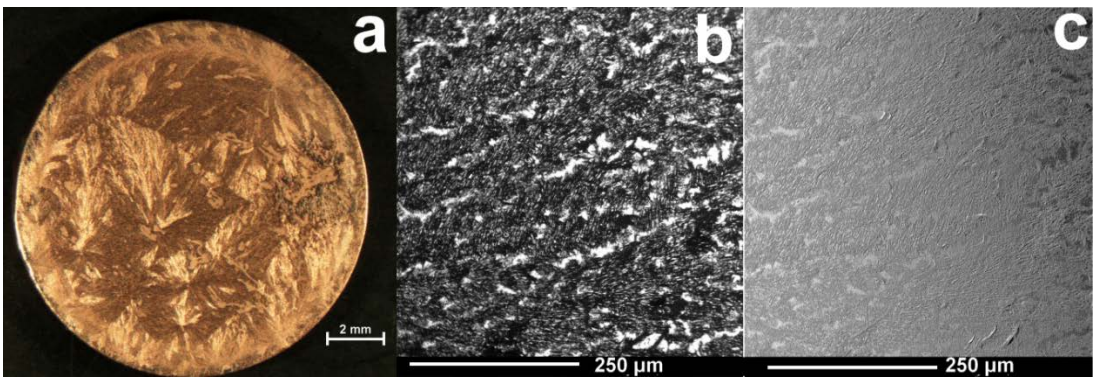

Figure 6.9: Sample treated for 24h in 0.15 M NaC_{10} (in ethanol), optical image (a), BS (b) and SE (c) images.

Figures 6.8 and 6.9 show the results of the copper coupons immersed in 0.15 M solutions of HC_{10} and NaC_{10} respectively. The difference in surface coverage between the sample treated with HC_{10} or NaC_{10} is evident. The sample treated with the latter solution presents a surface almost totally covered by a carboxylate layer, while the coupon immersed in an acid solution presents scattered crystals of copper decanoate on the surface, lightly visible in the optical micrograph.

On some samples it is possible to observe the formation of a thicker layer blue green layer where oxidized regions on the sample are present (especially on the unpolished back, as shown in Figure 6.10b). The thicker layer appears to be blue-green and XRD analyses (reported in Appendix E) demonstrate that this is composed of a mixture of copper hydroxides and copper and sodium carboxylate. The whitish colour of the coating formed on the upper surface (Figure 6.10a) can be ascribed to the presence of a mixed layer composed of sodium carboxylate and copper carboxylate, also observed for the heptanoate above and in previous studies [15]. On the other hand, the formation of this deposit on the back was evident exclusively when treating the samples with NaC_{12} in concentration higher than 0.1 M. No such green layer was observed with NaC_7 or NaC_{10}.

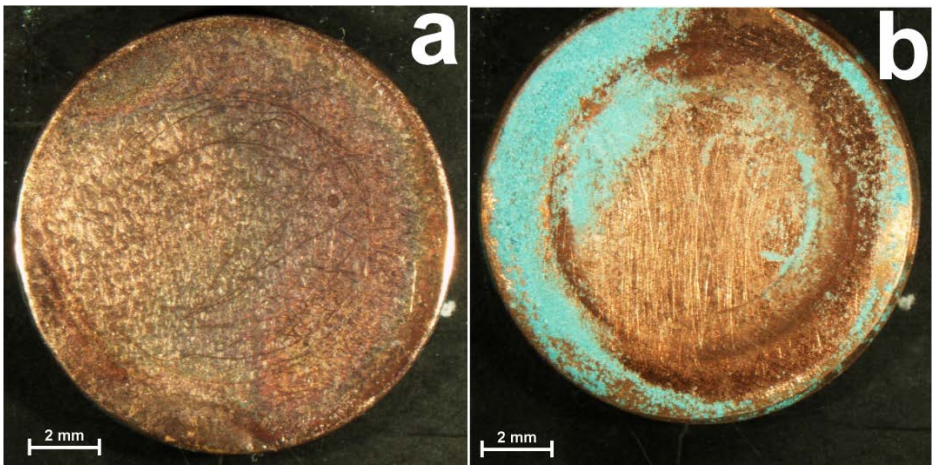

Figure 6.10: Optical micrographs of sample treated for 24h in 0.1 M NaC_{12} (in ethanol): front (a) and back side (b).

The reproducibility was a problem during these experiments. In a series of samples treated following the same protocol, very few reacted with the solution to form a coating. The irreproducibility of the coating formation is probably due to the

inhomogeneity of the solution. The "pH7" solutions are not homogeneous systems because they are composed of ethanol and water (added with the NaOH solution). Sodium carboxylates are dissolved in the water component, while copper carboxylates are dissolved in the ethanolic component of the solution. The use of NaOH in aqueous solution is necessary because sodium-carboxylates are not soluble in ethanol [16]. As a result a number of tests have been carried out using KOH instead of NaOH. KOH is more soluble than NaOH in ethanol [17] and it makes it possible to avoid the presence of water in the carboxylate solution. However, even then, it was not possible to obtain a uniform layer of copper-carboxylate on the surface.

6.3.3 Sodium carboxylate coatings on artificially corroded samples

In order to test the effects of carboxylate solutions on real objects, a set of corroded samples were prepared for the coating application. The samples were covered with different copper corrosion products: cuprite, nantokite, paratacamite and a mixture of copper chlorinated compounds.

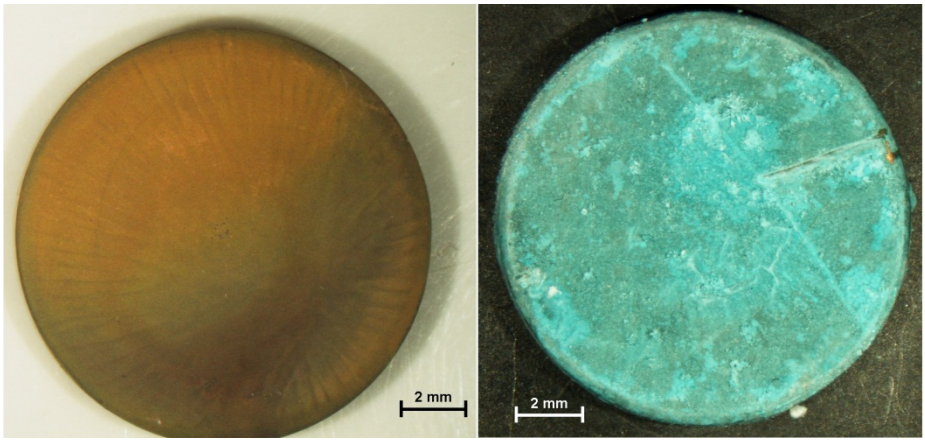

Figure 6.11: Optical micrographs of an artificially corroded sample (covered by a nantokite layer) before and after immersion in 0.15 M NaC_{12} for 24h.

The corroded samples were immersed in a dodecanoic acid (0.15 M) solution and a sodium dodecanoate (0.15 M) solution for 24 hours. After 24 hours of immersion the samples showed a blue-green colour, in some case a white deposit on the blue surface was also visible, probably related to the deposition of unreacted sodium-

dodecanoate. Figure 6.11 shows an example of the results obtained: on the left is a corroded copper coupon with a nantokite layer (4 µm thick); on the right is the same copper coupon after 24 h of immersion a sodium-dodecanoate solution 0.15 M in ethanol. In this example the colour of copper-carboxylate is evident. We can assume that the better reactivity of a corroded surface is due to the larger availability of copper ions on the surface. In this case, the coating appears soft and can be easily scratched by a finger nail.

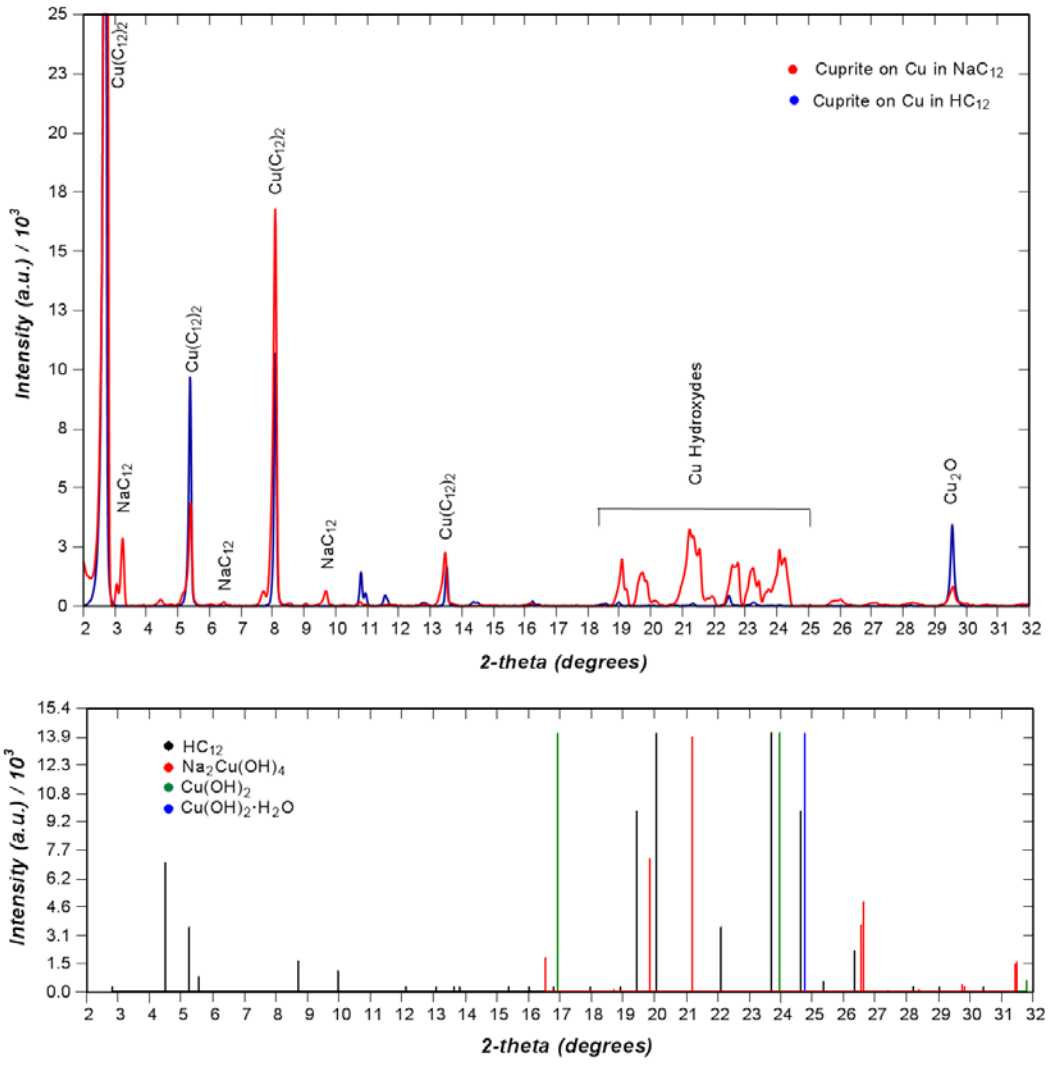

Figure 6.12: the above spectrum shows the comparison between XRD spectra (2theta range 2-32) obtained from corroded copper coupons (cuprite layer) immersed in 0.15 M ethanolic solution of HC_{12} (blue line) and NaC_{12} (red line). Below, the reference patterns for several Cu hydroxydes and for dodecanoic acid are shown in the 2-theta range 2-32 degrees.

XRD analyses were performed after the treatment in NaC_{12} and HC_{12}. Figure 6.12 shows the pattern from Cu coupons, covered by a cuprite layer, after the immersion in the coating solutions. Diffraction peaks of copper and cuprite are not visible in the pattern, which shows the two theta range 2-32 degrees, more interesting for the observation of carboxylate diffraction patterns.

The two diffractograms presents the same pattern, attributable to $Cu(C_{12})_2$, with the red spectrum (sample immersed in NaC_{12}) having extra peaks slightly shifted on the right. The presence of these peaks is attributable to the presence of NaC_{12}. In the two theta range between 17 and 24 degrees peaks due to the formation of copper-sodium hydroxides are also visible. The presence of copper hydroxides can be explained by the reaction of the copper surface with the NaOH added to the solution, since they were not detected in sample immersed in carboxylic acid solutions.

We observe that, on the sample immersed in NaC12 (red spectrum) the intensity of the diffraction peaks due to the reflection of NaC_{12} are less intense respect to the reflections of NaC_{12}, indicating a minor presence of the sodium carboxylate with respect to the copper carboxylate.

To summarize, copper coupons immersed in NaC_{12} 0.15 M ethanolic solution (which means dodecanoic acid partially neutralized with NaOH) seem to present a mixed layer constituted of mostly NaC_{12} and $Cu(C_{12})_2$. The preponderance of $Cu(C_{12})_2$ or NaC_{12} may depend on the availability of copper ions on the surface. The reason for this difference is that the process

$$Cu \rightarrow Cu^{++} \rightarrow Cu(C_{12})_2 \qquad (6.1)$$

is possibly slower than the precipitation of NaC_{12}, while the presence of an oxidized layer on the coupon surface seems to favour the formation of $Cu(C_{12})_2$ respect to the deposition of NaC_{12}.

6.3.4 Synchrotron radiation XRD study of copper carboxylate layers

We note above that the copper carboxylate layers only become apparent on the surface when the solvent evaporates. This was confirmed by time-lapse XRD experiments in the eCell on the XMaS beamline at the ESRF. A sequence of X-ray diffractograms taken over several hours shows no sharp features due to crystal growth.

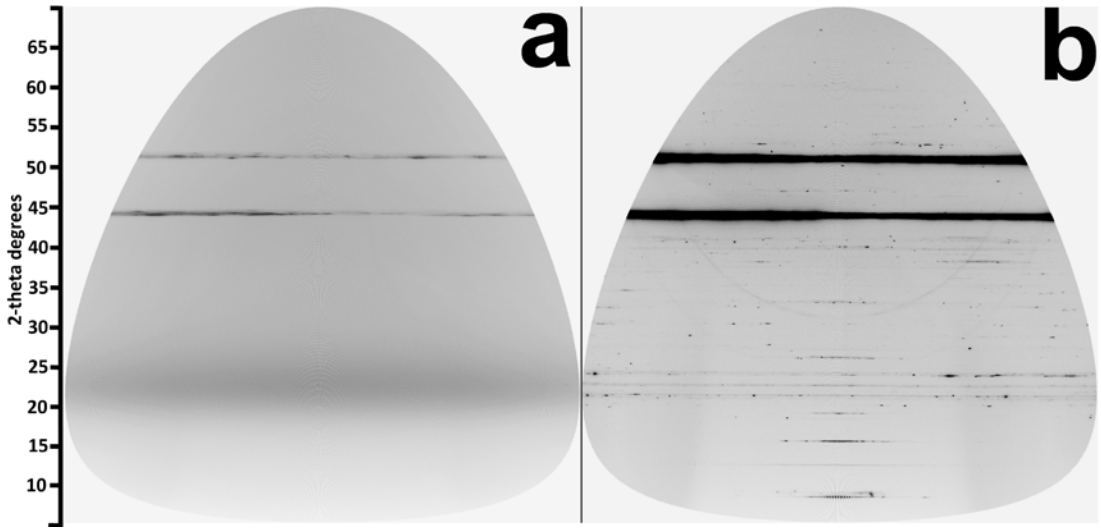

Figure 6.13: Diffraction images of a copper coupon, immersed for 12 hours in a 0.1 M NaC12 ethanolic solution, taken before the removal of the coating solution (wet surface, a) and at the end of the drying process (dry surface, b).

The images shown in Figure 6.13 were collected during the immersion time develop a diffuse band between scattering angles of 20° and 25° which indicates the presence of a gel or nanocrystalline layer either on the surface or in suspension immediately above it. This band is clearly visible in the image (taken after 8 hours in solution) in figure 6.13a, together with the two main diffraction peaks of copper at two theta angles 43.6° and 50.7°. In this image, the scattering of the copper is absorbed by the solution and its reflection bands show a low intensity. After this image was acquired, the solution was removed from the eCell and the sample was allowed to dry in air. The last Mar image of the drying sequence is presented in Figure 6.13b. The diffuse band has split into three reflections as the nanocrystals consolidate into larger formations on drying. It can therefore be concluded that compounds develop in nanocrystalline form close to the electrode surface during the immersion in the

solution, and are then deposited as crystals large enough for coherent scattering by evaporation of the solvent. The polycrystalline structure of the copper substrate, on the other hand, is visible by the two intense reflection bands at 43.6° and 50.7°. The deposition can also be observed in XRD patterns obtained from the image stack (by integrating along the rows of the images). The time-lapse sequence is presented in Figure 6.14 and the XRD pattern extracted from the sequence is shown in Figure 6.15. The crystallization process is fast but the compounds which grow are not identifiable as copper dodecanoate. Instead the spectra are similar to those from the reverse side of the coupons as described above, consisting of a mixture of copper hydroxides (mostly), copper dodecanaote and dodecanoic acid.

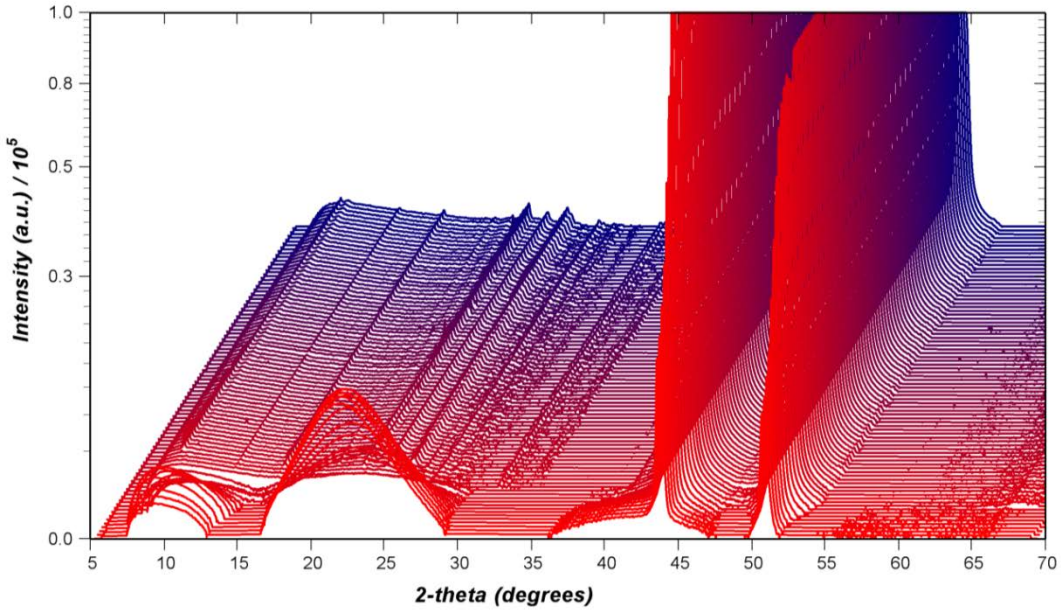

Figure 6.14: XRD diffractogram sequence of the drying process of copper immersed in a 0.15 M ethanolic solution of NaC_{12}.

The reflections from 17 degrees onwards, in fact, correspond to hydroxides of copper and sodium-copper. In contrast, a coupon grown and analysed in the laboratory in a solution of HC_{12} in ethanol showed a set of reflections very similar to that in Figure 6.12. Clearly, the process is hard to reproduce, and the presence of the sodium hydroxide leads to the formation of undesirable by-products.

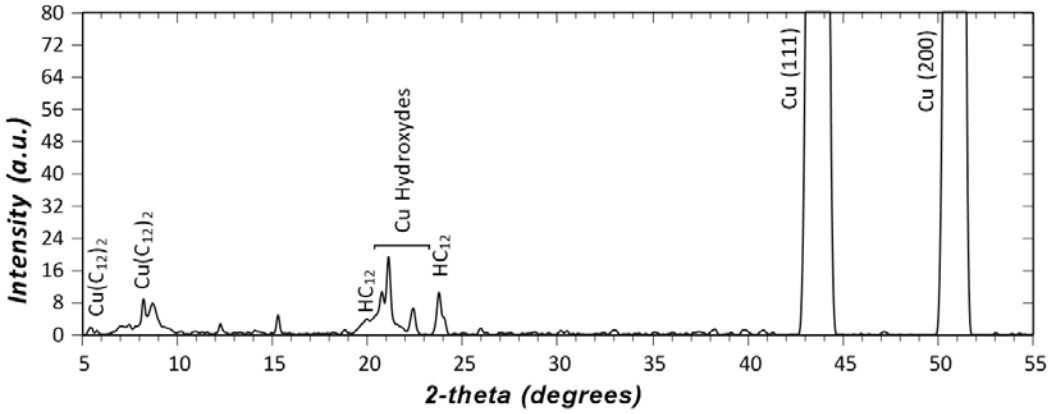

Figure 6.15: XRD pattern extracted from the last image of the drying sequence (2-theta range 5-55 degrees).

6.3.5 Evaluation of the corrosion inhibition

A further step in this research involved the measurement of the corrosion inhibition of the carboxylate coatings applied from ethanolic solution with electrochemical measurements such as polarization resistance and corrosion density measurements. For the electrochemical tests we selected only the samples that presented homogeneous coatings:

NaC_7: 0.05 M and 0.10 M immersed for 1, 6 and 24 hours
NaC_{10}: 0.05 M, 0.10 M and 0.15 M immersed for 1, 6 and 24 hours
NaC_{12}: 0.10 M and 0.15 M immersed for 1, 6 and 24 hours

Potentiodynamic curves of a set of copper coupons treated with different solutions are presented in Figure 6.16. All samples in the figure have been treated with the same conditions regarding polishing, concentration (0.10 M) and immersion time (24 hours).

This plot shows that the use of NaC_7 and NaC_{10} to coat the copper coupon does not improve the corrosion resistance: in fact, the corrosion potential (E_{corr}) is the same as for the uncoated copper and it is not possible to observe a decrease in the corrosion current density (i_{corr}). The treatment with 0.10 M NaC_{12} solution, on the other hand, gives a better inhibition as the corrosion current density is slightly reduced. Moreover, the slope of the anodic curve was not significantly reduced by the

presence of NaC_7 or NaC_{10}, indicating the ineffectiveness of the compound as corrosion inhibitor. The use of NaC_{12}, on the other hand, slows the corrosion rate of the copper, observable in a reduced slope of the anodic part of the curve between -0.40 and -0.35 V.

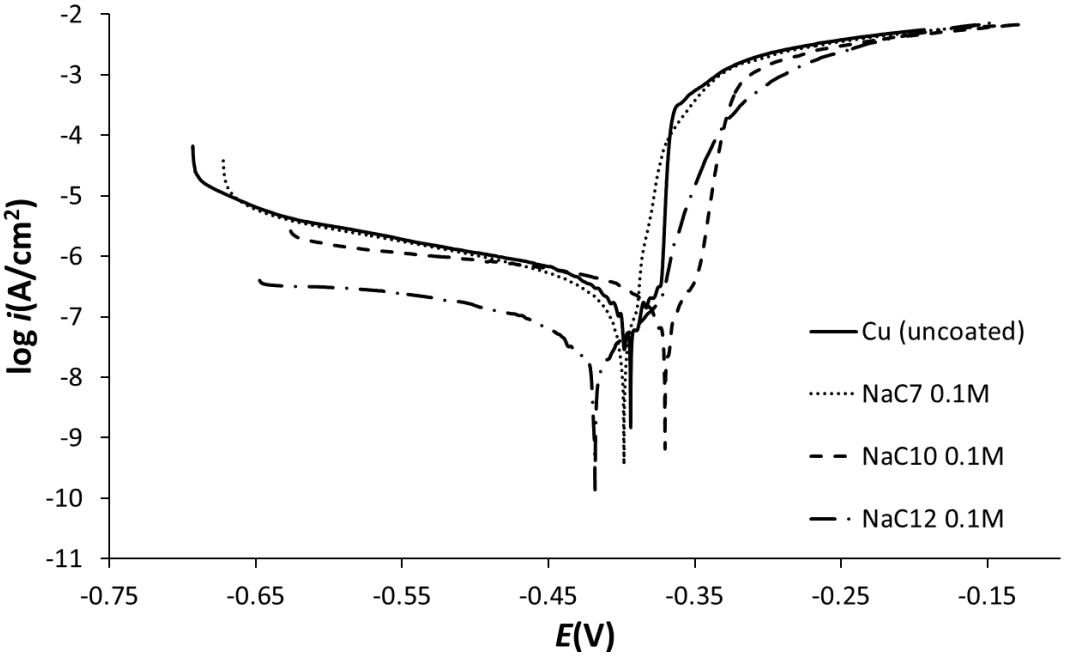

Figure 6.16: Potentiodynamic curves for samples treated in 0.1 M NaC_7 (dotted line), 0.1 M NaC_{10} (dashed line), 0.1 M NaC_{12} (dash-dot line) and uncoated copper (full line).

Table 6-I presents the average value (obtained from five measurements) of E_{corr}, the polarization resistance (R_p) and the current density (i_{corr}) for the samples coated with NaC_7, NaC_{10} and NaC_{12} and shows an increasing inhibition connected with the length of the carboxylic chain. The i_{corr} values, in fact, is decreasing with the increasing number of carbon atoms. The values presented here are the average values obtained from five repetitions of the measurements.

The data also demonstrate that the corrosion inhibition is variable and strictly dependent on the uniformity of the carboxylate layer. The highest values were obtained from samples where there was a uniform layer on the surface.

Although they show corrosion inhibition in some cases, copper-carboxylate layers appear unsuitable for application to real objects at least for three reasons: they introduce a new layer, changing the colour and general appearance, they are not resistant to accidental scratches and their softness is not good for the protection against pollutants. A number of solutions for addressing these issues could be

tested, for instance shorter immersion time, in order to get a thinner layer, even though this would not solve the problem of the coating colour, as all copper-carboxylates show a blue colour [16,18].

Table 6-I: Average value of E_{corr}, polarization resistance (R_p) and current density (i_{corr}) for copper coupons coated with NaC_7, NaC_{10} and NaC_{12}.

Sample	E_{corr} (V)	σ E_{corr}	R_p (Ω cm²)	σ R_p	i_{corr} (A/cm²)	σ i_{corr}
Copper (uncoated)	-0.44	0.01	3.9×10^3	3.5×10^2	1.5×10^{-6}	4.1×10^{-7}
NaC_7 0.1 M	-0.41	0.01	7.5×10^3	1.6×10^3	3.1×10^{-7}	2.3×10^{-7}
NaC_{10} 0.1 M	-0.37	0.01	2.6×10^4	1.3×10^4	1.7×10^{-7}	7.5×10^{-8}
NaC_{10} 0.15 M	-0.35	0.01	5.8×10^4	3.5×10^4	9.3×10^{-8}	5.2×10^{-8}
NaC_{12} 0.1 M	-0.39	0.01	1.1×10^6	1.4×10^6	1.6×10^{-8}	1.4×10^{-8}
NaC_{12} 0.15 M	-0.39	0.01	5.6×10^5	7.1×10^5	3.3×10^{-8}	3.8×10^{-8}

6.4 Conclusions

This chapter described the deposition of copper carboxylate layers achieved by immersion in ethanolic solutions of carboxylic acids and sodium carboxylates. This method allows the use of longer carboxylic acid (less soluble in water) and the preservation of a higher pH respect to the use of pure carboxylic acids.

Solutions of long-chain carboxylic acid in ethanol and "pH 7" solutions have been tested and the addition of NaOH improves the homogeneity of the layer with the risk that copper and copper-sodium hydroxides will also form in varying proportions. The carboxylate layer obtained once the solvent has evaporated, is easily removable, consists in-part of sodium carboxylate as well as the copper compound where NaOH was added, but does not create an efficient barrier against moisture and gaseous pollutants.

The study of the deposition of a copper-dodecanoate layer with SR-XRD showed that the $Cu(C_{12})_2$ does not grow on the electrode surface during immersion, but it is deposited by evaporation of the solvent.
Finally, colour and aesthetic appearance of the treated metal are not satisfying: thin layers of carboxylate coating are not effective against corrosion and thicker layers show a blue-green colour.
The results presented show that the deposition of copper carboxylate coatings from ethanolic solution does not at the moment provide a suitable route to surface protection in the conservation of historic metals, even though some corrosion inhibition can be achieved. Even then, the method presents reproducibility problems in the coating deposition and therefore in the inhibition efficiency.

References

[1] D.A. Scott, Copper and Bronze in Art – Corrosion, Colorants, Conservation, Getty Publications, Los Angeles, 2002.

[2] I.D. MacLeod, Bronze disease: an electrochemical explanation, in: Bulletin AICCM 7, AICCM, 1981: pp. 16–26.

[3] W.R. Fischer, B.D. Wagner, H. Siedlarek, B. Fussinger, I. Hanssel, N. von der Bank, The influence of chloride ions and light on the corrosion behavior of copper alloys in aqueous environments with special regard to bronze disease, in: I. MacLeod, S.L. Pennec, L. Robboiola (Eds.), Metal 95, Proceedings of the International Conference on Metals Conservation, Semur En Auxois 25-28 September 1995, James & James Ltd, London, 1997: pp. 89–94.

[4] E. Rocca, J. Steinmetz, Inhibition of lead corrosion with saturated linear aliphatic chain monocarboxylates of sodium, Corrosion Science, 43 (2001) 891–902.

[5] S. Mauchauffee, E. Meux, M. Schneider, Determination of the Solubility Products in Water at 20 °C of 32 Metallic Carboxylates, Industrial & Engineering Chemistry Research, 47 (2008) 7533–7537.

[6] R.T. Morrison, R.N. Boyd, Organic Chemistry, Prentice Hall PTR, London, 2002.

[7] R.G. Bates, M. Paabo, R.A. Robinson, Interpretation of pH measurements in alcohol-water solvents, Journal of Physical Chemistry, 67 (1963) 1833–1838.

[8] K. Leyssens, A. Adriaens, C. Degrigny, Electrochemical monitoring of the storage or stabilization of archaeological copper-based artifacts in sodium sesquicarbonate solutions, in: J. Bridgland (Ed.), ICOM-CC Preprints of the 14th Triennial Meeting, The Hague, 12-16 September 2005, James & James Ltd, London, 2005: pp. 301–309.

[9] M. G. Dowsett, A. Adriaens, C. Martin and L. Bouchenoire, The use of synchrotron x-rays to observe copper corrosion in real time, Analytical Chemistry 88 (2012) 4866-4872.

[10] M.G. Dowsett, A. Adriaens, Cell for simultaneous synchrotron radiation X-ray and electrochemical corrosion measurements on cultural heritage metals and other materials., Analytical Chemistry, 78 (2006) 3360–5.

[11] M. Dowsett, A. Adriaens, B. Schotte, G. Jones, L. Bouchenoire, Real time spectroelectrochemical growth and corrosion resistance monitoring of lead carboxylate coatings in an environmental cell (eCell), in: C. Degrigny, R. van Langh, I. Joosten, B. Ankersmit (Eds.), Metall 07: Proceedings of the International Conference on Metals Conservation. Amsterdam 17-21 September 2007, Rijksmuseum Amsterdam, Amsterdam, 2007: pp. 26–31.

[12] M. Dowsett, A. Adriaens, B. Schotte, G. Jones, L. Bouchenoire, In-situ spectroelectrochemical study of the growth process of a lead decanoate

coating as corrosion inhibitor for lead surfaces, Surface and Interface Analysis, 41 (2009) 565–572.

[13] N.-E. Ghermani, C. Lecomte, C. Rapin, P. Steinmetz, J. Steinmetz, B. Malaman, Structure and preliminary electron distribution of copper heptanoate from room-temperature X-ray data, Acta Crystallographica Section B Structural Science, 50 (1994) 157–160.

[14] International Centre for Diffraction Data database, release 2008, http://www.icdd.com/ (accessed 2/07/2013).

[15] S. Hollner, F. Mirambet, A. Texier, E. Rocca, J. Steinmetz, L. De Chimie, et al., Development of new non-toxic corrosion inhibitors for cultural property made of iron and copper alloys, in: V. Argyropoulos, A. Hein, M. Abdel Harith (Eds.), Proceedings of International Conference on Conservation Strategies for Saving Indoor Metallic Collections, Cairo 25 February – 1 March 2007, TEI of Athens, Athens, 2007: pp. 156–161.

[16] B. Zacharie, A. Ezzitouni, J.-S. Duceppe, C. Penney, A simple and efficient large-scale synthesis of metal salts of medium-chain fatty acids, Organic Process Research & Development, 13 (2009) 581–583.

[17] G.H. Aylward, T. Findlay, SI Chemical Data Book, 4th ed., J. Wiley & Sons Inc., Brisbane, 1998.

[18] C.H. Yoder, W.D. Smith, V.L. Katolik, K.R. Hess, M.W. Thomsen, C.S. Yoder, et al., The synthesis and analysis of copper (II) carboxylates, Journal of Chemical Education, 72 (1995) 267–269.

7. Conclusions

The research carried out and presented in this work has focused on different aspects of the corrosion of copper and copper alloys by means of electrochemical methods and complementary spectroscopic methods. The aim was to contribute to the improvement of strategies for preserving our cultural heritage. Three main applications were addressed: the corrosion study of copper-tin alloys, the application of voltammetry of microparticles for the characterization of copper alloys and their corrosion products, and the synthesis and characterization of protective coatings for copper surfaces.

Chapter 3, concerning, the corrosion of copper-tin alloys, aimed at studying the influence of the tin content on the corrosion behaviour of the alloys in various environments, including simulated marine environments and an urban environment. LSV and the related Tafel plots and polarization resistance measurements, together with SEM, XRF and XRD, allowed the characterization of the corrosion layers formed. Results showed that the tin content does not affect the types of corrosion product formed on the surface, however, a reduction of the corrosion rate was observed for alloys with a higher tin percentage. One should keep in mind here that the simulation experiments intend to approach realistic environments but nevertheless may still pose some limitations. The two-dimensional XRD analyses, in fact, highlighted the differences between corrosion layers formed by exposure to the atmosphere and corrosion layers formed in a corrosive solution. Further developments in this area may include other types of aggressive agents, extending the range of corrosive environments that can be simulated. Other research directions could involve the use of different alloy compositions and different surface finishing which could provide more information on the effect of mechanical polishing and chemical cleaning on the corrosion behaviour of copper and its alloys.

Voltammetry of microparticles (VMP) was used as a non-destructive technique to characterize copper-based archaeological artefacts from three excavated sites in

Flanders. In order to establish this, first a voltammetric database analysing of reference materials (metals and simulated corrosion products) was created. The analyses carried out allowed the qualitative identification of the alloy composition and of the copper corrosion products present on archaeological artefacts. Complementary analyses, performed by means of XRF and XRD, confirmed the results obtained from the VMP analyses.

VMP is shown to be effective for the characterization of corrosion layers, especiallyfor the detection of copper chlorides which are dangerous for the preservation of the objects. This is certainly an advantage of the technique that can help conservators and restorers, dealing with a large number of archaeological artefacts, in finding easily the objects that can be considered more in danger compared to objects with a stable patina. The selectivity of the technique towards the electroactive species present in the sample is one of the main advantages of VMP. By selecting different electrolytes, the separation between oxidation and reduction peaks of diverse electroactive species can be achieved, leading to the identification of all the elements and minerals present in the sample. The major drawback of the technique is certainly the high dispersion of the data, which may create difficulties for the identification of the minerals. This problem can be possibly reduced, but only partially. The dispersion of the data, in fact, may be due to heterogeneities in the archaeological samples, difficult to estimate and eliminate, but also to the experimental conditions. Future developments, therefore, should include more research on the effect of experimental parameters on the voltammetric response, in order to minimize the dispersion of the data.

In view of the application of VMP to other archaeological and historical artefacts, more research is needed not only in order to extend the range of reference copper corrosion products, but also in order to create a reference database for minerals of tin, lead and zinc which can occur in archaeological corrosion layers. The research, in particular, should be focussed on the testing of various electrolytes with the aim of having a sort of universal electrolyte able to discriminate the different minerals in the corrosion crust.

The last part of the research dealt with the development of a carboxylate based protective coating for copper surfaces. Two deposition methods (electrochemical

deposition from aqueous solutions and immersion in ethanolic solutions) have been tested and the coatings have been characterized by means of linear sweep voltammetry and Tafel extrapolation, ATR-FTIR, XRD, optical and electron microscopy.

The two deposition methods produced protective layers able to reduce the corrosion rate of the copper surfaces. The most effective results were obtained by using a carboxylic chain of twelve carbon atoms. In particular, the use of ethanolic solutions was preferred in order to have a practical and easy method for treating archaeological objects without use of water, which can favour the corrosion process. Both methods, unfortunately, showed reproducibility problems in both the deposition as well as in the inhibition. Further research will be needed to better understand the formation of copper carboxylates layers, in order to improve the reproducibility of the deposition process. Another drawback encountered during this research, which makes copper carboxylate unsuitable for the application in the preservation of historical copper (and copper alloys) artefacts, is the aesthetic appearance of the treated metals. Copper-carboxylates, in fact, are characterized by a blue-green colour, evident in the case of the deposition of a thick layer and when treating corroded objects. A change in the surface properties cannot be accepted when dealing with heritage metals, whose aesthetic characteristics should be preserved for the correct interpretation of the historical significance.

As a final consideration of this work, it must be emphasized that the role of electrochemistry in the study of cultural heritage materials can and should be extended. Besides corrosion studies, for which electrochemical methods are the main techniques, voltammetry of microparticles appears very promising for many applications in the field of heritage studies. Its characteristics, including its versatility, allow its use for the characterization of a broad range of materials (among them pigments and organic dyes) and its diffusion in conservation laboratories.

Nederlandstalige samenvatting

Het onderzoek in dit werk spitst zich toe op corrosiestudies van koper door middel van elektrochemische methoden en enkele complementaire spectroscopische methoden. Het doel omvat een bijdrage te leveren in de verbetering van conservatie-strategieën van het metalen culturele erfgoed. Drie aspecten worden behandeld: de corrosiestudie van koper-tin legeringen, de toepassing van voltammetrie van micropartikels (VMP) voor de karakterisering van koperlegeringen en corrosieproducten van koper, en de synthese en karakterisering van een beschermende deklagen voor koperen voorwerpen.

In het eerste deel wordt de invloed van het legerend element tin op het corrosiegedrag van de legeringen bestudeerd. Het onderzoek wordt uitgevoerd in verschillende milieus, waaronder een gesimuleerd marien milieu en een typisch stedelijk milieu. Lineaire voltammetrie, Tafel grafieken en polarisatieweerstandmetingen, samen met rasterelektronenmicroscopie (SEM), X-straalfluorescentiespectroscopie (XRF) en X-straaldiffractie (XRD) laten toe verschillende corrosie-aspecten (corrosiesnelheid, gevormde corrosielaag, morfologie, en dergelijke) te karakteriseren.

De VMP techniek wordt aangewend als niet-destructieve techniek om koper-gebaseerde voorwerpen uit drie Vlaamse archeologische sites the karakteriseren. De analysen laten toe om de samenstelling van de legering alsook deze van de corrosieproducten te bepalen. Complementaire analysen worden uitgevoerd met behulp van XRF en XRD.

Het laatste deel heeft tot doel carboxylaatdeklagen te optimaliseren en te karakteriseren naar hun corrosiebeschermende eigenschappen voor koperen oppervlakken. Twee verschillende depositietechnieken worden uitgetest (onderdompeling vs. elektrochemische depositie), alsook wordt geëxperimenteerd met oplossingen gebaseerd op ethanol. De karakterisering wordt uitgevoerd met behulp van hogervermelde technieken alsook met synchrotron XRD.

Het werk wordt afgesloten met conclusies aangaande het werk en een standpunt wat betreft potentieel toekomstig onderzoek in hetzelfde domein.

List of publications and activities

List of publications

- A. Elia, M. Dowsett, A. Adriaens, *Electrochemical characterization of bronze historical objects using voltammetry of microparticles*, accepted for publication in special issue Applied Physics A: Microchemistry in Art and Archaeology
- K. S. Lokesh, M. De Keersmaecker, A. Elia, D. Depla, P. Dubruel, P. Vandenabeele, S. Van Vlierberghe, A. Adriaens, *Adsorption of cobalt (II) 5,10,15,20-tetrakis(2-aminophenyl)-porphyrin onto copper substrates: characterization and impedance studies for corrosion inhibition*, Corrosion science 62 (2012), 73-82
- A. Elia, K. De Wael, M. Dowsett, A. Adriaens, *Electrochemical deposition of a copper carboxylate layer on copper as potential corrosion inhibitor*, Journal of Solid State Electrochemistry 16 (2012), 143-148.
- A. Elia, M. Dowsett, G. Jones, A. Adriaens, *Evaluation of Carboxylate-based Coatings for the Protection of Copper and Copper Alloys*, in YOCOCU: Contribute and Role of Youth in Conservation of Cultral Heritage, Palermo (Italy), 24-26 May 2010, (Eds A. Macchia, E. Greco, B.A. Chiarandá, N. Barbabietola) ateneo "La Sapienza", Rome, 2011, pp 203-212
- A. Elia, M. Dowsett, A. Adriaens, *On the use of alcoholic carboxylic acid solutions for the deposition of protective coatings on copper*, in Proceedings of the ICOM-CC Metal Working Group International Triennial Meeting, Charleston (SC), 10-15 October 2010, (Eds. P. Mardikian, C. Chemello, C.Watters, P. Hull) Metal 10, Clemson University, Clemson, 2010, pp.144-150
- T. Poli, A. Elia, O. Chiantore, *Surface finishes and materials: Fiber-Optic Reflectance Spectroscopy (FORS) problems in cultural heritage diagnostics*, e-Preservation Science 6 (2009), 174-179

- A. Elia, *Analisi di diagnostica conservativa della maschera S11059,* in: E. D'Amicone, M. Pozzi Battaglia (Eds.) Egitto mai visto. Le dimore di Assiut e Gebelein, Tipografia Editrice Temi, Trento, 2009, pp. 81-83
- A. Elia, *Olio di oliva da Cipro per la bellezza delle donne d'Egitto* in: E. D'Amicone, E. Fontanella (Eds.) Nefer: la donna nell'antico Egitto, Motta Editore, Milano, 2007, pp.173

Conference abstracts

- A. Elia, M. Dowsett, A. Adriaens, *Voltammetry of Microparticles for the characterization of copper and bronze corrosion products on Roman artefacts*, 2nd International Congress Chemistry for Cultural Heritage (CHEMCH) 2012, Istanbul 9-12 July 2012 (oral presentation)
- A. Elia, M. Dowsett, A. Adriaens, *Electrochemical characterization of bronze patinas on Roman archaeological objects*, Youth in Conservation of Cultural Heritage (YOCOCU) 2012, Antwerp 18-20 June 2012 (oral presentation)
- A. Adriaens, M. G. Dowsett, A. Elia, P-J. Sabbe, M. De Keersmaecker, M. Hand, J. Crawford , R. A. Grayburn and R. Morris, *Beauty and the synchrotron: collaboration between Ghent University (BE) and University of Warwick (UK)*, Cultural Heritage meets Science: The Interface, 14 September 2011, Mary Rose Trust Museum, Portsmouth, UK (poster contribution)
- A. Elia, A. Adriaens, P. Normile, M. Dowsett, *A Synchrotron Radiation Study of Copper Carboxylate Layers on the XMaS beamline*, Synchrotron Radiation to Art (Sr2A) 2010, Amsterdam, 7-10 November 2010 (poster contribution)
- A. Adriaens, M.G. Dowsett, P.A. Thomas, G.K.C. Jones, A. Elia, L. Bouchenoire, *Real time XRD monitoring of lead carboxylate growth in an environmental cell*, 51st Corrosion Science Symposium, Southampton, 1-3 september 2010 (poster contribution)
- M. G. Dowsett, A. Adriaens, M. Hand, J.B. Crawford, A. Elia, S. Brown, *X-ray excited optical luminescence for the study of problems in heritage metal*

corrosion, 51st Corrosion Science Symposium, Southampton, 1-3 september 2010 (poster contribution)

- A. Elia, M. Dowsett, A. Adriaens, *On the use of alcoholic carboxylic acid solutions for the deposition of protective coatings*, Metal 10, Charleston, South-Carolina, 11-15 october 2010 (oral presentation)
- A. Adriaens, M. Dowsett, G. Jones, A. Elia, L. Bouchenoire, *Real time XRD monitoring of lead carboxylate growth in an environmental cell*, 10th Biennial Conference on High Resolution X-Ray Diffraction and Imaging, Coventry 20-23 september 2010 (poster contribution)
- A. Adriaens, M. Dowsett, A. Elia, G. Jones, C. Martin, l. Bouchenoire, *Real time synchrotron XRD measurements of copper corrosion and conservation protocols*, 51st Corrosion Science Symposium, Southampton, 1-3 september 2010 (poster contribution)
- A. Elia, M. Dowsett, G. Jones, A. Adriaens**,** *Evaluation of Carboxylate-based Coatings for the Protection of Copper and Copper Alloys*, Youth in Conservation of Cultural Heritage (YOCOCU) 2010, Palermo, 24-26 May 2010 (poster contribution)
- A. Elia, A. Adriaens, M. Dowsett, G. Jones, *Evaluation of carboxylate-based coatings for the protection of copper and copper alloys*, Het 10de Vlaams Jongerencongres van de Chemie (VJC10), Blankenberge, 1-2 March 2010 (oral presentation)
- A. Adriaens, M. Dowsett, A. Elia, *In-situ time-resolved monitoring of copper corrosion using an automated electrochemical cell*, Synchrotron and Neutron workshop (SyNeW), Brussels, 23rd April 2009 (poster contribution)
- A. Elia, *Segreti dell'arte e della bellezza nell'antico Egitto. Le indagini chimiche svelano tecniche antiche*, Scienziati dell'arte, Torino, 14-24 April 2008 (oral presentation, poster)

Beamtimes attended at the ESRF

26-01-821: An investigation of ODXAS for measuring thin corrosion layers on heritage copper alloys and other materials (main proposer: Annemie Adriaens)

26-01-832: Parallel application of ODXAS and XAS for studying heritage metal corrosion in real time (main proposer: Annemie Adriaens)

SI 1625: Time resolved SR-XRD of electrochemical processes and controlled environment exposure on heritage lead (main proposer: Mark Dowsett)

EC 188: Time-resolved SR-XRD and XAS for the conservation/protection of heritage and other metals using XMaS (BM28) (main proposer: Mark Dowsett)

Beamtime attended at DESY

10008225: Full Field XRF camera tests and applications (main proposer: Laszlo Vincze)

Workshops and training schools

Electrochemistry in Historical and Archaeological Conservation (Leiden, 11-15 January 2010).

COST Training School: Indoor Air Quality in Museums, Galleries and Archives. Analytical Methods and Preventive Conservation Strategies (Vienna, 5-9 May 2009)

Electrolytic cleaning of metallic artefacts, Part I (Antwerp, 3-4 December 2009)

Electrolytic cleaning of metallic artefacts, Part II (Antwerp, 14-15 December 2010)